RPSEA

FINAL TECHNICAL REPORT

Document Number: 08121-2902-07.FINAL

Fiber-containing Sweep Fluids for Ultra Deepwater Drilling Applications

Contract Number: 08121-2902-07

March 3, 2012

Ramadan M. Ahmed
Assistant Professor
The University of Oklahoma
100 Boyd St., Norman, OK 73019

LEGAL NOTICE

This report was prepared by *The University of Oklahoma* as an account of work sponsored by the Research Partnership to Secure Energy for America, RPSEA. Neither RPSEA members of RPSEA, the National Energy Technology Laboratory, the U.S. Department of Energy, nor any person acting on behalf of any of the entities:

a. MAKES ANY WARRANTY OR REPRESENTATION, EXPRESS OR IMPLIED WITH RESPECT TO ACCURACY, COMPLETENESS, OR USEFULNESS OF THE INFORMATION CONTAINED IN THIS DOCUMENT, OR THAT THE USE OF ANY INFORMATION, APPARATUS, METHOD, OR PROCESS DISCLOSED IN THIS DOCUMENT MAY NOT INFRINGE PRIVATELY OWNED RIGHTS, OR

b. ASSUMES ANY LIABILITY WITH RESPECT TO THE USE OF, OR FOR ANY AND ALL DAMAGES RESULTING FROM THE USE OF, ANY INFORMATION, APPARATUS, METHOD, OR PROCESS DISCLOSED IN THIS DOCUMENT.

THIS IS AN INTERIM REPORT. THEREFORE, ANY DATA, CALCULATIONS, OR CONCLUSIONS REPORTED HEREIN SHOULD BE TREATED AS PRELIMINARY.

REFERENCE TO TRADE NAMES OR SPECIFIC COMMERCIAL PRODUCTS, COMMODITIES, OR SERVICES IN THIS REPORT DOES NOT REPRESENT OR CONSTIITUTE AND ENDORSEMENT, RECOMMENDATION, OR FAVORING BY RPSEA OR ITS CONTRACTORS OF THE SPECIFIC COMMERCIAL PRODUCT, COMMODITY, OR SERVICE.

Abstract

This report presents experimental and theoretical studies conducted on the rheology and stability of fiber-containing sweep fluids. In addition, the report shows results of our investigations on settling behavior of solids particles in fiber sweeps. Spherical glass particles with different diameters were used. We performed experiments using water and oil-based fluids. Fluid composition and fiber concentration were varied during the investigation.

Rheological properties of the fluid samples were measured before stability and settling velocity experiments. Even though 0.04 percent fiber content is recommended in the field for sweep application, tests were conducted varying fiber content from 0.00 to 0.08 percent. Results indicate the absence of excessive thickening, which is frequently observed in highly concentrated fiber suspensions. Because of their low fiber concentration, fiber sweeps are not vulnerable to excessive thickening.

The stability of fiber sweep determined the hole-cleaning performance of the fluid. During our investigations, we developed mathematical models based on hydrodynamic drag behavior of long cylinders. They predict the stability of non-Newtonian fiber suspensions. Model predictions showed good agreement with experimental results. Both theoretical analysis and experimental observation suggested the critical role of viscosity in maintaining the stability of the fluid. Highly viscous base fluids created stable fiber suspensions. However, viscosity was not the only parameter that controlled the stability of these fluids. The polymer type also played a great role. In general, xanthan gum-based fluids showed very good stability. In addition to the polymer type, the existence of structure in the fluid also stabilized the fluid. Oil-based muds (OBM and SBM) are structured fluids with a continuous oil phase and dispersed water droplets. Because of the surfactant (i.e., emulsifier), the fluid maintained its structure for sufficiently long time. The structure trapped fiber particles and kept them in the suspension without segregation. All oil-based fluids that were tested show excellent stability.

Settling velocity of cuttings is often used to assess hole-cleaning performance of drilling fluids. The addition of fiber into a drilling fluid substantially reduced the settling velocity of cuttings and improved carrying capacity of the fluid. The velocity reduction came from the improvement of the drag force that opposes the motion of the particle. When fiber particles were fully dispersed in the fluid, they tended to form a network structure that generated additional drag force (fiber drag). After obtaining settling velocity measurements, we were able to determine the contribution of the fiber drag to the total drag force. Due to the strong interactions between the fiber particles and the base fluid, the hydrodynamic component of the fiber drag dominated the drag that originated because of mechanical friction and fiber entanglement. As a result, the fiber drag was strongly related to viscous properties of the fluid. In this study, we developed a settling velocity model by predicting settling behavior of particles in fiber sweeps. The model accounted for the presence of fiber particle using the fiber drag coefficient. Model predictions showed a satisfactory agreement with experimental measurements.

Sweep experiments were conducted with fiber-containing water-based and synthetic-based drilling fluids to study wellbore cleaning performance. Extensive flow loop experiments were carried out by varying fiber concentration (up to 0.27 lb/bbl) in industry utilized water-based and synthetic-based drilling fluid formulations. Cuttings bed heights in the flow loop annulus were measured at different flow rates and pipe rotation speeds for the different fluid-fiber combinations at horizontal and inclined configurations. In addition, to investigate the hydraulic impact of the fiber, pipe viscometer and wellbore hydraulics experiments were conducted at varying fiber concentrations. Results showed that fiber sweeps substantially improved cuttings removal compared to the base fluid sweeps, despite similar equivalent circulating densities.

A mechanistic model was developed to predict critical cuttings transport velocity or equilibrium bed height in horizontal and inclined wellbores with fiber-containing fluids. The model was developed by considering fluid flow over a stationary bed of solid particles of uniform thickness. The model required a correlation for estimating the additional drag (i.e., fiber drag) resulting from the presence of fiber in the fluid. Settling velocity experimental data was used to provide a correlation for the fiber drag coefficient, and the sweep experiments were used to verify the model predictions. The critical transport velocity was measured by visual observation of the cuttings bed particles movement. The model predictions and experimental measurements showed good agreement at low flow rates. For fluids without fiber (i.e., base fluid), mechanistic model predictions were compared with published experimental results and with predictions of an existing model. The comparisons showed satisfactory agreement with measurements and better accuracy than the existing model.

Signature:  Date: March, 03, 2012

Table of Contents

Disclaimer	ii
Abstract	iii
Table of Contents	vii
List of Tables	x
List of Figures	xi
1. Executive Summary	1
2. Theoretical Study on Stability of Fiber Sweeps	4
2.1. Particle Settling Behavior	4
2.1.1. Classification of Particle Settling Behavior	4
2.1.2. Motion of Fibrous Particles	5
2.2. Modeling Rising Velocity of Particles	6
2.3. Non-Rising Particles under Static Conditions	8
2.4. Non-Rising Particles under Dynamic Conditions	11
2.5. Modeling Results	12
2.6. Conclusions	15
Nomenclature	16
References	17
3. Experimental Study on Stability of Fiber Sweeps	18
3.1. Scope	18
3.2. Experimental Setup and Procedure	18
3.3. Results	19
3.3.1. Effect of Base Fluid Rheology on Stability of Fiber Sweep	20
3.3.2. Effect of Temperature on Stability of Fiber Sweep	26
3.3.3. Comparison of Model Predictions with Experimental Results	27
3.4. Conclusions	28
Nomenclature	29
References	29
4. Rheological Properties of Fiber Sweeps	30
4.1. Introduction	30
4.2. Literature Review	32
4.3. Fiber Fluid Rheology	34

4.4. Experimental Investigations	36
4.4.1. Experimental Setup	36
4.4.2. Test Procedure	37
4.5. Experimental Results	38
4.5.1. Effect of Fiber Concentration	38
4.5.2. Effect of Temperature	44
4.5.3. Shear Viscosity Parameters	45
4.6. Conclusions	48
Nomenclature	48
References	49
5. Settling Behavior of Particles in Fiber-containing Drilling Fluids	51
5.1. Introduction	51
5.2. Settling in Fiber Suspensions	55
5.3. Experimental Study	56
5.3.1. Experimental Setup	57
5.3.2. Test Materials	58
5.3.3. Test Procedure	58
5.3.4. Test Results	59
5.4. Analysis of Results and Discussions	62
5.5. Model Predictions	63
5.6. Conclusions	64
Nomenclature	65
References	65
6. Hole Cleaning Performance of Fiber Sweeps	68
6.1. Introduction	68
6.2. Experimental Setup	69
6.3. Experimental Procedure	71
6.4. Experimental Test Matrix	76
6.4.1. WBM Test Matrix	76
6.4.2. SBM Test Matrix	77
6.5. Experimental Results	78
6.5.1. Dynamic Variation of Cuttings Bed Height	78
6.5.2. Effect of Fluid Types	79

6.5.3. Effect of Fiber Concentration	82
6.5.4. Effect of Inclination Angle	85
6.5.5. Effect of Flow Rate	87
6.5.6. Effect of Pipe Rotation	88
6.6. Pipe Viscometer Measurements	89
6.7. Wellbore Hydraulics	92
6.8. Conclusions	93
6.9. Guidelines	94
Nomenclature	95
References	96
7. Mechanistic Modeling of Hole Cleaning with Fiber Sweeps	97
7.1. Introduction	97
7.2. Forces Involved in Particle Transport	98
7.2.1. Gravity and Buoyancy Forces	99
7.2.2. Hydrodynamic Forces	99
7.2.3. Fiber Drag Force	101
7.2.4. Plastic Force	102
7.3. Near-Bed Velocity Profile	103
7.3.1. Newtonian Fluid	103
7.3.2. Non-Newtonian Fluid	103
7.4. Mechanistic Model Formulation	106
7.5. Experimental Results	107
7.5.1. Comparison of Model Predictions with Test Measurements	107
7.5.2. Comparison of Model Predictions with Published Data and Existing Model	108
7.6. Conclusions	110
Nomenclature	110
References	111

List of Tables

Table 2.1	Input data	12
Table 3.1	Test matrix for stability experiments	18
Table 3.2	One-hour stability of test fluids	20
Table 4.1	Test matrix of rotational viscometer measurements	36
Table 4.2	Fiber properties	36
Table 4.3	Rheological parameters of XG based fluid with varying fiber concentration at 72°F and 170°F	46
Table 4.4	Rheological parameters of PAC based fluid with varying fiber concentration at 72°F and 170°F	46
Table 4.5	Rheological parameters of XG/PAC (50%/50%) based fluid at 72°F and 170°F	47
Table 4.6	Rheological parameters of XG + Barite (12 ppg) based fluid at 72°F and 170°F	47
Table 4.7	Rheological parameters of PHPA based fluid with varying fiber concentration at 72°F and 170°F	47
Table 4.8	Rheological parameters of OBM and SBM with varying fiber concentration at 72°F and 170°F	47
Table 6.1	WBM flow loop test matrix and rheological properties	76
Table 6.2	SBM flow loop test matrix	76

List of Figures

Fig. 2.1	Free body diagram of a cylindrical particle rising in static fluid	6
Fig. 2.2	Vertical component of shear force acting on a fully suspended cylinder	9
Fig. 2.3	Differential element of a cylinder subject to shear force	9
Fig. 2.4	Shear force acting on a cylinder oriented vertically	10
Fig. 2.5	Critical yield stress as a function of fluid density for a non-raising particle	10
Fig. 2.6	Narrow slot representing annulus	11
Fig. 2.7a	Rising velocity vs. yield stress for horizontally oriented fiber in 8.33 ppg fluid with n=0.3	13
Fig. 2.7b	Rising velocity vs. yield stress for horizontally oriented fiber in 8.33 ppg fluid with n=0.6	13
Fig. 2.8	Rising velocity vs. yield stress for horizontally oriented fiber in 8.33 ppg fluid with n=1.0	13
Fig. 2.9	Rising velocity vs. yield stress for horizontally oriented fiber (n = 0.3 & K = 2.1 $lbfs^n/100\ ft^2$)	13
Fig. 2.10	Rising velocity vs. yield stress for horizontally oriented fiber (n = 0.6 & K = 2.1 $lbfs^n/100\ ft^2$)	14
Fig. 2.11	Rising velocity vs. yield stress for horizontally oriented fiber (n = 1.0 & K = 2.1 $lbfs^n/100\ ft^2$)	14
Fig. 2.12	Rising velocity vs. mud weight under dynamic conditions for vertically oriented fiber	15
Fig. 3.1	Fluid samples	19
Fig. 3.2	Unstable fluids after 1-hour test	19
Fig. 3.3	Graduated cylinder used for stability experiment	19
Fig. 3.4	One-hour stabilities of XG based fiber sweep at 170°F	21
Fig. 3.5	One-hour stabilities of PAC based fiber sweeps at 170°F	22
Fig. 3.6	One-hour stabilities of PHPA based fiber sweeps at 170°F	22
Fig. 3.7	One-hour stabilities of XG/PAC based fiber sweeps at 170°F	23
Fig. 3.8	One-hour stabilities of XG based weighted (12 ppg) fiber sweeps at 170°F	24
Fig. 3.9	Measured and predicted one-hour stability of oil-based fluids at 170°F	24
Fig. 3.10	Twelve-hour stabilities of XG based fluids at 170°F	24
Fig. 3.11	Twelve-hour stabilities of XG based fluids at 72°F	24
Fig. 3.12	One-hour stabilities of PAC based fluids at 72°F	25
Fig. 3.13	Half-hour stabilities of PAC based fluids at 170°F	25
Fig. 3.14	Apparent viscosity vs. shear rate of based fluids at 170°F	26

Fig. 4.1	Stand mixers	37
Fig. 4.2	Rotational viscometers	37
Fig. 4.3	Rheology of XG based fluid at 72°F and 170°F varying fiber and polymer concentrations	39
Fig. 4.4	Rheology of PAC based fluid at 72°F and 170°F varying fiber and polymer concentrations	40
Fig. 4.5	Rheology of XG/PAC (50%/50%) mix fluid at 72°F and 170°F	41
Fig. 4.6	Rheology of XG based weighted fluids (12 ppg) at 72°F and 170°F	42
Fig. 4.7	Rheology of PHPA based fluids at 72°F and 170°F varying fiber and polymer concentrations	43
Fig. 4.8	Rheology of weighted (12.2 ppg) oil-based fluids at 72°F and 170°F	44
Fig. 5.1	Schematic of the settling cylinder	57
Fig. 5.2	Rheologies of 0.5% PAC based fluids with different fiber concentrations	58
Fig. 5.3	Settling velocity of 2-mm glass bead vs. time in mineral oil	59
Fig. 5.4	Drag coefficient vs. particle Reynolds Number for base fluids	59
Fig. 5.5	Settling velocity particle in 0.5% PAC based fluid for different fiber concentrations	60
Fig. 5.6	Settling velocity particle in 0.25% XG based fluid for different fiber concentrations	60
Fig. 5.7	Comparison of fiber drag with viscous drag acting on a particle in 0.5% PAC based fluid	61
Fig. 5.8	Fiber drag coefficient vs. Reynolds Number	62
Fig. 5.9	Normalized fiber drag coefficient vs. Reynolds Number for different fluids	62
Fig. 5.10	Predicted vs. measured settling velocity for different PAC based fluids	63
Fig. 5.11	Predicted and measured settling velocity vs. fiber concentration for 0.5% PAC	63
Fig. 5.12	Predicted and measured settling velocity vs. fiber concentration for 0.25% XG	64
Fig. 6.1	Flow loop in inclined position	70
Fig. 6.2	Flow loop configuration/schematic	71
Fig. 6.3	Sieve analysis of silica sand, 8/16 mesh	71
Fig. 6.4	Synthetic-based fluid constituents	72
Fig. 6.5	Packaged components of synthetic-based fluid	73
Fig. 6.6	SBM component concentrations	73
Fig. 6.7	Emulsifier/Dispersator	73
Fig. 6.8	Annulus test section bed height measuring tapes	78

Fig. 6.9	Bed height vs. flow rate for XG based fluid sweep (no fiber), inclined annulus (8.33 ppg)	78
Fig. 6.10	Fluctuation of cuttings bed height due to drillpipe rotation	79
Fig. 6.11	Bed height vs. flow rate for WBM and SBM, no rotation, inclined annulus	80
Fig. 6.12	Percent reduction of bed height of WBM and SBM, no rotation, inclined annulus	80
Fig. 6.13	Apparent viscosity vs. shear rate for sweep base fluids, ~95°F	81
Fig. 6.14	Bed height vs. flow rate for WBM, no rotation, inclined annulus	82
Fig. 6.15	Comparison of fiber effectiveness for hole cleaning with WBM (8.33 ppg), inclined annulus	82
Fig. 6.16	Dimensionless bed height vs. flow rate for SBM, no pipe rotation	83
Fig. 6.17	Dimensionless bed height vs. flow rate for WBM, no pipe rotation, horizontal annulus	84
Fig. 6.18	Percent bed height reduction vs. fiber concentration for SBM, no pipe rotation	84
Fig. 6.19	Percent bed height reduction vs. flow rate for SBM, no pipe rotation	85
Fig. 6.20	Percent bed height reduction vs. flow rate for SBM, 25 rpm pipe rotation	85
Fig. 6.21	Percent bed height reduction vs. inclination angle for SBM	86
Fig. 6.22	Dimensionless bed height vs. flow rate for WBM base fluid, horizontal and inclined annulus	86
Fig. 6.23	Percent bed height reduction vs. flow rate for SBM base sweep, no fiber	87
Fig. 6.24	Effect of different pipe rotation speeds on the hole cleaning for WBM	88
Fig. 6.25	Percent bed height reduction vs. fiber concentration for SBM, Q = 20 gpm	89
Fig. 6.26	Pipe viscometer schematic	90
Fig. 6.27	Measured pressure loss as a function of flow rate in pipe viscometer, 90° orientation	91
Fig. 6.28	Friction factor vs. General Reynolds number in pipe viscometer, 90° orientation	91
Fig. 6.29	Annulus test section schematic	92
Fig. 6.30	Measured pressure loss as a function of flow rate in annulus, 90° orientation	92
Fig. 6.31	WBM Friction factor vs. General Reynolds number in annulus, 90° orientation	93
Fig. 7.1	Forces acting on a single bed particle	99
Fig. 7.2	Drag and lift force acting on the surface of a bed particle	100
Fig. 7.3	Stagnant fluid surrounding a bed particle (Ahmed et al. 2002)	103
Fig. 7.4	Bed height vs. flow rate for 2 mm cuttings in horizontal configuration	107
Fig. 7.5	Bed height vs. flow rate for 2 mm cuttings in inclined (70°) configuration	108

Fig. 7.6	Bed height vs. flow rate for 0.45 mm cuttings with PAC based fluid	109
Fig. 7.7	Bed height vs. flow rate for 0.45 mm cuttings with PAC based fluid	109

1. Executive Summary

Project Management Plan and Technology Status Assessment (Tasks 1 & 2): The project began with developing the project management plan and assessing the technology status. As required by RPSEA, the project management plan and technology status assessment report were submitted within 30 days of the award. The project management plan presents project work breakdown structure, schedules, key milestones, and planned expenditures for each Task.

Technology Transfer, Project Reporting and Other Activities (Tasks 3 & 4): Different technology transfer methodologies are being implemented to disseminate the outcomes of the project. Project outcomes have been presented in different meetings including: Six RPSEA TAC meetings and MPGE advisory board meeting. A paper on rheology of fiber sweeps (George et al. 2011) was presented at the 2011 AADE meeting. We participated in the 2011 Offshore Technology Conference (OTC), University showcase. Furthermore, a book chapter (George et al. 2012) and a journal article (Elgaddafi et al. 2012) have been accepted for publication.

Literature Review and Theoretical Study (Task 5): The research part of the project began with extensive literature review on fiber-containing fluid systems. Literature review and theoretical investigations on rheology, hydraulics, stability and carrying capacity of fiber-containing drilling sweeps were undertaken. The outcomes of this task that are presented in Sections 2, 4, and 5 were used to develop a mechanistic model to predict the hole cleaning performance of fiber sweeps. The model optimizes fiber sweep applications.

Bench-Top Experiments (Task 6): These experiments were aimed at developing fiber sweep formulations that have superior stability and optimum fiber concentration. We developed a stability model for fiber sweeps and theoretically analyzed their stability (Section 2). This helped us to select the ranges of base fluid properties that are suitable for fiber sweep applications. The stability of commonly used base fluids were tested and stable formulations identified (Section 3). Even though excessive thickening is a common problem with fibrous fluids, our rheology study (Section 4) did not demonstrate the presence of thickening in fiber sweeps. As the fiber concentration increased, the rheologies of test samples remained roughly the same. In addition to stability and rheology studies, extensive settling experiments were carried out (Section 5) to assess carry capacity of fiber sweeps. Based on theoretical analysis and experimental results, we developed a model that predicts the settling behavior of particles in fiber sweeps. The model was applied to formulate the mechanistic hole-cleaning model, which was developed in Task 8.

Flow Loop Experiments (Task 7): Extensive flow loop experiments were carried out to study rheology, hydraulics and hole cleaning performance of the base fluids and fiber sweeps. To conduct the experiments, first the flow loop was modified to perform fiber sweep tests. Fiber concentration, inclination angle, and pipe rotational speed were varied. Water-based and synthetic-based fluids were tested. Results showed the hole cleaning performance of the fiber sweep under different conditions.

Mechanistic Modeling (Task 8): Flow loop measurements may not be directly applied to evaluate the performance of sweep fluid in the field. However, they can be used to validate and calibrate models that are based on the generalized conservation laws and applicable for both field and lab-scale measurements. Therefore, in the final stage of the project, modeling study was carried out to formulate a mechanistic that predicted the performance of the sweep fluid under field conditions and optimized the application of fiber sweep technology. Flow loop measurements were utilized to evaluate and calibrate the model.

Deliverables of the project:

i. Report and publications presenting:
   - Literature review findings (Sections 2.1, 4.2 and 5.1) and data analysis (Sections 3.3, 4.5, 5.4 and 6.4)
   - Empirical correlations and semi-empirical models (Section 5.4)
   - Mathematical models (Sections 7, 5.2 and 2.2), and
   - Mechanisms and physical phenomena involved in the application of fiber sweep (Sections 2.1, 3, 4.1 and 5.1)

ii. Formulations of stable fiber-containing sweep fluids (Section 3.3)

iii. Experimental data describing
   - Particle settling velocity (Section 5.3)
   - Fiber drag (Section 5.4)
   - Rheology and stability under different temperature conditions (Sections 3 and 4)
   - Hydraulics and hole cleaning performance of fiber sweeps (Section 6)

iv. Recommendations and guidelines for field applications (Section 6.9)

References

George, M., Ahmed, R. and Growcock, F. 2011.Rheological Properties of Fiber-Containing Drilling Sweeps at Ambient and Elevated Temperatures, paper AADE-11-NTCE-35, presented at the AADE National Technical Conference and Exhibition, Houston, Texas, April 12-14, 2011.

George, M., Ahmed, R. and Growcock, F. 2012. Stability and Flow Behavior of Fiber-Containing Drilling Sweeps, Rheology, InTech, Rijeka, Croatia, ISBN: 978-953-51-0187-1, http://www.intechopen.com/books/rheology/stability-and-flow-behavior-of-fiber-containing-drilling-sweeps.

Elgaddafi, R., Ahmed, R., George, M. and Growcock, F. 2012. Settling behavior of spherical particles in fiber-containing drilling fluids, J. Pet. Sci. Eng. (2012), doi:10.1016/j.petrol.2012.01.020.

2. Theoretical Study on Stability of Fiber Sweeps

One of the major areas of concerns in the development of fiber sweep technology is fluid instability under borehole conditions. A recent experimental study (Ahmed and Takach 2008) demonstrated the presence of fiber separation in low-viscosity sweep fluids. Fiber particle separate or rise in the fluid due to the buoyant nature of the particles. The separation of the fiber particle substantially reduces the performance of the sweep fluid.

2.1 Particle Settling Behavior

In contrast to the manufacturing industry, where fiber suspensions are common, the conditions to which the sweep fluids are subjected can be extremely severe. Modern technological advances within the oil and gas industry have taken some of the unpredictability out of the well construction phase. Despite this, there is still no ability to attenuate the harsh environmental conditions that exist within the wellbore, such as high temperature and high pressure, which necessitate the use of thermally stable, high specific gravity fluids. These circumstances, unique to the oil and gas industry, and other intangibles, preclude a large majority of previous work on the flow behavior of homogeneous, non-Brownian suspensions within a controlled environment. Another dissimilarity is the relative specific gravities of the suspended particles and the suspending medium. There is a large quantity of experimental, mathematical, and numerical studies on the settling behavior of spherical and non-spherical particles. However, in the case of fiber sweeps, the relative gravities are reversed, as the specific gravities of the synthetic fiber and sweep fluid is less than and greater to water, respectively. This relation encourages buoyancy, and the fibers tend to rise within the suspension. Despite the opposing directions of motion, the fibers and fiber networks still exhibit similar general motion and phenomena.

2.1.1 Classification of Particle Settling Behavior

The settling behavior of particles can be divided into four generally accepted classifications, whose definitions can be revised to reflect the purpose of this study (Scholz 2006):

- **Class I:** Unhindered settling of discrete particles. The singular particle undergoing this settling behavior will accelerate until a terminal settling velocity is reached, where the hydrodynamic drag and gravitational force are balanced. Stokes' Law is commonly used to describe this motion of spherical particles.
- **Class II:** Settling of a dilute suspension of flocculent particles. The randomly moving particles collide and become entangled, and form aggregates (flocs), which can have increased settling velocities compared to a single fiber.
- **Class III:** Hindered and zone settling. Particle concentration is increased to a point where

discrete settling no longer occurs. All particles consolidate and displace the liquid phase, which gives rise to a new upward flow of liquid. This reciprocal motion reduces the overall particle settling velocity and is called hindered settling. In large surface area settling applications with high particle concentration, the whole suspension may tend to settle as a "blanket" (zone settling).

- **Class IV:** Compression settling (compaction and consolidation). As the settling continues, a compressed layer forms at the bottom of the settling column. As the compression layer is created, a concentration gradient forms extending upward from the lower sludge region to an increasingly dilute solids particle concentration.

2.1.2 Motion of Fibrous Particles

Class I and II can be used to describe the motion of synthetic fibers within a low concentrate suspension. The modeling study considers Class I motion, which simply describes the forces and rising velocity of a single fiber suspended in a fluid. This prediction can be extrapolated to determine the rising velocity of a dilute suspension of fiber particles, or Class II motion. Due to the minimal scale of this research, hindered or zonal settling is readily apparent. While the fibers do rise to the surface of the test cylinders within the extents of the experiments, there is no true compaction or compression of the fibers at the liquid surface.

The settling motion of a particle is simply a classification of its motion. The settling motion of a fibrous particle is much more complex (Qi et al. 2011). In the absence of extraneous forces, a sphere settles in a purely vertical direction. The inconsistent, asymmetrically shaped flexible fiber suspended in a fluid can exhibit profligate behavior in three dimensions, as well as drift horizontally during its vertical ascent/descent (Herzhaft and Guazzelli 1999). The rising velocity of these fibers also depends on the fiber concentration and orientation of the high-aspect ratio particles. Experimental studies investigating dilute and semi-dilute cylindrical or spheroid particles indicate that concentration is vital in understanding the settling behavior (Qi et al. 2011; Kuusela et al. 2001, 2003; Koch and Shaqfeh 1989; Herzhaft et al. 1996, 1999). The overall consensus regarding the settling behavior of fiber suspensions was the ability of the fiber flocs to settle faster than an individual fiber. As the fiber concentration increased, the fibers actually exhibited hindered settling, and the mean velocity actually decreased below that of a single fiber.

The previous studies mentioned were concerned with phenomena of a similar nature and relevant to this work. However, due to the particular focus of this study, the ideas and conclusions gathered from literature must be extrapolated and generalized to correlate to the rising tendency of the fibers. This study showed rising velocities of fiber particles within a suspension, based on theoretical models and experimental results.

2.2 Modeling Rising Velocity of Particles

The purpose of this modeling study was to predict the behavior of the synthetic monofilament fiber suspended in fluids with varying rheological properties. In order for the fiber to perform as efficiently and effectively as possible, the fluid suspending the fiber was engineered to promote the fiber's wellbore cleaning capabilities. Thus, a theoretical study was conducted to determine the desirable base fluid properties and formulate sweep fluids that are stable under borehole conditions.

For the sake of simplicity and to provide easier comparison between fibers oriented perpendicular (horizontally) and parallel (vertically) to the direction of motion, the analysis only considered a single fiber suspended in the fluid (Class I settling behavior). This assumption ignored the effect of fiber-fiber interaction and fiber concentration. The fiber-fiber interaction phenomenon and the fiber concentration in the fluid were shown to influence the stability of the fiber-fluid system (Ahmed and Takach 2008). This analysis also addressed two orientations of the fiber: perpendicular to the direction of motion of the fiber (horizontal) and parallel to the direction of motion of the fiber (vertical). These orientations represent the boundaries within which the fiber can theoretically orient. However, it has been shown that single settling fiber will orient itself horizontally (Fan et al. 2004; Kuusela et al. 2001, 2003; Qi et al. 2011). This stable orientation is also irrespective of fluid velocity, and will eventually return to the horizontal position if acted upon by an outside force (Qi et al. 2011). Liu and Joseph (1993) investigated how a slender particle is affected by liquid properties, particle density, length, and shape. They found that only particle concentration and the end shapes influenced particle orientation during settling. This agrees with studies by Herzhaft et al. (1996, 1999), which concluded that orientation of a settling spheroid is almost independent of aspect ratio, but it is correlated to suspension concentration.

As the fiber concentration is increased, the hydrodynamic interactions between the fibers will upset the stable horizontal fiber. With increasing fiber concentration, the fiber will show greater tendency to orient parallel toward the direction of motion (Herzhaft et al. 1996; Qi et al. 2011). By analyzing both cases, we predicted the rheological properties of the base fluid that can keep the fiber in suspension for a sufficient length of time.

To determine the velocity at which the submerged fiber particles move upward to the surface of the liquid, the sum of the forces in the vertical direction (y-axis) are set equal to zero. As shown in **Fig. 2.1,** the forces acting on the fiber moving within the column of fluid are buoyancy (F_b), hydrodynamic drag (F_D) and gravity ($m \cdot g$). In this case, the fiber is assumed to be oriented horizontally (perpendicular to the direction of motion of the fiber). The projected surface area of a fiber particle, dependent upon particle

orientation, is needed to compute the drag force. In this case, the fiber is horizontally oriented, and the generalized equation of the force balance in the vertical (y) direction is:

$$\sum F_y = F_b - F_D - mg = 0 \quad \text{……..……...……} \quad (2.1)$$

The forces acting on the fiber are written in terms of their variables. Thus:

$$V_p \rho_f g - \frac{1}{2}\rho_f C_{D,h} U_{p,h}^2 A_{p,h} - \rho_p V_p g \quad \text{…...……} \quad (2.2)$$

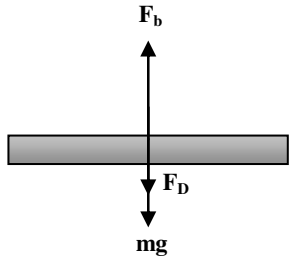

Fig. 2.1 Free body diagram of a cylindrical particle rising in static fluid

where $U_{p,h}$ is the rising velocity of horizontally oriented particle. For horizontal orientation, the projected area is $A_{p,h} = L \; x \; d$, and the volume of the fiber particle $V_p = \frac{1}{4} \pi d^2 L$. After inserting the expressions of projected area and fiber volume and rearranging the variables, the formula for the rising velocity of the particle is:

$$U_{p,h} = \left[\frac{\pi d g}{2} \left(\frac{\rho_f - \rho_p}{\rho_f} \right) \frac{1}{C_{D,h}} \right]^{\frac{1}{2}} \quad \text{……...…..…..…} \quad (2.3a)$$

A similar analysis for a vertically oriented particle yields the following rising velocity expression:

$$U_{p,v} = \left[2Lg \left(\frac{\rho_f - \rho_p}{\rho_f} \right) \frac{1}{C_{D,v}} \right]^{\frac{1}{2}} \quad \text{……...…..……...……} \quad (2.3b)$$

The drag coefficients of the fiber particle must be estimated to predict the rising velocities using the above equations. Hole cleaning fibers are more or less straight and they can be considered as a long cylinder for drag force calculation. Drag coefficient correlations and charts for long cylinders are well documented in the literature. For cylinders oriented perpendicular to the flow (i.e., cross flow), Perry (1984) presented a chart that can be approximated with the equation given below.

$$Log(C_{D,h}) = \frac{0.9842 - 0.554 Log(\mathrm{Re})}{1 + 0.09 Log(\mathrm{Re})} \quad \text{……..……} \quad (2.4)$$

This correlation is valid for Reynolds Numbers (Re) ranging from 10^{-3} to 10. It has been used extensively in this study, as most lab experiments involving fibers primarily exist in a Reynolds Number range less than 1.

The drag coefficient of a cylinder oriented in the direction of the flow is only a function of the aspect ratio (L/d). Based on available data in the literature (Hoerner 1965), the following equation has been developed to estimate the drag coefficient, C_{Dv}:

$$C_{D,v} = 0.825 + \frac{0.317}{1+\left(\frac{l/d}{1.54}\right)^{4.23}} \quad \text{..... (2.5)}$$

As shown in Eqn. (2.4), the drag coefficient of a cylindrical fiber under cross flow condition is a function of the Reynolds number, which is generally expressed as $Re = \rho U_{p,h} d/\mu$ (i.e., the ratio of inertial force to viscous force). This definition holds true for Newtonian fluids, which possess a linear relationship between shear stress and shear rate. However, the fluids that are often utilized in fiber sweep applications are non-Newtonian. Hence, the Reynolds Number needs to be redefined using the apparent viscosity function as $Re = \rho U_{p,h} d/\mu_{app}$. The viscosity for Newtonian fluids is an actual property of the fluid, and is constant despite the shear rate. However, for non-Newtonian fluids, the apparent viscosity varies with shear rate and rheological parameters of fluid. Applying the Yield Power Law (YPL) rheology model, the apparent viscosity, μ_{app}, is expressed as:

$$\mu_{app} = K(\dot{\gamma})^{n-1} + \tau_y(\dot{\gamma})^{-1} \quad \text{..... (2.6)}$$

This study is to determine the desirable Yield Power Law (YPL) fluid properties that must keep the fiber in suspension in order to create efficient momentum transfer mechanisms between the sweep fluid and cuttings bed. Hence, only fluids with sufficient yield stress and/or increased low shear rate viscosity can be utilized to keep the fibers in suspension.

2.3 Non-Rising Particles under Static Conditions

A horizontally oriented cylindrical particle, suspended in YPL fluid (**Fig. 2.2**), may not rise to the top, but remain suspended in the fluid depending on the yield stress of the fluid (Dedegil 1987). A static condition prevails when the forces in the vertical direction acting on the particle are balanced. For a fully suspended static particle, the momentum balance, Eqn. (2.1) can be rewritten to include the static shear force acting on the particle in lieu of the drag force that is present under dynamic conditions. By taking a differential

element of the cylindrical fiber, the vertical component of the maximum static shear stress (i.e., yield stress) acting on the fiber can be determined (Fig. 2.2). The direction of the shear stress acting on the cylinder depends on the location of the differential element as shown in Fig. 2.2. The stress acts on the area represented by the differential element shown in **Fig. 2.3** is expressed as:

$$dA = LRd\theta \quad \text{.....} \quad (2.7)$$

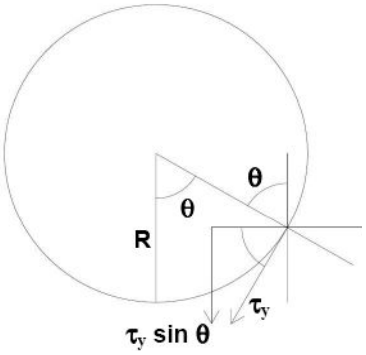

Fig. 2.2 Vertical component of shear force acting on a fully suspended cylinder

Then, the vertical component of the shear force acting on the differential element is:

$$dF_{shear} = dA \cdot \tau_y \sin\theta = LRd\theta \cdot \tau_y \sin\theta \quad \text{.....} \quad (2.8)$$

In a fiber oriented vertically and horizontally, shear stresses act on the circumferential and end areas. However, the end areas are negligible when compared to circumferential area of the cylinder. This further simplifies the analysis. Neglecting the forces acting on the cylinder ends, the overall vertical component of the shear force is subsequently obtained by integrating Eqn. (2.8). After simplification, the vertical component of the stress force acting on horizontally oriented cylinder becomes:

$$F_{s,h} = 2dL\tau_y \quad \text{.....} \quad (2.9)$$

The above equation predicts the maximum value of the shear force acting on the cylinder. For the sake of simplicity, the analysis is only concerned with a single fiber suspended in fluid. The cylinder is considered to be non-rotating and constantly perpendicular to the direction of motion of the fiber. In addition, as stated earlier, the calculations ignore the fiber-fiber interactions, which will influence the momentum balance. Writing the force balance in the vertical direction and replacing the drag force with the shear force in Eqn. (2.1), we get:

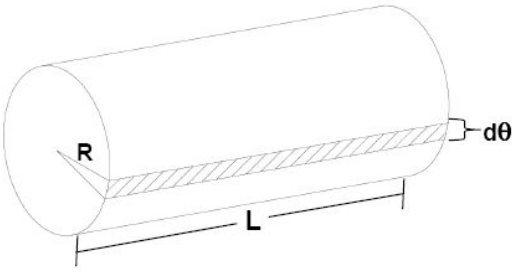

Fig. 2.3 Differential element of a cylinder subject to shear force

$$\sum F_y = 0 = V_p\rho_f g - 2dL\tau_y - \rho_p V_p g \quad \text{.....} \quad (2.10)$$

Replacing the particle volume V_p with $\pi d^2 L/4$, and grouping like terms results in:

$$2dL\left[\frac{\pi dg}{8}\left(\rho_f - \rho_p\right) - \tau_y\right] = 0 \quad \text{..... (2.11)}$$

For a fiber particle oriented in the vertical direction (**Fig. 2.4**), the shear stress acts vertically along the length of the fiber particle. By taking a circular differential element of height (dh) and circumference (πd), the shear force can be written as:

$$F_{s,v} = \pi d\tau_y \int_0^L dh = \pi dL\tau_y \quad \text{..... (2.12)}$$

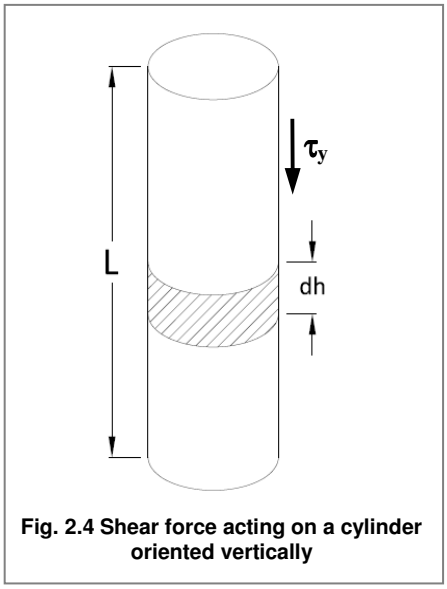

Fig. 2.4 Shear force acting on a cylinder oriented vertically

Once again rewriting the force balance equation to include the shear force acting on a vertical oriented particle, and grouping like terms results in:

$$\frac{\pi dL}{4}\left[dg\left(\rho_f - \rho_p\right) - 4\tau_y\right] = 0 \quad \text{..... (2.13)}$$

For this study, the dimensions of the fiber are known and fixed. Therefore, in order to determine the fluid property that can hold the fibers is suspension, Eqns. (2.11) and (2.13) must be rewritten to solve for critical shear stress as a function of density difference and fiber diameter for a fiber oriented horizontal and vertical, respectively. For a fiber oriented horizontal, the critical yield stress is:

$$\tau_{y,h} = \frac{\pi dg}{8}\left(\rho_f - \rho_p\right) \quad \text{..... (2.14)}$$

For a vertically oriented fiber particle, the critical yield stress is calculated as:

$$\tau_{y,v} = \frac{dg}{4}\left(\rho_f - \rho_p\right) \quad \text{..... (2.15)}$$

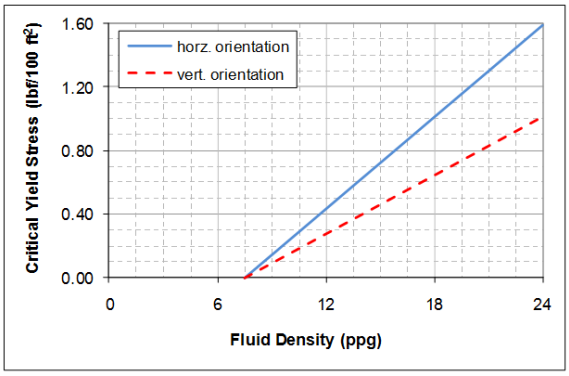

Fig. 2.5 Critical yield stress as a function of fluid density for a non-rising particle

For this analysis, the fiber size and density are known. Thus, the critical yield stress is essentially a function of the fluid density, and increases linearly with density. **Figure 2.5** presents the yield stress required to keep a fiber particle with specific gravity of

0.9, length of 10 mm, and diameter of 100 μm vertically oriented. Theoretically, very small yield stress (less than 1.5 lbf/100 ft^2) is needed to keep the fiber in suspension.

2.4 Non-Rising Particles under Dynamic Conditions

The models developed in Section 2.1 are for fiber particles rising in static fluid. They do not account for other flow phenomena such as the lateral motion and deformation of the fluid, and hydrodynamic diffusion effects. Eqns. (2.3) and (2.4) are appropriate for understanding rising behavior of fibers under static conditions. However, this study is to determine the hole cleaning efficiency of the fiber particles in real world situations such as flowing in the annulus during drillstring rotation. The shearing motion of the fluid in the annulus will affect the apparent viscosity that subsequently influences the behavior of fiber particles in the base fluid. To model the behavior of fiber under dynamic conditions accurately, the overall shear rate must be computed from the primary and secondary flow shear rates. As the sweep fluid is flowing in the annulus, it is subjected to primary and secondary flows. The primary flow is the gross flow of the fiber-fluid suspension in the annulus. For a fluid flowing in the annulus, the shear rate varies from zero to its maximum value, which occurs at the inner wall. Using the narrow slot approximation technique, the shear at any point in the annulus is given as (Miska 2007):

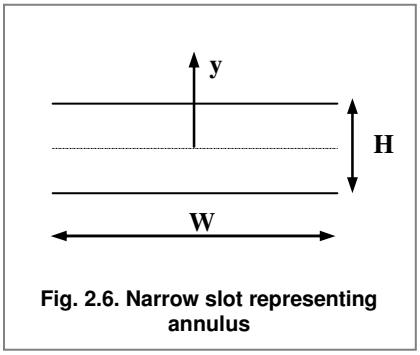

Fig. 2.6. Narrow slot representing annulus

$$\dot{\gamma}(y) = \frac{1}{K^n} \cdot \left[y\left(\frac{dp}{dL}\right) - \tau_y \right]^{\frac{1}{n}} \quad \text{..... (2.16)}$$

Equation (2.16) can be integrated to calculate the average shear rate as:

$$\dot{\gamma}_{ave} = \frac{1}{W(H/2)} \int_0^{H/2} \dot{\gamma}(y) W dy \quad \text{..... (2.17)}$$

For YPL fluids, due to the presence of the plug zone, the average shear rate (i.e., primary share rate) calculation procedure is complex. However, the shear rate in plug zone is zero and the average shear rate is expected to be very low. For Power Law fluid, Eq. (2.17) yields:

$$\dot{\gamma}_{ave} = \dot{\gamma}_{primary} = \frac{1/K^n (dp/dL)^{1/n} (H/2)^{1/n}}{W(n+1/n)} \quad \text{..... (2.18)}$$

The width of the slot W = $\pi(d_o + d_i)/2$ and the clearance H = $(d_o - d_i)/2$. The primary shear rate is a function of, flow geometry, properties of the fluid and pressure gradient or annular velocity.

The rising motion of the particle induces the secondary flow, which is a function of the fiber particle rising velocity and the particle diameter:

$$\dot{\gamma}_{secondary} = \frac{U_p}{d_p} \quad \text{(2.19)}$$

Knowing that shear rate is the magnitude of the deformation tensor, the resultant shear rate scalar can be determined by the Eucledian norm:

$$\dot{\gamma}_{total} = \sqrt{\dot{\gamma}^2_{primary} + \dot{\gamma}^2_{secondary}} \quad \text{(2.20)}$$

2.5 Modeling Results

In order to predict the behavior of the fiber under dynamic conditions, the annular velocity and hydraulic diameter were assumed based on conventionally observed values (**Table 2.1**). For a dynamic condition, the rising velocity of the fiber particle can be determined applying the rising velocity equations in combination with the resultant shear rate. To predict the possible results of the subsequent bench-top experiments, sensitivity analysis was conducted using the model. By varying certain properties of the fluids and determining the resulting rising velocities, the behavior of the fibers in suspension were investigated. For the sensitivity analysis, the rising velocity of a horizontally oriented fiber was determined under dynamic conditions varying the yield stress, fluid behavior index "n", fluid density and consistency index "K" (**Figs. 2.7** to **2.11**).

Table 2.1 Input data

Fiber Diameter	=	0.0001 m
Fiber Length	=	0.01 m
Fiber Density	=	897.04 kg/m^3
$U_{annulus}$	=	3.00 ft/sec
	=	0.9144 m/sec
$D_{hydraulic}$	=	3.50 in
	=	0.0889 m
K	=	1.32 N-s^n/m^2
n	=	0.52

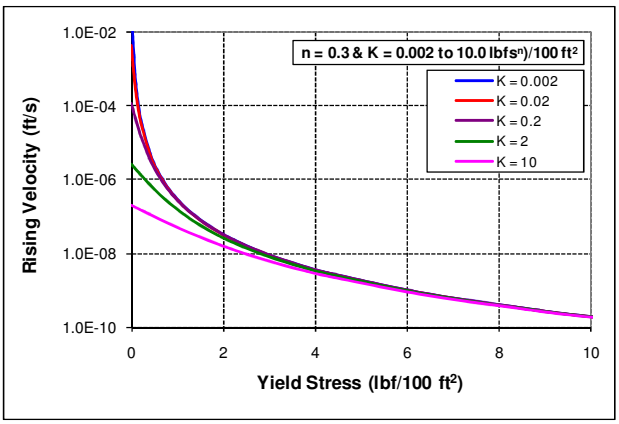

Fig. 2.7a Rising velocity vs. yield stress for horizontally oriented fiber in 8.33 ppg fluid with n=0.3

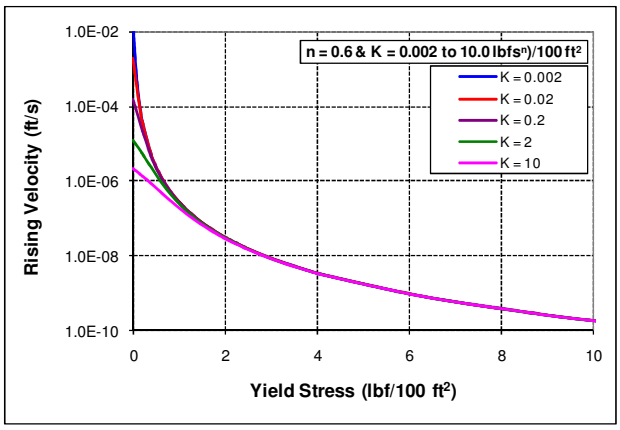

Fig. 2.7b Rising velocity vs. yield stress for horizontally oriented fiber in 8.33 ppg fluid with n=0.6

Fundamental principles of non-Newtonian fluids must be applied in explaining the results presented from **Figs. 2.7** to **2.8**. As the consistency index increases, the rising velocity decreases. According to Eqn. (2.6), the apparent viscosity of the fluid increases when the consistency index is increased. Fibers suspended in high viscosity fluid experience more resistance to their natural buoyant tendency and decreased rising velocity. Also apparent in these figures is the merging of floating velocities as the yield stress increases, regardless of the consistency component. This indicates that as the yield stress of the fluid increases, the consistency index term in Eqn. (2.6) becomes increasingly irrelevant in determining the Reynolds Number and rising velocity. It is apparent that the consistency index has marginal effect on the rising velocity of the fiber.

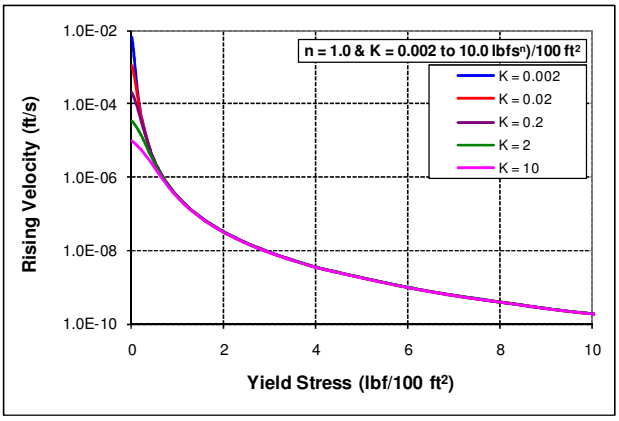

Fig. 2.8 Rising velocity vs. yield stress for horizontally oriented fiber in 8.33 ppg fluid with n=1.0

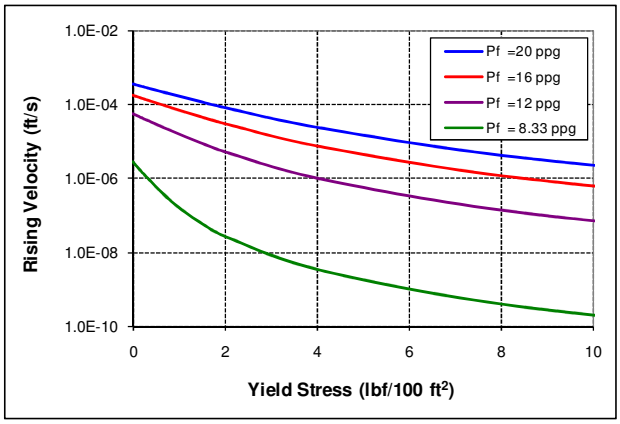

Fig. 2.9 Rising velocity vs. yield stress varying fluid density for horizontally oriented fiber particle (n = 0.3 and K = 2.1 lbfsⁿ/100 ft²)

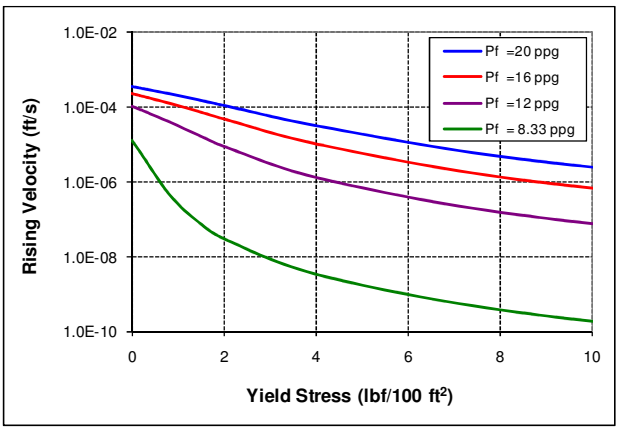

Fig. 2.10 Rising velocity vs. yield stress varying fluid density for horizontally oriented fiber particle (n = 0.6 and K = 2.1 lbfs^n/100 ft^2)

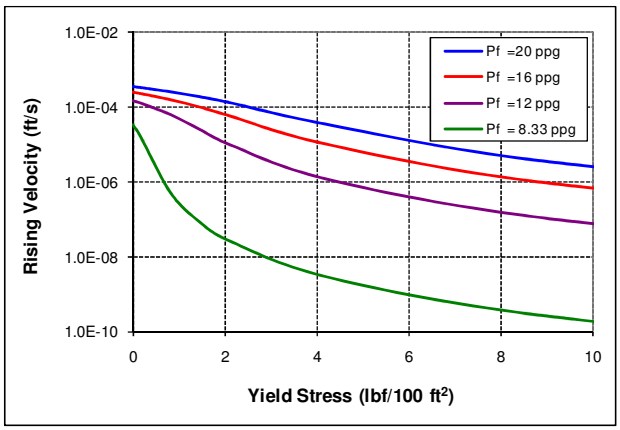

Fig. 2.11 Rising velocity vs. yield stress varying fluid density for horizontally oriented fiber particle (n = 1.0 and K = 2.1 lbfs^n/100 ft^2)

The yield stress and inherent "n" value of a specific fluid characterizes the degree to which the fluid behavior is non-Newtonian. Another trend worth investigating from **Figs. 2.7** to **2.8** is the relative closeness of the rising velocity plots for different fluids with respect to their fluid behavior indices. It is observed that as the fluid behavior index "n" increasingly deviates from unity, the spread of the rising velocity plots at low yield stress values tends to increase. A careful examination of Figs 2.7 and 2.8 reveals that the increase in the value of "n" substantially increases the rising velocity in fluids with high "K" values. Even though this is unusual observation, analysis of Eqn. (2.6) shows that, at low shear rates (i.e., shear rates less than 1 s^{-1}), decreasing the values of "n" results in increased apparent viscosity.

To explore the effect of yield stress on the upward motion of the fiber particles further, the rising velocity of a horizontal fiber was analyzed varying the yield stress, fluid density and flow behavior index. From **Figs. 2.9** to **2.11**, it can be seen that as the density of the fluid increased, the rising velocity increased. This was attributed to buoyancy; as the fluid became denser than the fiber, the fiber tended to ascend to the surface faster. This also correlates to the fact that the less dense fluids require smaller yield stresses to decrease the rising velocity or indefinitely suspend the fibers.

For a vertically oriented fiber particle, the rising velocity strictly relies on the fiber dimensions and density difference between the particles and the fluid. As shown from Eqn. (2.5), when the fiber particle orients itself in the direction of motion, the drag coefficient becomes independent of the Reynolds Number and rheological properties of the fluid. Due to the high aspect ratio and low drag coefficient of the fiber, the rising velocity of a vertically oriented fiber particle is very high. For a given fiber density, the rising velocity increases with the increase in mud density (**Fig. 2.12**). Due to the flexibility of the fiber and high hydraulic instability, vertical configuration is difficult to maintain; therefore, predicted values do not reflect the actual rising speeds. In real situations, fibers are not perfectly straight. They also orient

randomly under static conditions. Under dynamic conditions, their orientation to some extent is influenced by the flow field.

2.6 Conclusions

A mathematical model was developed to predict the rising velocity of fiber particles suspended in fluid. Sensitivity analysis was undertaken to examine the effects of fluid properties on the rising behavior of buoyant fiber particles. The following conclusions were made based on the results of the analysis:

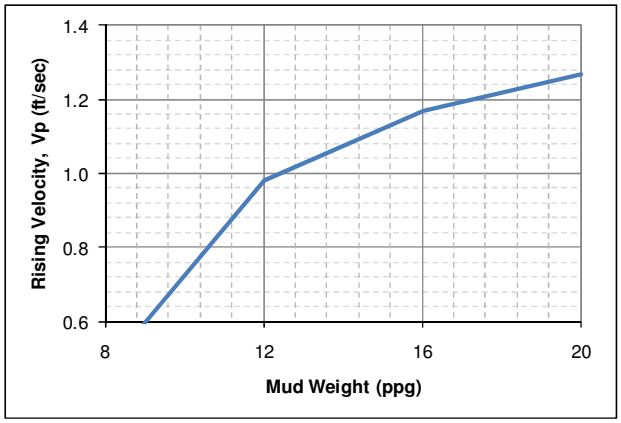

Fig. 2.12 Rising velocity vs. mud weight under dynamic conditions for vertically oriented fiber

- In highly shear-thinning fluids with no measurable yield stress, the rising velocity of the fiber was sensitive to the consistency index (K).
- As the flow behavior index "n" decreased, the fluid became increasingly shear-thinning. The decrease in "n" allowed for a greater influence of "K" on the rising velocity of the fiber for a given yield stress.
- Fluid density had a greater magnitude of influence on rising velocity at high yield stress values.
- The model developed for a vertically oriented fiber particle over-predicted the rising velocity, while the model formulated for a horizontal particle provided reasonable predictions.

Nomenclature

$A_{p,h}$ = projection area of horizontally oriented particle

$A_{p,v}$ = projection area of vertically oriented particle

$C_{D,h}$ = Drag coefficient for a horizontally oriented particle

$C_{D,v}$ = Drag coefficient for a vertically oriented particle

d = diameter of fiber particle

d_i = inner diameter of annulus

d_o = outer diameter of annulus

D_h = hydraulic diameter ($D_{outer} - D_{inner}$)

F_B = Buoyancy force

F_D = Drag force

g = gravitational acceleration

K = consistency index

L = length of the fiber

m = Mass of a fiber particle

n = flow behavior index

Re = Reynolds Number

R = particle radius (m)

$U_{p,h}$ = rising velocity of particle

$U_{p,h}$ = rising velocity of a horizontally oriented fiber particle

$U_{p,v}$ = rising velocity of a vertically oriented fiber particle

W = weight of a fiber particle

V_P = volume of a fiber particle

Greek Letters

$\dot{\gamma}$ = Shear rate

$\dot{\gamma}_{ave}$ = Average shear rate

$\dot{\gamma}_{primary}$ = Primary shear rate

$\dot{\gamma}_{secondary}$ = Secondary shear rate

$\dot{\gamma}_{total}$ = Total/overall shear rate

μ = fluid viscosity

μ_{app} = Apparent fluid viscosity

θ = Angle

ρ_f = Fluid density

ρ_p = Density of a particle

τ_y = yield stress

$\tau_{y,h}$ = critical yield stress for a horizontally oriented particle

$\tau_{y,h}$ = critical yield stress for a vertically oriented particle

References

Ahmed, R.M. and Takach, N.E. 2008. Fiber Sweeps for Hole Cleaning. Paper SPE 113746 presented at the Coiled Tubing and Well Intervention Conference and Exhibition, The Woodlands, Texas, 1-2 April. doi: 10.2118/113746.

Dedegil, M.Y. 1987. Drag Coefficient and Settling Velocity of Particles in Non-Newtonian Suspensions. *Journal of Fluids Engineering* **109** (3): 319-323.

Fan, L, Mao, Z., and Yang, C. 2004. Experiment on Settling of Slender Particles with Large Aspect Ratio and Correlation of the Drag Coefficient. *Ind. Eng. Chem. Res.* 43 (23): 7664-7670.

Herzhaft, B., Guazzelli, E., Mackaplow, M., & Shaqfeh, E. 1996. Experimental Investigation of a Sedimentation of a Dilute Fiber Suspension. *Phys. Rev. Lett.* **77** (2): 290-293Hoerner, S. F. (1965): Fluid-Dynamic Drag. Hoerner Fluid Dynamics, Brick Town, New Jersey.

Herzhaft, B. & Guazzelli, E. 1999. Experimental Study of Sedimentation of Dilute and Semi-Dilute Suspensions of Fibres. *J. Fluid Mech.* **384**: 133-158Metzner, A.B. and Reed, J.C. 1955. Flow of Non-Newtonian Fluids – Correlation of the Laminar, Transition, and Turbulent-flow Regions. *A.I.Ch.E. Journal* **1** (4): 434-440.

Koch, D. & Shaqfeh, E. 1989. The Instability of a Dispersion of Sedimenting Spheroids. *J. Fluid Mech.* **209**: 521-542.

Kuusela, E., Hofler, K., & Schwarzer, S. 2001. Computation of Particle Settling Speed and Orientation Distribution in Suspensions of Prolate Spheroids. *J. Eng. Math.* **41** (2-3): 221-235.

Kuusela, E. & Lahtinen, J. 2003. Collective Effects in Settling of Spheroids Under Steady-State Sedimentation. *Phys. Rev. Lett.* **90** (9): 1-4.

Liu, Y.J. & Joseph, D.D. 1993. Sedimentation of Particles in Polymer Solutions. *J. Fluid Mech.* **255**: 565-595.

Miska, S. 2007. Advanced Drilling, Course Material, University of Tulsa.

Perry, R.H. and Green, D.W. 1984. *Perry's Chemical Engineering Handbook. 6th Edition*. Japan: McGraw-Hill.

Qi, G.Q., Nathan, G.J., & Kelso, R.M. 2011. Aerodynamics of Long Aspect Ratio Fibrous Particles Under Settling. Paper AJTEC2011-44061 presented at the ASME/JSME 8th Thermal Engineering Joint Conference, Honolulu, Hawaii, USA, 13-17 March.

Scholz, M. 2006. *Wetland Systems to Control Urban Runoff.* Amsterdam, The Netherlands: Elsevier.

3. Experimental Study on Stability of Fiber Sweeps

The current investigation involved experimental studies of the stability of the fiber in various fluids at ambient and high temperatures. Several base fluids were chosen to simulate typical drilling and sweep fluids utilized in the field.

3.1 Scope

The purpose of this investigation was to determine how well various base fluids hold the fiber in suspension under ambient and high temperature conditions. The fibers had a specific gravity of approximately 0.9, which was less dense than the typical fluids in which they are suspended. Therefore, their natural tendency was to rise to the surface of the fluid and form fiber lumps. If the fibers rose while suspended in the fluid, the hole cleaning performance of the fluid diminished and fiber lumps might plug some of the downhole tools. As discussed previously, fiber sweep is mainly applied to reduce cuttings in the wellbore. The fluids utilized for the sweep operations must possess properties conducive to maintaining a uniform fiber concentration throughout the bulk volume without increasing the ECD.

3.2 Experimental Setup and Procedure

Stability experiments were conducted using 250 ml graduated cylinders. Stand mixers were used to prepare the test fluid. Test samples were placed in a laboratory oven to maintain high temperature conditions. All fluids were prepared using the same process, unless otherwise specified by the fluids' respective product literature or laboratory preparation guidelines. Multiple polymeric fluids were tested, as well as oil-based and synthetic-based muds. Each polymeric fluid was mixed at varying concentrations (**Table 3.1**). The process used for preparing the fluids followed these steps:

Table 3.1 Test matrix for stability experiments

	Base Fluid (lb / bbl)	Weighting Agent	Fiber Concentration (lb / bbl)
Water-Based Mud [WBM]	**Xanthan Gum [XG]** (0.35, 0.87, 1.75, 2.62)	- 8.33 ppg	0.00, 0.07, 0.14, 0.21, 0.28
	Polyanionic Cellulose [PAC] (0.35, 0.87, 1.75, 2.62)	- 8.33 ppg	0.00, 0.07, 0.14, 0.21, 0.28
	XG / PAC [1 : 1] (0.35, 0.87, 1.75, 2.62)	- 8.33 ppg	0.00, 0.07, 0.14, 0.21, 0.28
	Xanthan Gum [XG] (0.87, 1.75, 2.62)	*Barite 12.1 ppg*	0.00, 0.10, 0.20, 0.30, 0.40
	PHPA (0.17, 0.35, 0.52)	- 8.33 ppg	0.00, 0.07, 0.14, 0.21, 0.28
OBM	**Mineral Oil-Based**	*Barite 12.2 ppg*	0.00, 0.10, 0.20, 0.30, 0.40
SBM	**Internal-Olefin-Based**	*Barite 12.1 ppg*	0.00, 0.10, 0.20, 0.30, 0.40

Step 1. **Preparation of Base Fluid**: The fluid samples were initially mixed in bulk using a stand mixer to begin hydration of the polymer. Hot water was used to accelerate the hydration time. The polymeric fluids were then placed in a blender, mixed for 30 minutes, and left to sit for 24 hours to ensure complete hydration.

Step 2. **Preparation of Samples**: After sitting static for 24 hours, the fluids were re-agitated using a stand mixer to ensure uniformity of the samples. The bulk fluid was then divided into 300 milliliter (ml) individual samples based on fiber concentration (**Fig. 3.1**). Fiber was added to the

samples by volumetric concentration in increments of 0.07, 0.14, 0.21, and 0.28 lb/bbl for unweighted, water-based fluid (approx. 0.02, 0.04, 0.06, and 0.08 percent by weight for 8.33 lb/gal mud).

Step 3. **Heating the Samples**: The samples were placed in the oven for approximately 10 minutes to preheat the fluid. They were removed from the oven and re-agitated with the stand mixer to ensure fiber uniformity. The fluid samples were then immediately transferred to 250 ml graduated cylinders, and placed in the oven for one hour.

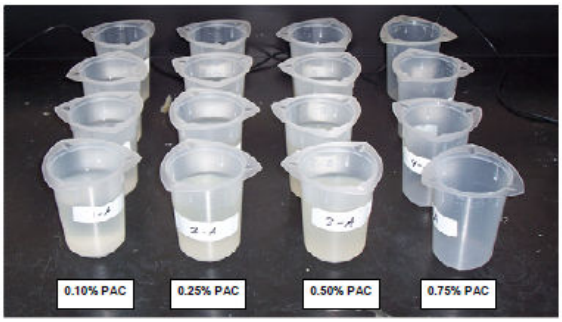

Fig. 3.1 Fluid samples

Step 4. **Extracting the Fiber**: The graduated cylinders were promptly removed from the oven after one hour. Under quiescent conditions, buoyant fiber particles move toward the surface of the sample increasing the fiber concentration in the upward direction. In unstable fluids, most of the fiber particles reach the surface of the sample (**Fig. 3.2**) after one hour. Using a 60 cubic centimeter (cc) syringe, the top 50 ml of the fluid (**Fig. 3.3**) were extracted from the cylinders and placed in separate beakers. Water and surfactant were mixed in with the fiber-fluid to aid in cleaning the fibers.

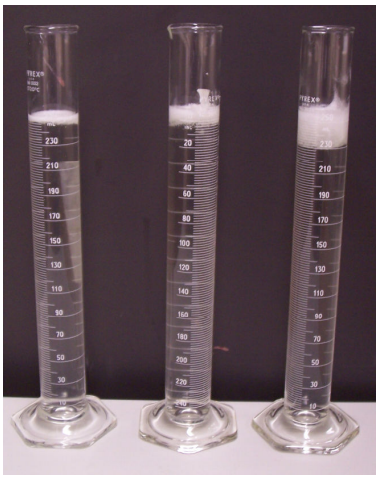

Fig. 3. 2 Unstable fluids after 1-hour test

Step 5. **Weighing the Fiber:** The fibers were separated from the fluid using a screen, and remixed with water and surfactant to further clean the fibers. The fibers were then screened again, dried in an oven, and weighed.

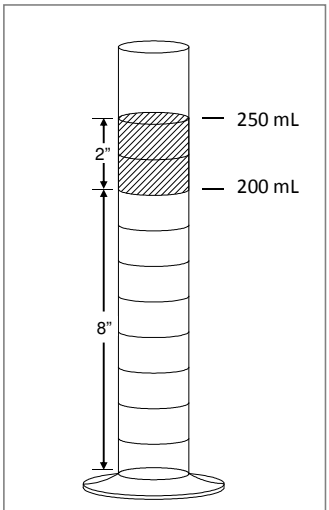

Fig. 3. 3 Graduated cylinder used for stability experiment

3.3 Results

The stability of the fiber-fluid suspension was tested for various fluids at varying polymer concentration. The results of high temperature (170ºF) stability experiments are summarized in **Table 3.2**. Depending on the fluid type, increasing the polymer concentration may or may not provide experimental and/or visual evidence of increasing stability. The purpose of this study was to predict the stability of the fiber sweeps in actual field conditions. Therefore, all experiments were run at high temperature to simulate wellbore conditions. For the sake of comparison, a few stability

experiments were also conducted at ambient temperature.

As discussed previously, the low density of the fiber resulted in a proclivity to rise to the surface. This was apparent when mixing a small amount of fiber with water, as the fiber almost immediately surfaced. With all other variables held constant, an increase in fluid density theoretically resulted in a shorter rising time. Experiments were conducted to test this hypothesis.

3.3.1 Effect of Base Fluid Rheology on Stability of Fiber Sweep

One goal of the research was to determine if the physical properties of the base fluids influence the stability of the suspension. The non-Newtonian fluids tested portrayed non-linear relationships between shear stress and shear rate. That is, they exhibited an apparent viscosity, a unique viscosity for an infinitely changing unique shear rate. For Newtonian fluids, the viscosity defines the material, since the shear stress or shear rate can be determined at any point if the viscosity is known. However, the apparent viscosity cannot define the fluid because it is ever changing with the flow. Nevertheless, the apparent viscosity provides a much needed approximate numerical comparison between the fluids, as well as a basis for understanding the mechanisms that provide for a stable fiber-fluid suspension. It is also important to note that these samples were not subjected to any shearing motion during the stability portion of the experiment. This was a static test, and the only shear present was exerted by the fiber itself as it moves upward in the fluid. The polymers and fluids tested were pseudo plastic, and exhibited shear-thinning behavior. In other words, the apparent viscosity decreased with increasing shear rate. Relating this to practical applications, as the fluid circulates through the annulus, it was subjected to varying shear rate. As the apparent viscosity decreased in response to an increase in shear rate, the ability of the fluid to maintain stability suffered. For this phase of the investigation, this characteristic was not included in the analysis.

Table 3.2 One-hour stability of test fluids

Polymer	Stable	Unstable
0.10% XG		X
0.25% XG	X	
0.50% XG	X	
0.75% XG	X	
0.10% PAC		X
0.25% PAC		X
0.50% PAC		X
0.75% PAC		X
1.20% PAC		X
0.10% XG+PAC		X
0.25% XG+PAC		X
0.50% XG+PAC	X	
0.75% XG+PAC	X	
0.25% XG+Barite (12 ppg)	X	
0.50% XG+Barite (12 ppg)	X	
0.75% XG+Barite (12 ppg)	X	
0.25% XG+Barite (16 ppg)	X	
0.50% XG+Barite (16 ppg)	X	
0.75% XG+Barite (16 ppg)	X	
0.05% PHPA		X
0.10% PHPA		X
0.15% PHPA	X	
OBM (8.1 ppg)	X	
OBM (12.2 ppg)	X	
SBM (7.9 ppg)	X	
SBM (12.1 ppg)	X	

Multiple stability experiments were conducted at high temperature and a few were conducted at ambient temperature. **Figures 3.4 to 3.14** present the test results along with model predictions. The results are

presented in terms of final fiber concentration of the top layer (i.e., the top 50 ml of the 250 ml graduated cylinder) as a function of initial fiber concentration. The plots show stable and unstable fluid lines. The unstable fluid line illustrates the maximum fiber concentration that would occur in the top layer if all the fiber particles migrate into this layer. The stable line shows the initial fiber concentration in the top layer that does not change with time because of full stability. Results complement the rheological analyses of these fluids. The fluids that are believed to naturally possess or those that have been designed to have yield stress generally showed better performance. Xanthan gum (XG), a very common drilling fluid viscosifier, also used in the food industry due to its yield properties, showed anticipated results (**Fig. 3.4a**). All except the thinnest fluid (0.10 percent XG) were able to show complete stability. To further test the stability of Xanthan gum (XCD) based fluids, the test duration was extended to 12 hours (**Figs. 3.10** and **3.11**). At high temperature, the two thinner fluids showed unstable behavior, but the thicker fluids were able to retain their yield stress and keep the fibers in suspension. At ambient temperature, there was no visual or experimental conclusion to show that the fiber had even begun to rise within the fluid.

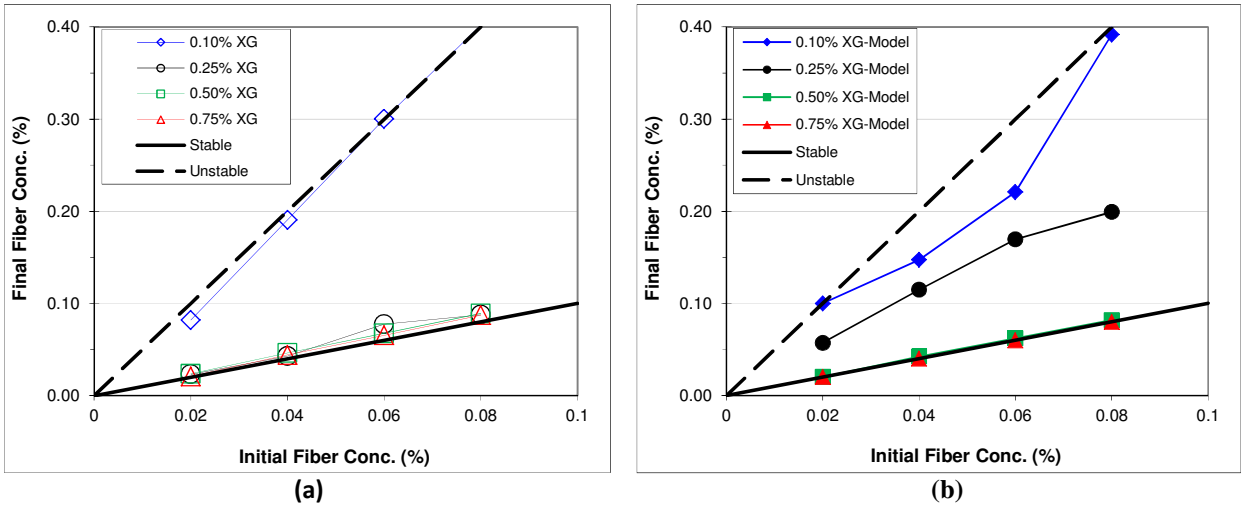

Fig. 3.4 One-hour stabilities of XG based fiber sweep at 170°F: a) lab experiments; and b) mathematical model

The polyanionic cellulose (PAC) polymeric fluid showed no stability (**Fig. 3.5a**). PAC is typically used as a shale inhibitor - not for its cuttings carrying capacity or for sweeps. However, the solution remains clear when mixed with water, and is a good tool for observing the fibers in suspension. In an attempt to determine if the polyanionic cellulose (Polypac R) fluid had any potential as a fiber suspension fluid at high temperature, the experiment time was shortened to 30 minutes (**Fig. 3.13**). In this short amount of test duration, the fiber in the thicker fluid had not yet migrated to the surface, while the thinner fluids once again showed no stability. As per the experimental results, the PAC fluid mixed at 0.25 percent w/w showed unexpected stability. Upon visual inspection, the fiber appeared to have grouped in the middle of the cylinder, preventing the majority of the fiber from rising to the top part of the cylinder. The

hydrodynamic and mechanical effects between the container wall and the rising fibers caused the formation of a fiber plug (lump) that did not move. This bridging created a plug for the lower fibers, which in turn became entangled. This phenomenon persisted under quiescent condition for the length of the experiment and subsequent fiber sample removal. After moving the cylinder with the fiber-fluid, the bridging behavior was overcome, and the fiber-plug rose to the surface in a matter of minutes.

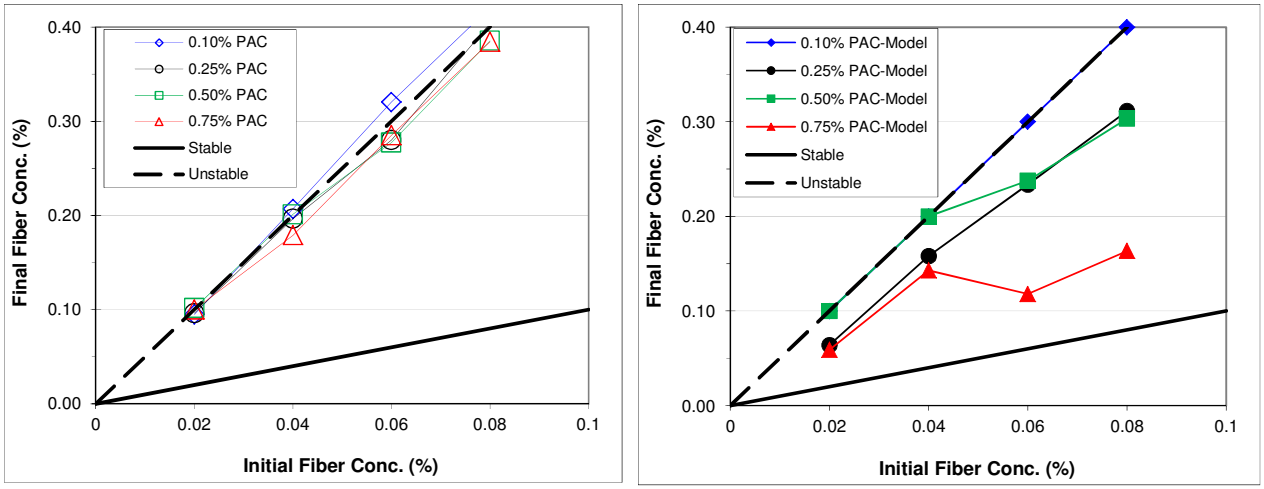

Fig. 3.5 One-hour stabilities of PAC based fiber sweeps at 170°F: a) lab experiments; and b) mathematical model

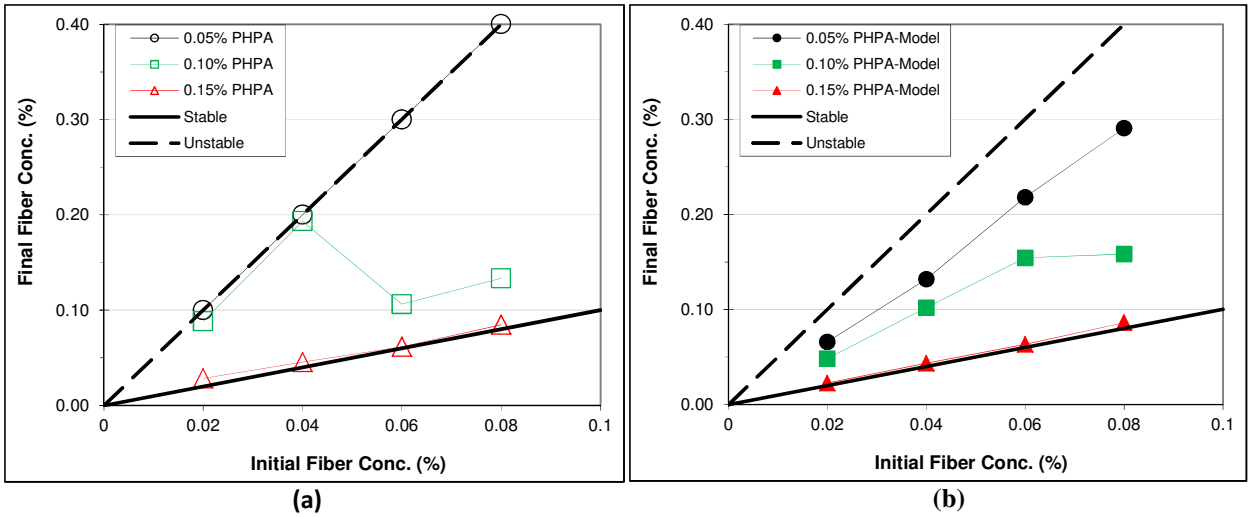

Fig. 3.6 One-hour stabilities of PHPA based fiber sweeps at 170°F: a) lab experiments; and b) mathematical model

Another clear fluid tested during the experiments was Partially-Hydrolyzed Polyacrylamide (PHPA), which is often utilized as a shale stabilizer in drilling applications. Following the experimental procedure and mixing at concentrations commonly used in the field, the thickest fluid (0.15 percent PHPA) showed stable behavior (**Fig. 3.6a**), while the thin fluid (0.05 percent PHPA) became unstable. The intermediate viscosity fluid (0.10 percent PHPA) was essentially unstable. At high fiber concentrations, the

experimental results showed stable behavior, but this is probably attributable to the formation of fiber plug (i.e., bridging). In an effort to control the stability of the polymeric fluids, XG and PAC were mixed at a one-to-one ratio using the same total polymer concentrations as previous tests. (Fig. 3.7a). Unfortunately, the addition of the XG resulted in an opaque fluid, and visual clues to the mixed fluid's stability were impossible. The stability experiment results showed the two thinner fluids to be unstable, while the two thicker fluids were able to completely hold the fiber in uniform concentration.

Drilling fluids are usually weighted in order to control formation pressure and support the borehole wall. As the magnitude of difference in specific gravity between the fiber and fluid widens as the fluid density increases, the fiber is pushed upwards with greater buoyancy force**. Figs. 3.8** and **3.9** depict the results of the weighted fluid stability experiments. Despite the increased buoyancy force acting on the fiber particle, the experiments showed that the yield stress of the XG fluid prevented the particle from rising. The weighted and unweighted oil-based mud (OBM) and synthetic-based mud (SBM) demonstrated similar stability behavior (**Fig. 3.9**). In these two fluid systems, increasing the density by the addition of barite had no detrimental effect on the stability of the suspension. The fluids were formulated to provide properties advantageous to drilling applications. They exhibited relatively low shear stress but had sufficient yield stress to prevent the fibers from rising.

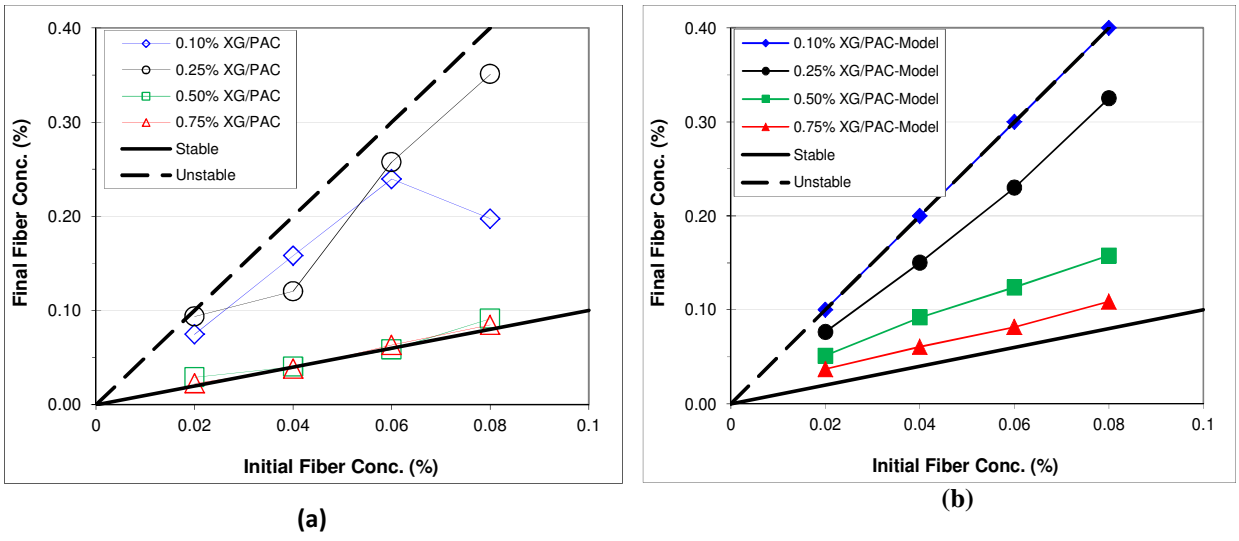

Fig. 3.7 One-hour stabilities of XG/PAC based fiber sweeps at 170°F: a) lab experiments; and b) mathematical model

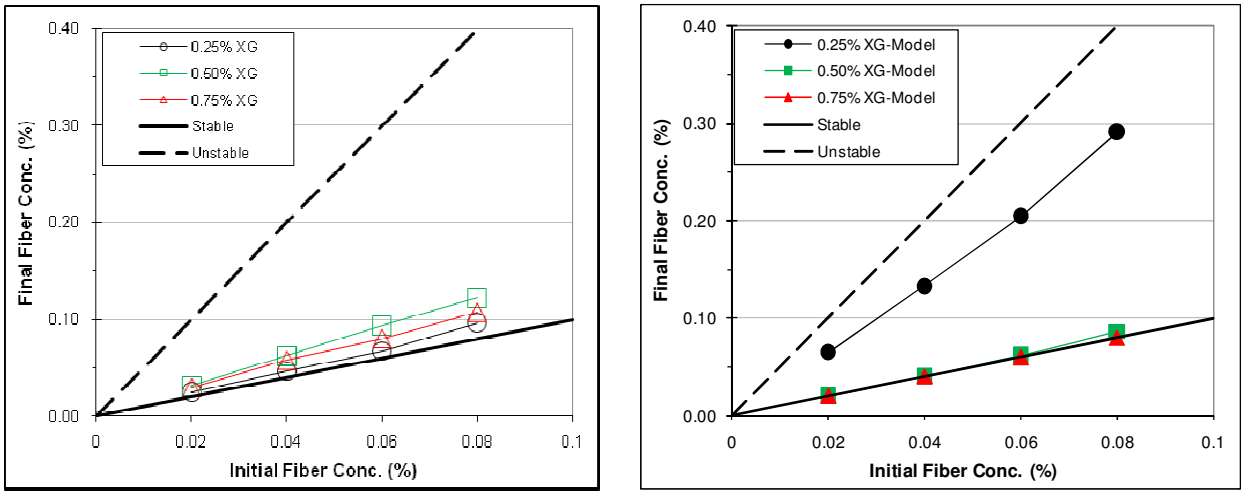

Fig. 3.8 One-hour stabilities of XG based weighted (12 ppg) fiber sweeps at 170°F: a) lab experiments; and b) mathematical model

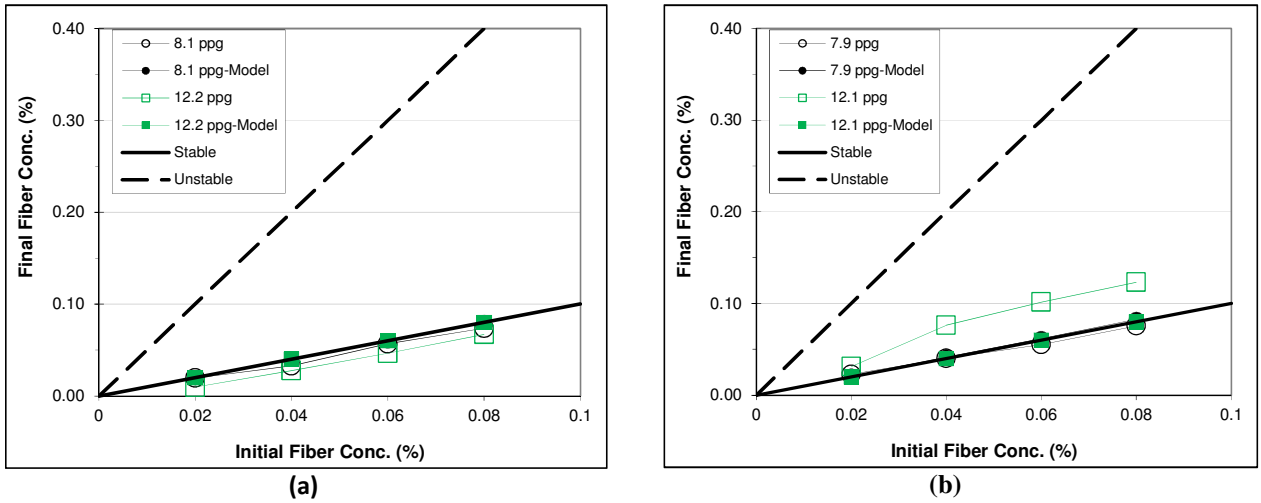

Fig. 3.9 Measured and predicted one-hour stability of oil-based fluids at 170°F: a) OBM; and b) SBM

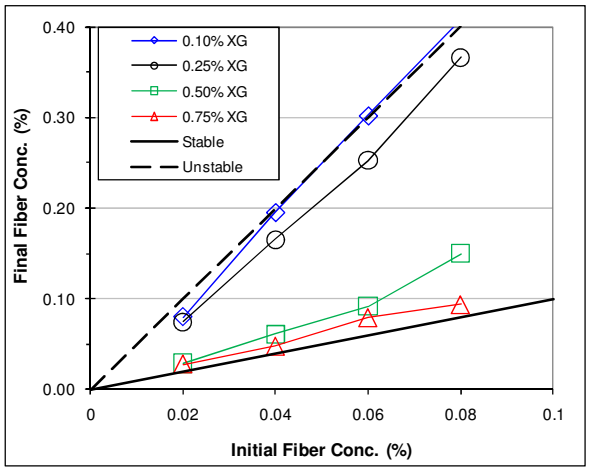

Fig. 3.10 Twelve-hour stabilities of XG based fluids at 170°F

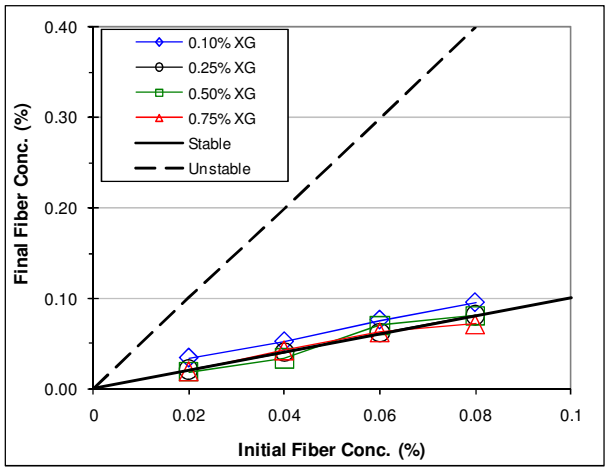

Fig. 3.11 Twelve-hour stabilities of XG based fluids at 72°F

Intuitively, the magnitude of the fluid's resistance to deformation or viscosity should provide a good indication of its internal ability to resist flow. Therefore, an increase in a fluid's viscosity would result in an increase in the ability to hold particles in suspension. In relation to this research, an increase in polymer concentration would result in higher viscosity, which in turn would yield a more stable fiber suspension. Visual observation of the fluids while mixing could also provide insight into the probable stability. The rheological study on fibrous fluids that was undertaken previously was reconciled with the stability experiment results to compare the apparent viscosities of the stable and unstable fluids (**Figs. 3.14a** and **3.14b**). Figure 3.14a shows a few low viscosity fluids, some of which were unstable. This data contradicts the original hypothesis that the fluid's viscosity or rheological properties would determine its ability to maintain stability. Easily apparent is the viscosity profile of the 1.20 percent PAC fluid, overall the most viscous fluid present in the figure. Despite its relatively high viscosity, this fluid was unstable (**Fig. 3.14a**). In addition, present in this figure are three stable fluids (0.25 percent XG, 0.50 percent XG/PAC, and 0.15 percent PHPA). It is important to note that these fluids exhibited lower apparent viscosity at low shear rate than the 1.20 percent PAC fluid. The 0.25 percent XG fluid even exhibited lower viscosity than the 0.75 percent PAC fluid, which was also unstable.

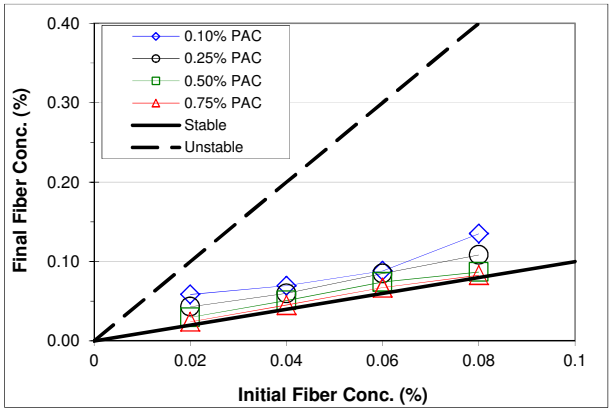

Fig. 3.12 One-hour stabilities of PAC based fluids at 72°F

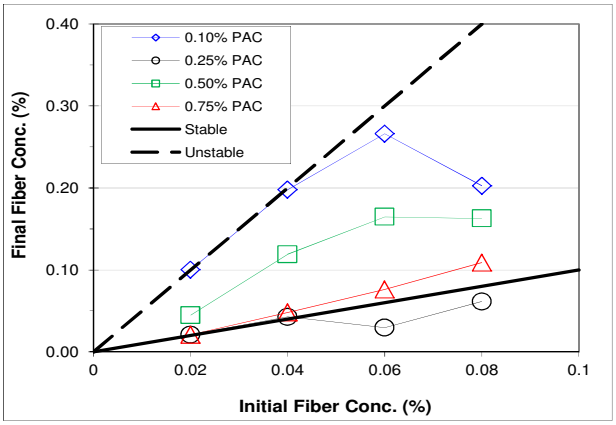

Fig. 3.13 Half-hour stabilities of PAC based fluids at 170°F

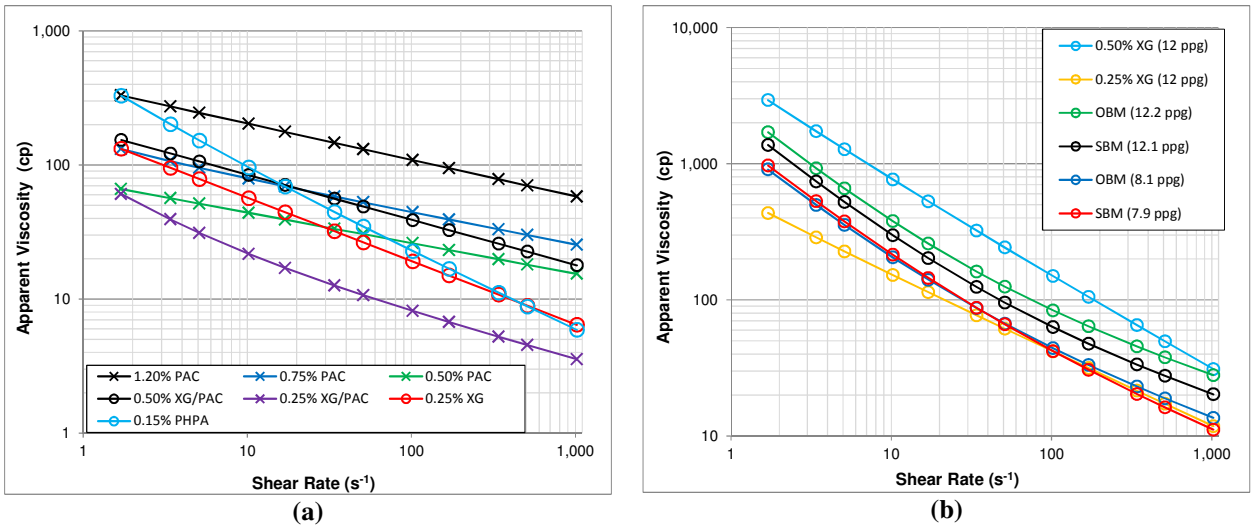

Fig. 3.14 Apparent viscosity vs. shear rate of based fluids at 170°F: a) low-viscosity fluids; and b) high-viscosity fluids

In general, XG based fluids showed better stability than other tested polymeric fluids. Xanthan gum polymer may have structure than can easily tangle with the fiber particles. Figure 3.14b depicts various stable high-viscosity fluids that were tested. The advantages of the oil-based and synthetic-based mud become apparent, since they form stable fiber sweeps. Oil-based muds are invert-emulsion. With dispersed phase (i.e., water phase) ranging from 20 to 30 percent, they exhibit strong structure that can hinder the movement of fiber particles. Therefore, even though rheological properties play great role in maintaining the fiber in suspension, other properties of the fluid such as the type of polymer or the presence of fluid structure may have some influence on the stability of fibrous fluid.

3.3.2 Effect of Temperature on Stability of Fiber Sweep

As stated previously, most of the experiments were carried out at 170°F, recreating the wellbore environment to the operational extent of the laboratory equipment. A few experiments (**Figs. 3.11** and **3.12**) were conducted at ambient temperature (72°F) to establish a relationship between temperature and stability of fiber suspensions. As expected, the suspensions were almost stable under ambient conditions. In contrast, **Figs. 3.10** and **3.5a** show the instabilities of thin fluids at high temperature (170°F). This confirms that the increase in temperature adversely affects the rheological properties of the fluids. However, this influence declines as the fluids becomes more viscous and increasingly non-Newtonian in nature.

Xanthan gum-based fluids were stable even under high temperature conditions. To observe instability, the test duration was extended to 12 hours. Then, thin fluids were able to show instability. When comparing **Fig. 3.12** with Fig. **3.5a**, the effect of temperature on the rheological properties of the PAC

fluid becomes apparent. While the ambient temperature experiments were able to show favorable results, increasing the temperature had adverse effects.

3.3.3 Comparison of Model Predictions with Experimental Results

The rising velocity model presented in Section 2 was developed to predict the stability of the fiber suspension or determine fluid properties necessary to prevent the separation of fiber particles. These models took into account various forces acting on each individual particle while suspended in the fluid, such as the buoyancy force created by the difference between fiber and fluid density, and the gravitational forced exerted on the fiber particle. The model was formulated to predict rising velocities for particles oriented horizontal and vertical. This was done to simulate the two extreme cases of particle motion within the fluid. The rheological parameters of the fluids obtained from viscometeric measurements were inputs into both models to compare model predictions with the actual experimental measurements. As the tested fluids exhibit non-Newtonian behavior, the rising velocity of the fiber particles becomes a function of rheological parameters of the fluid. The Yield Power Law (YPL) model is the most accurate constitutive equation to describe the majority of drilling fluids currently used in the industry. From the rheological measurements, the parameters of the test fluids were determined using regression analysis and used in the models. By determining the distance the fiber particles rose in one hour and the amount of fiber that entered into the top layer in that period, we were able to estimate the final concentrations of the top layer. Model predictions shown from **Figs. 3.4** to **3.9** were obtained using the horizontal orientation model. These results compared favorably with the test results. Predominately, the predictions were consistent with the measurements. However, in some cases, discrepancies were substantial. For instance, PAC based fluids did not show the ability to hold the fiber in suspension, but the model predictions for highly viscous fluid (0.75 percent PAC) showed some form of intermediate stability at high fiber concentrations.

The predictions of the vertical orientation model were also compared with measurements, but the results were very dissimilar. The model predicted all fluids to be unstable. This contradicted the experimental results, which demonstrated many of the fluids tested to be stable. When comparing the two mathematical models, the dimensional terms differed. For both models, the area projected to the fluid flow depended on the orientation of the fiber. If the fiber was oriented perpendicularly, the rectangular profile variables (length x diameter = 1.0×10^{-6} m^2) were the governing dimensions, and the vertical orientation profile was the circular end area ($\frac{1}{4}\pi d^2 = 7.85\times10^{-9}$ m^2). However, this only partially explained the difference. The drag coefficient (C_D) was also present in both equations and was inversely proportional to rising velocity because it counteracts the buoyancy force.

For a vertically oriented particle, drag force resisting the rising fiber is exclusively related to the fiber aspect ratio (Hoerner 1965) and independent of the fluid properties. Conversely, for a horizontally oriented particle, the drag force is implicitly related to the Reynolds Number (Perry 1984). The rather large aspect ratio in comparison to the rectangular projected area and fluid property dependency resulted in a vertically oriented particle rising velocity anywhere from three to five orders of magnitude greater than that for horizontally oriented particles.

Fluid density is one of the controllable model parameters that has a marked influence on the stability fiber sweep. The equation used to determine the rising velocity is a function of the difference between fluid density and particle density. Mathematically, the rising velocity increases as the difference between the two densities increases. In theory, an increasingly dense fluid results in a fiber moving upward instantaneously to the surface. However, the increased viscosity associated with weighted fluid hinders the barite particles that tend to settle in the fluid under static conditions. For instance, the model prediction for the stability of the weighted XG based fluids (**Fig. 3.8b**) shows both favorable and unfavorable results, while the experimental results indicated stable fluids with a slight departure from complete uniformity for the two thicker fluids. With its current formulation, the model considers a single particle rising in the fluid. It does not account for the hindering effect of barite particles. This model will be improved in the next phase of the project.

The oil-based and synthetic-based muds showed (**Fig. 3.9**) remarkable stability, both experimentally and mathematically. After performing the rheological and regression analyses, the weighted and unweighted fluids for both muds exhibited higher yield stress. All fiber-fluid combinations tested showed stable behavior. This was reinforced with the mathematical model predictions of similar results.

3.4 Conclusions

This study was undertaken to investigate the stability of fiber sweeps at ambient and high temperature conditions. Experiments were conducted using different base fluids (water-based and oil-based fluids) with varying fiber concentrations. Fibers were extracted from the samples after the test and weighed to determine the final fiber concentration in the top layer. This data was used to determine if the fiber rose while in the fluid sample, or if uniformity persisted throughout the length of the experiment. These measurements were compared with stability predictions obtained from the mathematical model. After analyzing and comparing all the data to date, the following inferences were made:

- Horizontally oriented particle model predictions were in general concurrence with the experimental data, and reasonable real-time application performance could be predicted using the

model. The vertically oriented particle model overestimated rising velocity of fibers in all fluids tested which did not reflect experimental results, and would not provide accurate predictions.

- Despite the dominant effect of fluid rheology on the stability of fiber sweeps, other properties of the fluid, such as the type of polymer, the presence of fluid structure, or hindering effect of other particles, considerably influenced stability.

- Selecting the type of polymer used for drilling sweep applications was critical in designing fluids that stable under downhole conditions.

- Oil-based and synthetic-based fluids had high fiber stability. This could be attributed to the high yield stress that they exhibited and the presence of emulsion structure in the two-phase system.

Nomenclature

U_p = Particle floating velocity (m/sec)

d = Particle diameter (m)

D_h = Hydraulic diameter ($D_{outer} - D_{inner}$)

ECD = Equivalent circulating density

K = Consistency index

n = Fluid behavior index

OBM = Oil-based mud

PAC = Polyanionic cellulose

PHPA = Partially Hydrolyzed Polyacrylamide

SBM = Synthetic-based mud

XG = Xanthan Gum

Greek Letters

μ_{app} = apparent viscosity

τ_y = yield stress

References

Hoerner, S. F. (1965): Fluid-Dynamic Drag. Hoerner Fluid Dynamics, Brick Town, New Jersey.

Perry, R.H. and Green, D.W. 1984. *Perry's Chemical Engineering Handbook. 6th Edition*. Japan: McGraw-Hill.

4. Rheological Properties of Fiber Sweeps

Fiber-containing sweeps (fiber sweeps) are effective tools for wellbore cleaning in horizontal wells. It has been shown that adding fiber to traditional sweeps can result in an increase in cuttings removal and reduction in cuttings bed thickness, which reduces the amount of torque and drag in horizontal wells. Despite some reported successes in the field and favorable research results, the fluid and fiber properties that define and influence fiber sweep rheology are not fully understood.

The hole-cleaning capabilities of weighted sweeps, high and low viscosity sweeps, and tandem sweeps are well documented. However, these conventional sweep methods often result in an increase in equivalent circulating density (ECD). Fiber-containing sweeps, which have promise to overcome this ECD disadvantage, are becoming popular alternatives. However, little detail is known about the flow and cuttings-carrying properties of these slurries.

This article presents the rheological measurements carried out on fiber-containing sweep fluids. Tests were conducted using various unweighted and weighted water-based, mineral oil-based and internal olefin-based drilling fluids with concentrations of a monofilament synthetic fiber ranging up to 0.4 lb/bbl. The rheology was measured at ambient and 170ºF. The study shows that fiber concentration has minimal effect on viscosity, indicating a negligible increase in ECD while providing improved sweep efficiency. These results can be useful for formulating sweep fluids utilized in deepwater applications.

4.1 Introduction

Poor hole cleaning can lead to an increase in non-productive time and costly drilling problems such as stuck pipe, premature bit wear, slow rate of penetration, formation fracturing, and high torque and drag (Ahmed and Takach 2008). A number of field-tested techniques have been introduced over the years to improve hole cleaning, cuttings transport, and prevent the formation of cuttings beds in the wellbore. Previous studies indicate that cuttings transport in directional wells is dependent on fluid rheology, wellbore inclination angle, rotary speed of the drillpipe, flow rate, wellbore geometry, and other drilling parameters (Valluri et al. 2006). Considering these factors, the most economical and easily employed procedures involve adding viscosifiers and weighting agents to the drilling fluid to increase the ability of the fluid to transport cuttings to the surface. In addition, increasing the flow rate has the ability to re-suspend cuttings, with the maximum pump rate generally provided the best hole cleaning conditions. However, pressure losses and the equivalent circulating density (ECD) must be considered when increasing the flow rate. Experience shows that optimal hole cleaning occurs with turbulent flow, but turbulent flow can erode the filter cake and borewall, as well as increase ECD. Therefore, using laminar flow at maximum flow rate, paired with fiber sweeps and mechanical agitation such as drillstring rotation

and reciprocation, is usually the preferred method for removing cuttings beds (Cameron et al. 2003). However, these methods often only slow the formation and buildup of cuttings beds and are not very effective at removing cuttings beds. In response to these problems, drilling fluid sweeps are utilized. The sweeps remove cuttings that cannot be transported to the surface during normal fluid circulation while drilling and provide additional vertical lift to the cuttings. Sweeps can be performed in all well inclinations from vertical to horizontal, as required by wellbore conditions. In deviated, highly inclined, and extended reach drilling (ERD) wells, sweeps are an essential tool to facilitate wellbore cleaning.

In highly deviated wellbores and especially ERD wells, the cuttings transport performance of a drilling fluid generally diminishes. Some highly shear-thinning fluids, such as are used in milling operations, are an exception; even in horizontal wells, the strong viscous coupling between the rotating drill string and fluid can bring up even metal shavings and fist-sized rock. In highly deviated wellbores, the fluid velocity has little vertical component, reducing the ability of the drilling fluid to suspend and carry the cuttings. The increased wellbore length results in higher ECD that limits the flow rate and provides more opportunity for the cuttings to form a bed on the low side of the wellbore. In addition, the drillpipe rests on the low side of the wellbore in horizontal sections, forcing the majority of the fluid to the high side and further encouraging the formation of cuttings beds. Inadequate hole cleaning is common with ERD wells.

Sweeps containing traditional fibrous lost circulation materials (LCM) have been shown to decrease cuttings and silt beds, as well as reduce torque and drag and improve the rate of penetration (Cameron et al. 2003). These materials generally refer to organic fibers or plant-derived abrasive substances. Experimental studies (Ahmed and Takach 2008) and field applications (Bulgachev and Pouget 2006) have shown that specially designed sweeps containing synthetic monofilament fibers show improved hole cleaning efficiency over comparable non-fiber sweeps. While these and other cases demonstrate favorable results when utilizing fiber sweeps, the method for designing these sweeps is still not fully developed. Visually observing shaker screens to determine whether cuttings transport rate is constant or changing and plotting these trends versus the sweep volume and fiber concentration are the predominant methods of monitoring hole-cleaning efficiency.

When fully dispersed in the sweep fluid, fibers form a stable network structure that tends to support cuttings due to fiber-fiber and fiber-fluid interactions. The fiber-fiber interactions can be by direct mechanical contact and/or hydrodynamic interference among fiber particles. Mechanical contact among fibers improves the solids-carrying capacity of the fluid (Ahmed and Takach 2008). Mechanical contact between the fibers and cuttings beds aid in re-suspending cuttings deposited on the low-side of the wellbore. As the fibers flow through the annulus, mechanical stresses develop between the settled cuttings

and the fibers. These mechanical stresses result in a frictional force that helps to re-suspend the cuttings while the fiber networks carry the solids to the surface. Also aiding in the solids transport is the fiber-fiber interaction that enables the fiber network to move as a single phase This fiber network can separate from the fluid phase. Therefore, at the surface of the cuttings bed the fiber may have a higher velocity than the fluid phase, which is typically very low. These fast moving fibers can therefore transfer more momentum to the deposited solids, overcoming the static frictional forces and initiating movement.

This study was undertaken to determine the effect of a fiber on drilling fluid rheology. This monofilament synthetic material is used in hole-cleaning sweeps throughout the industry. Tests were conducted of various unweighted and weighted water-based, mineral oil-based and internal olefin-based drilling fluids with a range of fiber concentrations. The rheology was measured at ambient and 170°F. The results are expected to be useful for formulating sweep fluids in deviated and deepwater applications.

4.2 Literature Review

Hole-cleaning sweeps may be classified as high-viscosity; high-density; low-viscosity; combinations; and tandem (Hemphill and Rojas 2002). Factors that govern sweep selection include hole angle, fluid density, lithology, cuttings diameter, drill pipe rotation, and fracture gradient (Power et al. 2000). In deepwater and deviated wells, the drilling window between the fracture gradient and pore pressure generally narrows with increasing depth and hole angle, respectively, reducing the available options for hole cleaning sweeps. In addition, long horizontal departures are common in order to reduce the environmental impact. This, combined with the marginal operating window, necessitates a strict adherence to a manageable ECD. To manage the ECD properly, drilling fluid rheology must be optimized for the conditions, and the wellbore must be as free of cuttings as possible.

Surface torque and the ability of the rig to overcome it is an important factor when deciding the feasibility of drilling a well, especially an extended read drilling (ERD) well. The friction generated between the wellbore and the drillstring in long horizontal sections creates the surface torque. Hole tortuosity in ERD wells further reduces the ability of the drilling fluid to adequately carry cuttings to the surface. Leaving cuttings behind adds resistance to the drillstring, which proportionately increases wellbore friction and surface torque (Maehs et al. 2010). The incorporation of fibrous lost circulation material (LCM) in the drilling fluid proved a major factor in reducing torque 25 percent on ultra-extended reach wells (Cameron 2001). In drilling an extended reach well in Abu Dhabi, the incorporation of fibrous hole cleaning sweeps resulted in a dramatic decrease in torque and drag and increased the rate of cuttings return to the surface by 50 percent (Cameron et al. 2003). While drilling Wytch Farm extended reach wells, it was observed that the addition of fibrous LCM affected the measurable torque and drag (Robertson et al. 2005). In this

case, the LCM was added both to the whole mud system and supplemented with sweeps. It is thought that the sweeps initiated the decrease in torque, and the LCM in the drilling fluid maintained the reduced torque levels. The mechanism by which the fibrous LCM decreased the torque was believed to be better hole cleaning and increased lubricity. The manner in which these mechanisms developed and operated is not fully understood, but one explanation is that the fibers intertwined to form a mesh, which scoured the wellbore. The fibers could also have acted as little roller bearings, increasing the lubricity of the drillstring, further reducing torque (Robertson et al. 2005).

Flexible fibers in suspension form three-dimensional networks that exhibit shear strength and viscoelastic properties because of the mechanical entanglement. At higher concentrations, the fiber suspension is capable of supporting a load and transmitting shear stress through the entire flow regime (Swerin 1997). The mechanical entanglement of the fiber networks can actually hold particles in suspension, preventing or slowing their segregation. As such, fiber fluid suspensions have also been shown to be an effective transport mechanism for hydraulic fracturing proppant (Bivins et al. 2005). In fiber free fluids, settling proceeds according to Stokes' Law. However, in suspensions with fibers, Stokes' Law cannot be applied directly. The sedimentation process may be better characterized as hindered settling. Fibers interfere with particle settling, generating additional drag, and a distinct liquid-particle boundary does not develop. A slot test was conducted to evaluate the proppant transport capability and settling prevention property of the fiber. Proppant in the fiber slurry was stable, and all proppant remained in suspension during the test. Graphical data showed a decrease in settling velocity of greater than one order of magnitude, as compared to fluid with no fiber. Furthermore, under the test conditions it was determined that the minimum fluid viscosity to ensure adequate proppant transport was about 100 cp at 100 s^{-1} shear rate (Bivins et al. 2005).

The addition of fiber to a fluid also delays the onset of turbulent flow, thus reducing drag and maintaining the flow in the laminar regime (Gupta et al. 2002). When fibers are added to a shear flow, the fiber particles orient themselves in the direction of the deformation tensor. This realignment enhances the fluid's ability to resist amplification of disturbances. The critical Reynolds Number increases as well as the general stability of the fluid as the fiber volume fraction and aspect ratio increase (Gupta et al. 2002). It has also been shown that the presence of fiber or fiber flocs can reduce the intensity of turbulence and encourage plug flow (Xu and Aidun 2005). This property of fiber-laden fluids is beneficial for hole cleaning operations as higher pump rates may be used while keeping the fluid in laminar flow. Turbulent flow while beneficial for wellbore cleaning, can erode the filter cake, resulting in lost circulation or formation damage.

4.3 Fiber Fluid Rheology

Controlling the rheology of the drilling and sweep fluids is essential to maintain favorable wellbore hydraulics and hole cleaning efficiency. This is of utmost importance when drilling extended and ultra-extended reach wells in deepwater where the pressure window often requires a minimum overbalanced wellbore pressure condition. In such environments, the pressure and temperature ranges rise to levels that are difficult to emulate in laboratory experiments, making it difficult to predict the rheology of the fluids downhole precisely.

To predict the transport properties and performance of fiber fluid sweeps in downhole conditions, the basic rheology of the base fluid and suspension must be understood. The proposed formulations for such fiber sweeps will be most effective when the rheology has been accurately modeled and fine-tuned for specific wellbore eccentricities. To begin to grasp how the fluid behaves, the relationship between shear stress and shear rate must be known. This is denoted as the shear viscosity profile, which is an aspect of the rheology of a fluid that is thought to control laminar flows in pipes, annuli, and other geometries. The most common shear viscosity models used to characterize non-Newtonian drilling fluids include:

- Bingham-Plastic (BP)

$$\tau = YP + PV \cdot \gamma$$

- Power Law (PL)

$$\tau = K\gamma$$

- Yield Power Law (YPL)

$$\tau = \tau_y + K\gamma^n$$

where τ = shear stress at the wall, γ = shear rate, YP = yield point, PV = plastic viscosity, K = consistency index, n = fluid behavior index, and τ_y = yield stress. It will be noted that thixotropic effects like gel strength are not included in these treatments.

As cuttings carrying capacity is a desirable trait of drilling fluid, a measurable yield stress must be present to hold the cuttings in suspension. The classic viscosity model used for drilling fluids is the Bingham-Plastic or pseudoplastic model. Here the shear stress rises linearly with shear rate, with a slope given by PV. The intercept on the τ axis, YP, is often identified with the carrying capacity of the fluid. Most drilling fluids exhibit a non-linear shear stress-shear rate relationship, which is best described by the Yield Power Law model. The YPL model is useful in describing a wide range of polymer-based, oil-based, and

synthetic-based drilling fluids, from low shear rate to high shear rate. For fluids with yield stress (τ_y), such as the YPL fluid, a certain shear stress must be overcome before flow can initiate. Without yield stress, the fluid simply follows the Power Law (PL) model. The other two curve-fitting parameters describe the rheology of PL fluid. K is the viscosity of the fluid at a shear rate of 1.0 s^{-1}, therefore providing an effective description of fluid viscosity at low shear rates. The flow behavior index, "n", indicates the shear-thinning tendency of the fluid. In Newtonian fluids, where viscosity is constant, "n" is equal to one. Reducing "n" creates a fluid that is shear-thinning, which decreases the effective annular viscosity and flattens the annular velocity profile, increasing the overall hydraulic efficiency.

Recently, the viscosity profiles of synthetic-based drilling fluids were measured from 80°F to 280°F and from zero to 5000 psig (Demirdal et al. 2007). The study showed the rheology to be extremely sensitive to downhole conditions, with the yield stress and consistency index drastically changing with varying temperature and pressure. The overall trend was that these parameters decreased with increasing temperature, and increased with increasing pressure. The evaluation also showed that the Yield Power Law model continued to describe the shear stress-shear rate relationship at all pressure and temperature conditions. Another study developed a simulator to determine the cuttings transport efficiency of drilling fluid under high-temperature and high-pressure conditions (up to 200°F and 2,000 psi). The experimental trend showed that higher temperatures diminished the cleaning efficiency of the fluid (Yu et al. 2007). Recent experiments studied water-based drilling foam and the effect of temperature on the cuttings concentration in a horizontal wellbore (Zhu 2005). The results showed that cutting concentration in the annulus generally increased as the fluid temperature increased.

Previous studies (Demirdal et al. 2007; Yu et al. 2007) show that temperature significantly alters the viscosity of drilling fluid and ultimately influences the cuttings transport efficiency. As the rheological properties change, so too does the fluid's ability to exert viscous and drag forces on the cuttings and the fiber. As the fluid becomes thinner with elevated temperature, the amount of momentum transferred to the cuttings is diminished. The thin fluid also loses its ability to maintain a uniform fiber concentration while flowing in the annulus. This separation decreases the hole cleaning effect of the fiber.

In designing a fiber-fluid formulation for wellbore cleaning sweeps, certain rheological parameters give a good indication of how well the sweep will perform. The yield stress and yield point of the fluid represent the amount of force required to move the fluid. At the same time, if the fluid possesses adequate yield stress to prevent the natural buoyancy of the fiber, the fiber will not separate. The yield stress indicates how well the sweep will maintain uniformity when circulating up the annulus.

4.4 Experimental Investigations

The current investigation involves experimental studies of the rheology of fiber-containing sweep fluids. Several base fluids were chosen to simulate the various drilling and sweep fluids utilized in the field (**Table 4.1**). A specially processed 100 percent virgin synthetic monofilament fiber was supplied for this research (**Table 4.2**), and was mixed with the base fluids at varying concentrations.

Table 4.1 Test matrix of rotational viscometer measurements

	Base Fluid (lb / bbl)	Weighting Agent	Fiber Concentration (lb / bbl)
Water-Based Mud [WBM]	**XG** (0.35, 0.87, 1.75, 2.62)	None 8.33 ppg	0.00, 0.14, 0.28
	PAC (0.35, 0.87, 1.75, 2.62)	None 8.33 ppg	0.00, 0.14, 0.28
	XG / PAC [50%/50%] (0.35, 0.87, 1.75, 2.62)	None 8.33 ppg	0.00, 0.14, 0.28
	XG (0.87, 1.75, 2.62)	*Barite 12.1 ppg*	0.00, 0.20, 0.40
	PHPA (0.17, 0.35, 0.52)	None 8.33 ppg	0.00, 0.14, 0.28
OBM	**Mineral Oil-base** [VERSACLEAN® System]	*Barite 12.2 ppg*	0.00, 0.20, 0.40
SBM	**Internal-Olefin-base** [NOVAPLUS® System]	*Barite 12.1 ppg*	0.00, 0.20, 0.40

Table 4.2 Fiber properties

Material	=	Polypropylene
Spec. Grav.	=	0.91
Length	=	0.40 in (10 mm)
Diameter	=	0.004 in (100 μm)
Melting Point	=	325°F – 350°F

The water-based fluids included fluids prepared with xanthan gum (XCD) at two mud weights, polyanionic cellulose (Polypac R), xanthan gum (XG), partially hydrolyzed polyacrylamide (PHPA) and mixtures of XG and PAC. Formulations were prepared with a broad range of concentrations of these polymers. Also tested were weighted mineral oil-based and internal olefin-based drilling fluids.

4.4.1 Experimental Setup

The shear viscosity experiments were conducted using stand mixers (**Fig. 4.1**), rotational viscometers (Chandler 35 and Fann 35A, **Fig. 4.2**), thermocup, mud balance, and a laboratory oven. The Chandler 35 rotational viscometer has 12 speeds and was modified to include a 1/5 spring. The weaker spring allowed for more sensitive and accurate measurements in the low shear rate range and reported all dial readings at five times (5x) higher than actuality. Both viscometers were calibrated and tested using multiple fluids of varying viscosities to ensure that readings were comparable.

Fig. 4.1 Stand mixers

Fig. 4.2 Rotational viscometers

4.4.2 Test Procedure

The steps required to prepare the samples and record measurements are as follows:

Step 1. **Preparation of Base Fluid:** Bulk base fluid samples were prepared by mixing water, viscosifiers, and barite. Immediately after mixing, all water-based fluids were covered and left undisturbed for a minimum of 24 hours to ensure full hydration. The fluids were then re-agitated, and a uniform sample was obtained to determine the specific gravity using the mud balance.

Step 2. **Preparation of Samples:** After fluids were mixed and hydrated (if necessary), individual samples were weighed and organized according to the polymer and fiber concentration. Fiber was added to the samples at weight concentrations of 0.02, 0.04, 0.06, and 0.08 percent. For the unweighted water-based fluids, 0.08 percent corresponded to 0.28 lb/bbl fiber, whereas for the 12-ppg water-based and non-aqueous fluids it corresponded to 0.4 lb/bbl fiber.

Step 3. **Viscometer Measurements at Ambient Temperature:** After all samples were prepared, the rheologies of the base fluids were measured using two rotational viscometers (Chandler 35 and Fann 35A). If the viscosity of the fluid being measured exceeded the spring capacity of the Chandler 35, the less sensitive but larger range Fann 35A was utilized for the higher shear rate measurements.

Step 4. **Viscometer Measurements at High Temperature:** Samples were placed in an oven for heating. The oven was set at approximately 180°F, and samples were agitated every 15 minutes to ensure uniformity. Once a sample was heated to 170°F as confirmed by a mercury thermometer, the

sample was removed from the oven and mixed for 30 seconds using a stand mixer. This mixing time was deemed adequate to achieve uniform re-dispersion of the fibers. Immediately after mixing, a portion of the sample was poured into the thermocup. Using a mercury thermometer, the thermocup temperature was adjusted to achieve a constant fluid temperature of 170°F. The viscometer measurements were taken using the procedure described in Step 3.

4.5 Experimental Results

The shear stress of each fluid was measured from 1 rpm to 600 rpm at ambient and elevated temperature. When circulating through the annulus, most parts of the fiber sweep are in the plug flow regime. Therefore, the low shear rate range is more significant when analyzing and predicting the behavior of these fiber sweeps under downhole conditions. However, to provide a general understanding of fiber sweeps, **Figs. 4.3** to **4.8** show the results of the viscometer measurements for the entire shear rate range.

Experiments were conducted with four (4) increasing levels of fiber concentration (Step 2). For the majority of the fluids tested, the trends were consistent as fiber concentration increased. To reduce data clutter, only the intermediate (0.14 lb/bbl) and high (0.28 lb/bbl) fiber concentrations were included in the figures for the water-based drilling fluids.

4.5.1 Effect of Fiber Concentration

One goal of the research was to determine the effect that adding fiber and increasing the fiber concentration has on the rheology of the fluid. As it has been shown in previous studies (Ahmed and Takach 2008), adding fiber to fluid has an insignificant effect on the flow behavior of the fluid. According to field results and supporting theories stated previously, adding fiber to the fluid may actually improve the hole cleaning performance without affecting the rheological properties of the fluid. After analyzing the results of the viscometer experiments, we found that the fiber had no predictable influence on the fluid rheology. In most cases, the addition of fiber to the base fluid resulted in a slight increase in shear stress (**Figs. 4.4a, 4.5c, 4.7b**). Other times, the base fluid exhibited a higher shear stress than the fiber fluid (**Fig. 4.6c**). Despite these deviations from the base fluid, the magnitude of their departure from the baseline was relatively insignificant. Careful observation of these figures shows that at shear rates less than 10 s^{-1}, the shear stress values for the majority of the figures were almost identical (**Figs. 4.6c** and **4.7b**).

In another case, two similar polymeric fluids showed contradicting trends. The high-temperature, weighted fiber fluid mixed with 0.87 lb/bbl XG polymer (**Fig. 4.6a**) showed the most common characteristic, with the shear stress increasing with fiber concentration. This was apparent in the low shear rate range, but the fiber concentration lost influence in the higher shear rate range. Conversely, the

high-temperature, weighted fiber fluid mixed with 1.75 lb/bbl XG mud (**Fig. 4.6b**) indicated an opposing trend, with fiber concentration reducing shear stress throughout the shear rate range measured. Despite this peculiarity, the change in shear stress in the region of interest (low shear rate) was of little consequence. At the shear rate 51.09 s^{-1}, the difference in shear stress between the base fluid and 0.4 lb/bbl fiber fluid (**Fig. 4.6a**) was 15 percent.

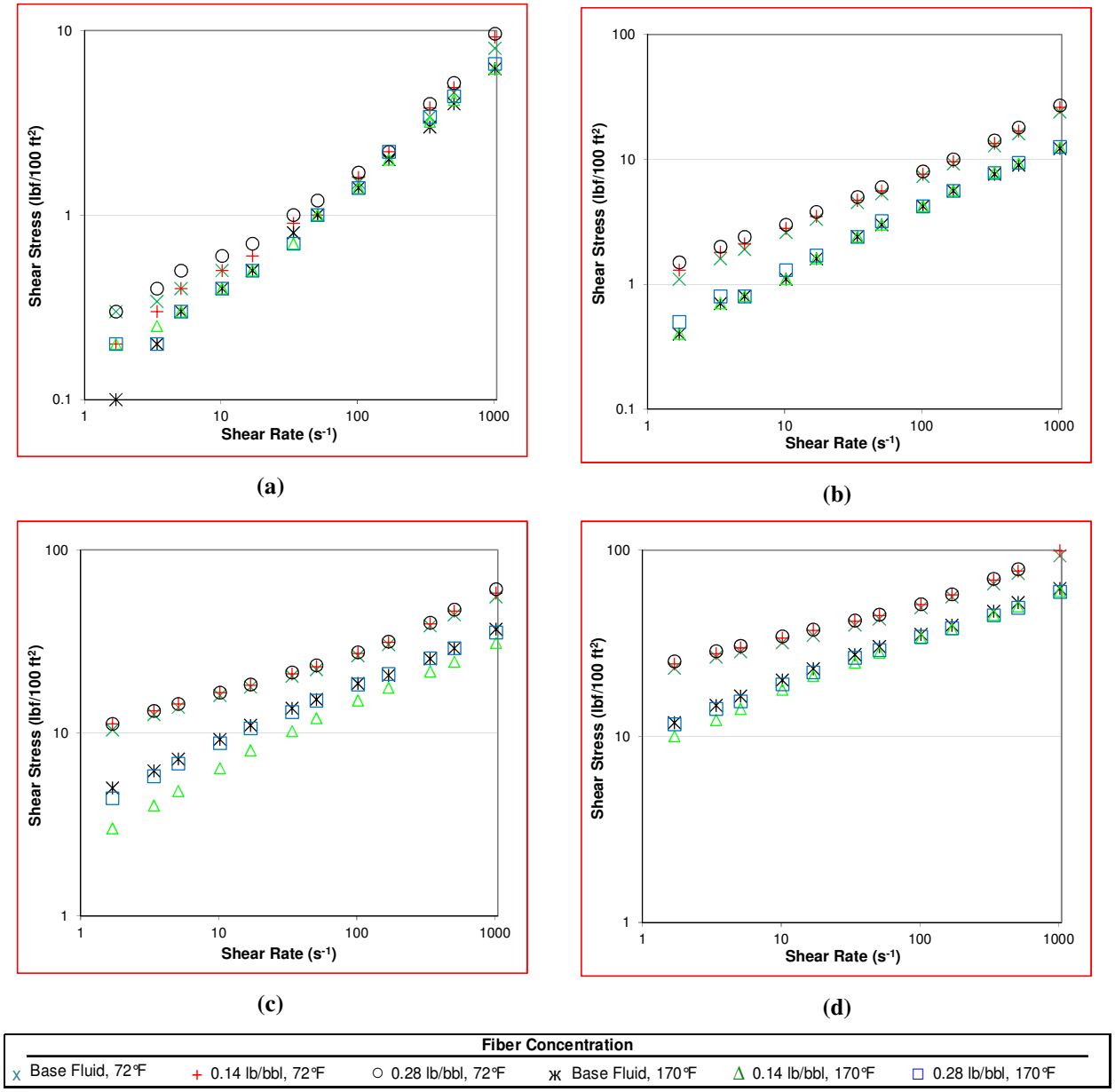

Fig. 4.3 Rheology of XG based fluid at 72°F and 170°F varying fiber and polymer concentrations: a) 0.35 lb/bbl XG; b) 0.87 lb/bbl XG; c) 1.75 lb/bbl XG; and d) 2.62 lb/bbl XG

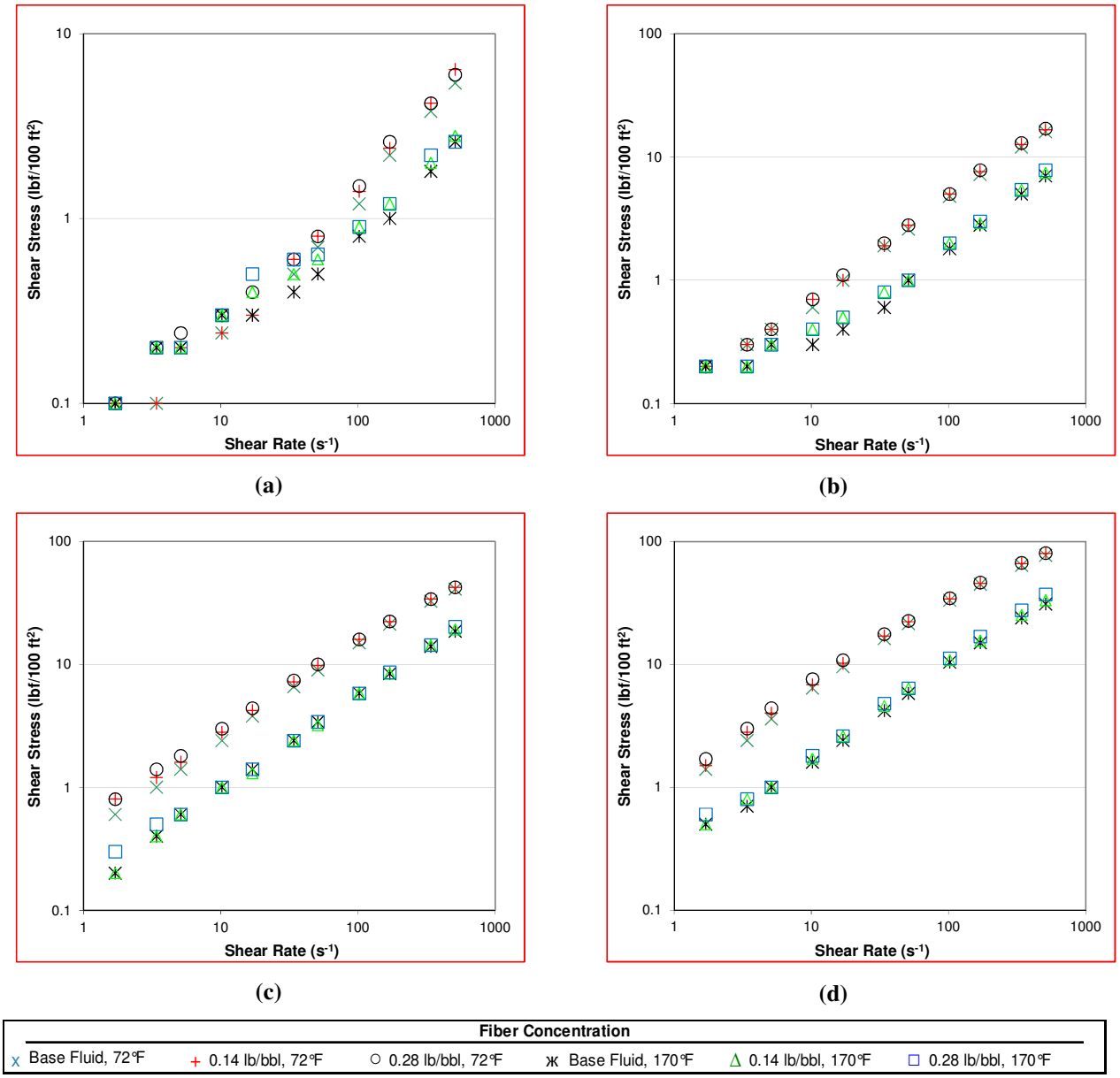

Fig. 4.4 Rheology of PAC based fluid at 72°F and 170°F varying fiber and polymer concentrations: a) 0.35 lb/bbl PAC; b) 0.87 lb/bbl PAC; c) 1.75 lb/bbl PAC; and d) 2.62 lb/bbl PAC

Another important point was the remarkably minor influence that fiber concentration has on shear stress in the oil-based and synthetic-based muds. Even at low shear rates, the change in shear stress ranged from 4 to 6 percent for most cases, with the extreme difference of 8.8 percent at 51 s^{-1} (**Fig. 4.8a**). This finding is encouraging, as fiber can be added to sweeps to enhance hole cleaning without fear of increasing the ECD. Oil-based and synthetic-based muds are often used in harsh, not-easily accessible environments where there is concern for shale interaction and environmental impact. These well locations often require high-angle wells to reduce the footprint and target multiple formations. Fiber sweeps may be employed to

reduce the cuttings beds in these extended reach horizontal wells in which pressure loss along the annulus is a major concern.

In every case, the addition of fluid had no impact on the general shape of the shear stress versus shear rate plots. The approximate model for the base fluid accurately described the behavior of the fiber fluid, at ambient and high temperature.

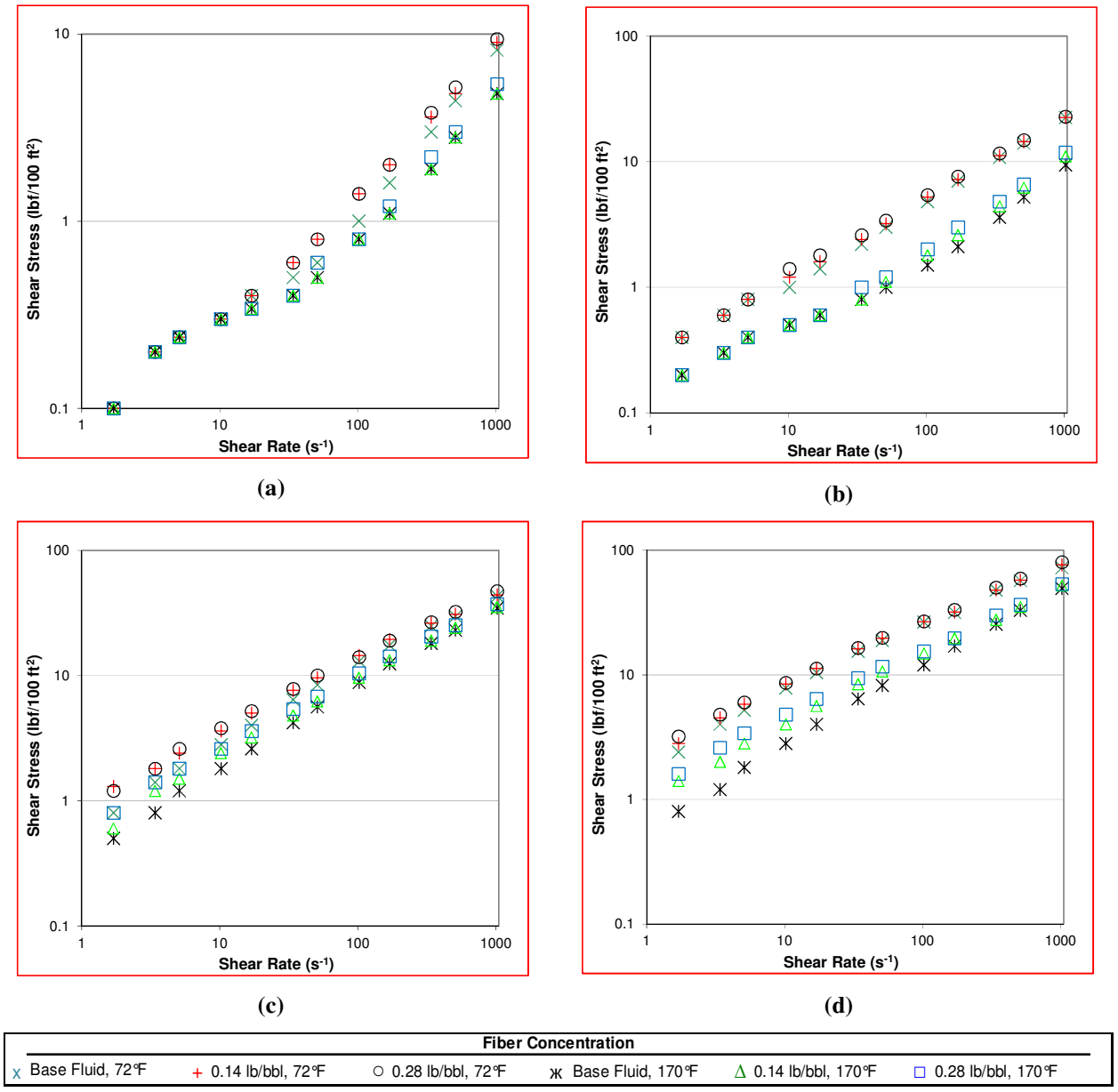

Fig. 4.5 Rheology of XG/PAC (50%/50%) mix fluid at 72°F and 170°F varying fiber and polymer concentrations: a) 0.35 lb/bbl XG/PAC; b) 0.87 lb/bbl XG/PAC; c) 1.75 lb/bbl XG/PAC; and d) 2.62 lb/bbl XG/PAC

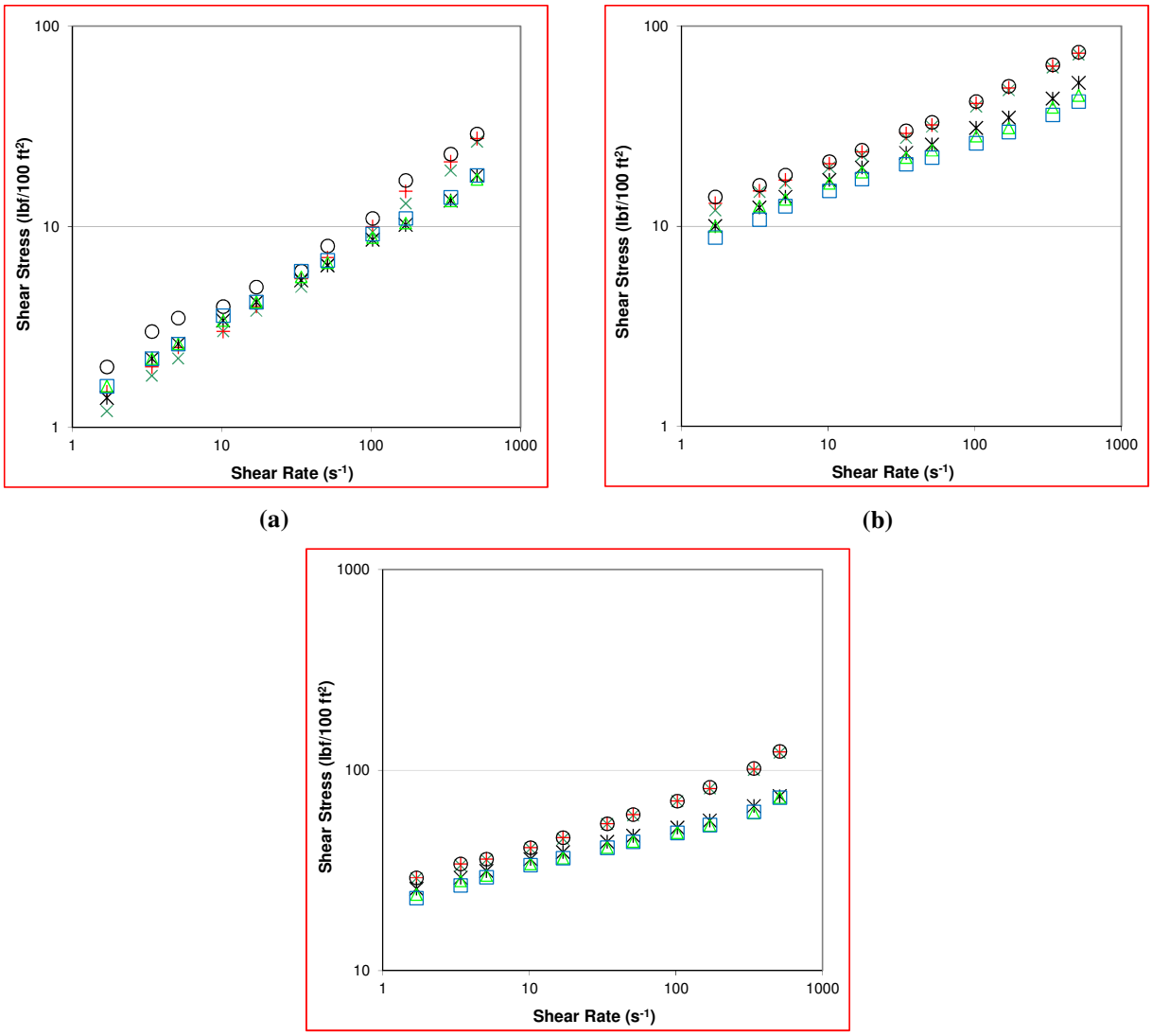

Fig. 4.6 Rheology of XG based weighted fluids (12 ppg) at 72°F and 170°F varying fiber and polymer concentrations: a) 0.87 lb/bbl XG; b) 1.75 lb/bbl XG; and c) 2.62 lb/bbl XG

In a study conducted by Ahmed and Takach (2008), the hole-cleaning efficiency of fiber sweeps was compared to base fluid (viscous) sweeps. The experiments were carried out in a flow loop with varying inclination angles, measuring the cuttings bed height and frictional pressure loss during sweep circulation. For the same annular velocity, the fiber sweeps generally showed a reduced bed height in the flow loop annulus. Annular pressure loss was recorded as a function of time for various flow rates. The results indicated that frictional pressure loss was approximately equal for the base fluid and fiber sweep. In one instance, the fiber sweep pressure loss was less than that exhibited by the base fluid. Pipe viscometer experiments were also conducted comparing flow curves of the base fluid and fiber sweep. Viscometer

pressure loss was measured as a function of flow rate. At low flow rates (laminar, plug flow regime), pressure loss for the base fluid and fiber sweep were equal and the flow curves were similar. A similar conclusion was drawn from a previous study (Xu and Aidun 2005) comparing velocity profiles as a function of fiber concentration. The inclusion of a small amount of fiber had minimal effect on the velocity profile at low Reynolds Number flow.

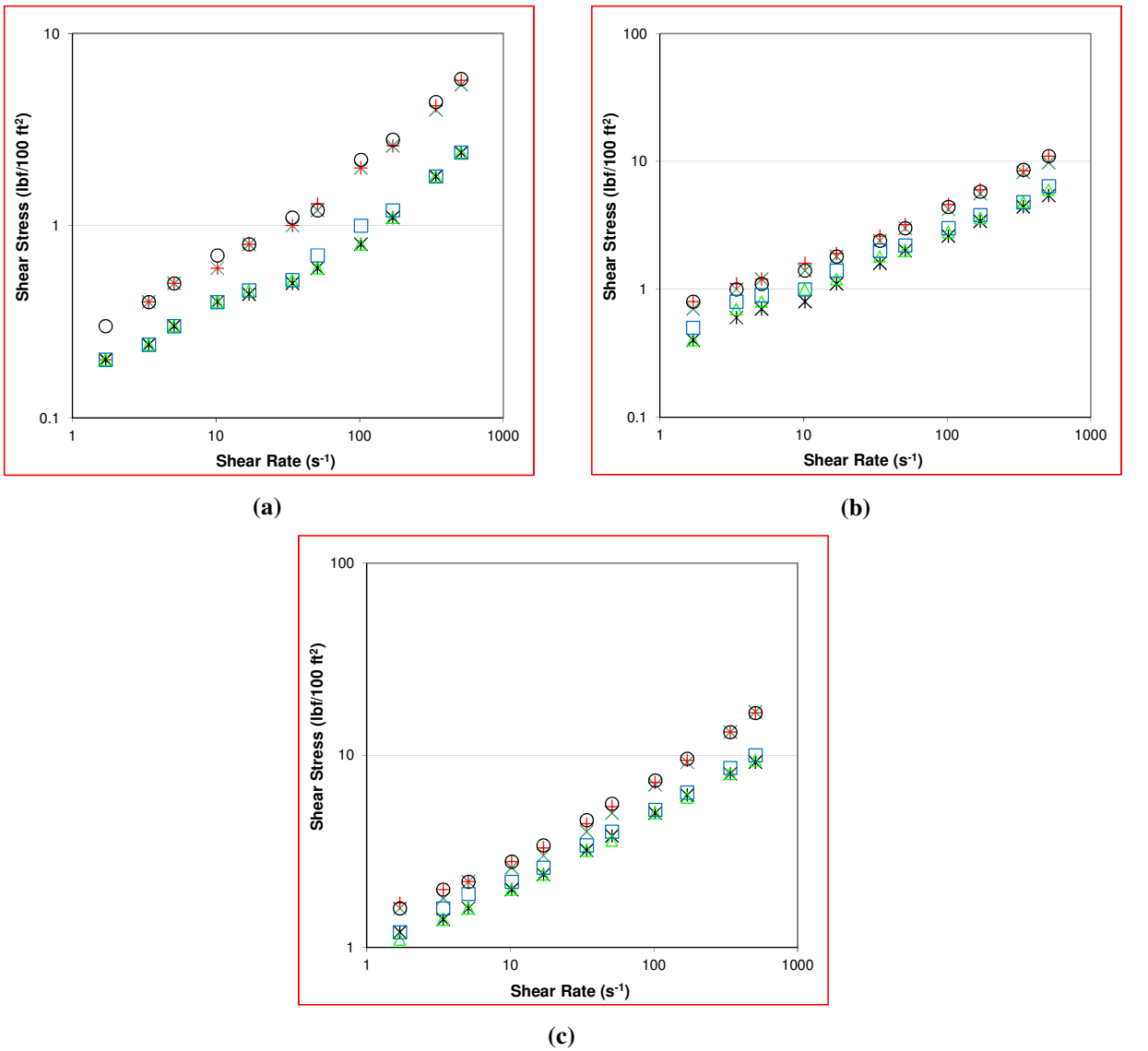

Fig. 4.7 Rheology of PHPA based fluids at 72°F and 170°F varying fiber and polymer concentrations: a) 0.17 lb/bbl PHPA; b) 0.35 lb/bbl PHPA; and c) 0.52 lb/bbl PHPA

4.5.2 Effect of Temperature

In order to reproduce the behavior of the fiber fluid under downhole conditions, the ambient temperature experiments were repeated at high temperature, as shown from **Fig. 4.3** to **Fig. 4.8**. The general trend exhibited in all the fluids studied was that the fluid's ability to flow increases with temperature. The warmer temperatures created a "thin" fluid that was more easily deformed. This enhanced tendency for deformation diminished the fluid's ability to project its inherent flow resistance.

Ann important trend became apparent when analyzing temperature influence on viscosity at different fiber concentrations. As mentioned previously, adding fiber or increasing fiber concentration showed a general tendency for slightly higher viscosity measurements at ambient temperature when compared to the base fluid. In most cases, this same trend was observed in the high-temperature measurements (**Figs. 4.5c** and **4.5d**). However, in some fluids, the increased temperature nullified the influence of fiber concentration (**Fig. 4.3b**). In these instances, adding fiber to the fluid resulted in an increase in viscosity at ambient temperature. However, when taking measurements of the same fluid at high temperature the fiber showed little or no influence on the viscosity.

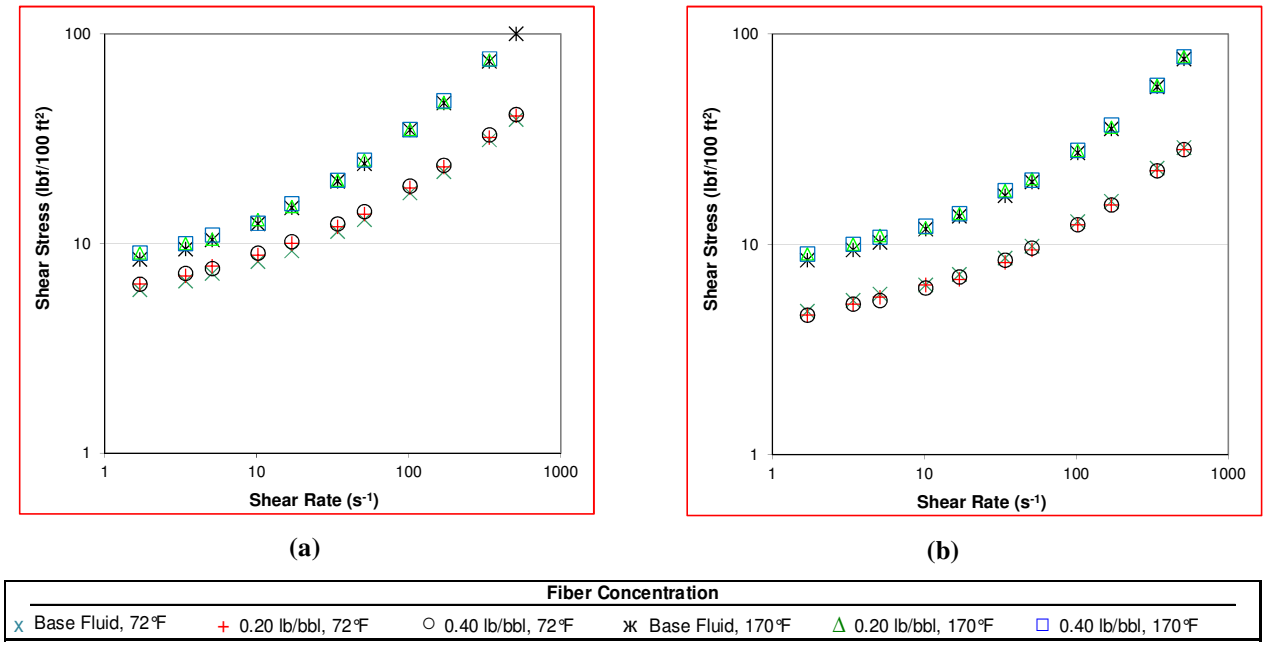

Fig. 4.8 Rheology of weighted (12.2 ppg) oil-based fluids at 72°F and 170°F varying fiber concentrations: a) OBM; and b) SBM

The oil-based and synthetic-based muds showed remarkable performance at ambient and high temperature. Regardless of temperature, fiber had an insignificant influence on viscometric measurements. Throughout the entire shear rate range, the percentage difference between base fluid and fiber fluid remained low and relatively constant. None of the water-based fluids tested showed this level

of control over the entire shear rate range at both temperatures.

The temperature of the fluids was altered to provide a closer representation to actual downhole conditions. However, elevated pressure conditions in the wellbore were not considered in this study, partly as a consequence of the operational capability of the equipment available for these experiments. Previous studies investigated the effect of elevated pressure on the rheology of various fluids. Zhou et al. (2004) conducted experiments to investigate aerated mud cuttings transport in an HPHT flow loop. The effect of elevated pressure (up to 500 psi) was found to have minimal influence on cuttings concentration.

Another study (Alderman et al. 1988) investigated the influence of high temperature and high pressure on water-based mud. The viscous behavior of the fluids in the HPHT conditions reflected the characteristics of their respective continuous phases: a weak pressure dependence and an exponential temperature dependence. It was also shown that the fluid yield stress was essentially independent of pressure, but highly influenced by temperature. Other studies concentrating on the pressure and temperature effects on cement slurry rheology gave similar results. The plastic viscosity of the cement slurry showed little increase with increasing pressure (up to 5000 psi) in relation to the significant effect of increased temperature up to 260°F (Ravi and Sutton 1990).

4.5.3 Shear Viscosity Parameters

The first step in analyzing the fiber fluid shear viscosity was to record all the viscometer shear stress measurements. Least-square regression was performed to determine the rheological parameters for all fluid-fiber-temperature formulations (**Tables 4.3 through 4.8**). The coefficient of determination, R^2, represents how well the measured shear stress values correlate with the values predicted by the Yield Power Law model. An R^2 value of 1.00 represents an exact match of experimental data with the predictive model data. The vast majority of the experimental data points fit the regression model extremely well.

Table 4.3 Rheological parameters of XG based fluid with varying fiber concentration at 72°F and 170°F

Composition		Rheological Properties							
		72 °F				170 °F			
Fluid	Fiber Conc. (lb / bbl)	τ_y	k	n	R^2	τ_y	k	n	R^2
		lbf/100 ft^2	lbf-s^n/100 ft^2			lbf/100 ft^2	lbf-s^n/100 ft^2		
XG 0.35 lb/bbl	0.00	0	0.04	0.76	1.00	0	0.09	0.61	0.99
	0.14	0	0.08	0.65	0.99	0	0.06	0.68	1.00
	0.28	0	0.08	0.65	0.99	0	0.06	0.67	0.99
XG 0.87 lb/bbl	0.00	0	0.80	0.48	1.00	0	0.34	0.53	1.00
	0.14	0	0.75	0.50	1.00	0	0.34	0.54	1.00
	0.28	0	0.77	0.50	1.00	0	0.40	0.51	1.00
XG 1.75 lb/bbl	0.00	4.75	5.06	0.33	1.00	0	4.41	0.31	1.00
	0.14	6.24	4.38	0.35	1.00	0	2.69	0.36	0.99
	0.28	6.34	4.27	0.36	1.00	0	4.03	0.32	1.00
XG 2.62 lb/bbl	0.00	13.33	8.76	0.31	1.00	0	10.83	0.25	1.00
	0.14	14.33	8.97	0.31	1.00	0	9.04	0.28	1.00
	0.28	16.15	8.08	0.33	1.00	0	10.43	0.25	1.00

As discussed previously, the shear viscosity models are mathematical relations that approximately represent the measured data using curve-fitting parameters. Some properties believed to exist in some polymers do not always manifest themselves. For instance, XG fluids typically exhibit a yield stress only at high concentrations. In our study, at low concentrations XG fluids best fit the regular Power Law model without a yield stress. This yield stress value increased as polymer concentration increases and the fluid became more viscous at low temperature (**Table 4.3**). However, at high temperature (170°F) even the higher concentration fluids did not show a yield stress value. Regardless, neither PAC (**Table 4.4**) nor PHPA (**Table 4.7**), by contrast, was anticipated to show a yield stress. Indeed that was the case, except for a couple of PHPA cases. However, the uncertainty in the yield stress in all of these cases can be expected to be approximately 1 lb/100 ft^2.

Table 4.4 Rheological parameters of PAC based fluid with varying fiber concentration at 72°F and 170°F

Composition		Rheological Properties							
		72 °F				170 °F			
Fluid	Fiber Conc. (lb / bbl)	τ_y	k	n	R^2	τ_y	k	n	R^2
		lbf/100 ft^2	lbf-s^n/100 ft^2			lbf/100 ft^2	lbf-s^n/100 ft^2		
PAC 0.35 lb/bbl	0.00	0	0.03	0.84	0.99	0	0.05	0.61	0.97
	0.14	0	0.03	0.85	0.99	0	0.06	0.60	0.99
	0.28	0	0.04	0.77	0.99	0	0.08	0.57	0.98
PAC 0.87 lb/bbl	0.00	0	0.09	0.82	1.00	0	0.02	0.92	0.99
	0.14	0	0.10	0.82	1.00	0	0.04	0.84	0.99
	0.28	0	0.11	0.81	1.00	0	0.04	0.85	0.99
PAC 1.75 lb/bbl	0.00	0	0.44	0.74	1.00	0	0.16	0.77	1.00
	0.14	0	0.56	0.70	1.00	0	0.15	0.78	1.00
	0.28	0	0.61	0.69	1.00	0	0.15	0.78	1.00
PAC 2.62 lb/bbl	0.00	0	1.22	0.68	0.99	0	0.28	0.76	1.00
	0.14	0	1.36	0.67	0.99	0	0.32	0.75	1.00
	0.28	0	1.52	0.65	0.99	0	0.27	0.79	1.00

Table 4.5 Rheological parameters of XG/PAC (50%/50%) based fluid with varying fiber concentration at 72°F and 170°F

Composition		Rheological Properties							
		72 °F				170 °F			
Fluid	Fiber Conc. (lb / bbl)	τ_y lbf/100 ft²	k lbf-s^n/100 ft²	n	R^2	τ_y lbf/100 ft²	k lbf-s^n/100 ft²	n	R^2
XG/PAC 0.35 lb/bbl	0.00	0	0.05	0.71	0.98	0	0.06	0.60	0.97
	0.14	0	0.05	0.72	0.99	0	0.06	0.60	0.97
	0.28	0	0.05	0.74	0.99	0	0.05	0.62	0.97
XG/PAC 0.87 lb/bbl	0.00	0	0.19	0.69	1.00	0	0.08	0.66	0.99
	0.14	0	0.25	0.65	1.00	0	0.07	0.71	0.99
	0.28	0	0.29	0.63	1.00	0	0.08	0.71	1.00
XG/PAC 1.75 lb/bbl	0.00	0	0.66	0.62	1.00	0	0.38	0.66	1.00
	0.14	0	0.98	0.56	1.00	0	0.53	0.62	1.00
	0.28	0	0.98	0.57	1.00	0	0.66	0.59	1.00
XG/PAC 2.62 lb/bbl	0.00	0	2.17	0.53	0.99	0	0.61	0.64	1.00
	0.14	0	2.48	0.51	1.00	0	1.09	0.56	1.00
	0.28	0	2.64	0.50	1.00	0	1.36	0.53	1.00

Table 4.6 Rheological parameters of XG+Barite (12 ppg) based fluid with varying fiber concentration at 72°F and 170°F

Composition		Rheological Properties							
		72 °F				170 °F			
Fluid	Fiber Conc. (lb / bbl)	τ_y lbf/100 ft²	k lbf-s^n/100 ft²	n	R^2	τ_y lbf/100 ft²	k lbf-s^n/100 ft²	n	R^2
XG+Barite 0.87 lb/bbl 12 ppg	0.00	0.52	0.55	0.62	0.99	0	1.05	0.46	0.99
	0.20	0.84	0.50	0.64	1.00	0	0.95	0.47	0.99
	0.40	1.09	0.77	0.58	0.99	0	1.07	0.46	0.99
XG+Barite 1.75 lb/bbl 12 ppg	0.00	7.06	4.23	0.45	0.99	3.48	5.78	0.34	0.99
	0.20	8.02	4.07	0.46	1.00	3.64	5.78	0.32	0.99
	0.40	9.20	3.91	0.46	1.00	1.07	6.93	0.29	1.00
XG+Barite 2.62 lb/bbl 12 ppg	0.00	16.91	10.14	0.36	1.00	7.64	16.37	0.22	1.00
	0.20	17.03	10.31	0.36	1.00	9.59	13.35	0.24	0.99
	0.40	17.09	10.25	0.36	1.00	6.64	15.07	0.23	0.99

Table 4.7 Rheological parameters of PHPA based fluid with varying fiber concentration at 72°F and 170°F

Composition		Rheological Properties							
		72 °F				170 °F			
Fluid	Fiber Conc. (lb / bbl)	τ_y lbf/100 ft²	k lbf-s^n/100 ft²	n	R^2	τ_y lbf/100 ft²	k lbf-s^n/100 ft²	n	R^2
PHPA 0.17 lb/bbl	0.00	0	0.17	0.55	0.99	0	0.06	0.56	0.99
	0.14	0	0.16	0.56	0.99	0	0.06	0.56	0.99
	0.28	0	0.10	0.64	0.99	0	0.07	0.55	0.99
PHPA 0.35 lb/bbl	0.00	0	0.34	0.54	1.00	0	0.30	0.47	1.00
	0.14	0	0.31	0.56	1.00	0	0.35	0.45	1.00
	0.28	0.51	0.22	0.62	1.00	0	0.38	0.45	0.99
PHPA 0.52 lb/bbl	0.00	1.05	0.40	0.58	1.00	0	0.59	0.44	1.00
	0.14	1.07	0.46	0.56	1.00	0	0.61	0.43	1.00
	0.28	0	0.61	0.69	0.99	0	0.72	0.42	1.00

Table 4.8 Rheological parameters of OBM and SBM with varying fiber concentration at 72°F and 170°F

Composition		Rheological Properties							
		72 °F				170 °F			
Fluid	Fiber Conc. (lb / bbl)	τ_y lbf/100 ft²	k lbf-s^n/100 ft²	n	R^2	τ_y lbf/100 ft²	k lbf-s^n/100 ft²	n	R^2
OBM (12.2 ppg)	0.00	6.92	1.03	0.72	1.00	5.09	0.69	0.63	1.00
	0.20	7.63	0.93	0.74	1.00	5.35	0.79	0.61	1.00
	0.40	7.61	0.96	0.73	1.00	5.32	0.83	0.61	1.00
SBM (12.1 ppg)	0.00	7.21	0.88	0.69	1.00	4.15	0.52	0.62	0.99
	0.20	7.84	0.86	0.70	1.00	3.97	0.51	0.62	0.99
	0.40	7.86	0.85	0.70	1.00	3.96	0.50	0.63	1.00

4.6 Conclusions

This study was conducted to investigate the effects of temperature and fiber concentration on the rheology of fiber-containing sweeps. Rheology experiments were conducted using rotational viscometers to measure the rheology of base fluids and fiber-containing fluids at ambient temperature and 170°F. The shear viscosity profiles of fiber sweep fluids were compared using graphical and curve-fitting regression analyses. Based on the experimental results and data analysis, the following conclusions were made:

- The addition of fiber up to 0.08 weight percent has a minor effect on the fluid's shear viscosity profile, whether at ambient temperature or 170°F. Some instances showed slight increases in viscosity, while others showed a decrease with increasing fiber concentration.
- Increasing the temperature of the fluid decreased the non-Newtonian behavior of the fiber fluid and decreased the viscosity throughout the shear rate range of 2 to $1000^{s^{-1}}$.
- In most cases, as fiber concentration increased, the viscosity showed increasingly non-Newtonian behavior: in the Yield Power Law model, n decreased while K and τ_y increased.
- Neither oil-based nor synthetic-based fluids exhibited any significant shear viscosity sensitivity to fiber concentration at ambient temperature or at 170°F. It may be possible for oil-based or synthetic-based mud sweeps to be utilized in the field with no increase in ECD.

Nomenclature

BHA = Bottomhole Assembly
BP = Bingham Plastic
ECD = Equivalent circulating density
ERD = Extended reach drilling
K = Consistency index (lbf-s^n/100 ft^2)
N = Flow behavior index
ppg = Pounds per gallon
PAC = Polyanionic Cellulose
PHPA = Partially Hydrolyzed Polyacrylamide
PL =Power Law
XG = Xanthan Gum
YPL =Yield Power Law

Greek Letters

τ = Shear stress (lbf/100 ft^2)
τ_y = Yield stress (lbf/100 ft^2)

γ = shear rate (s^{-1})

μ = Viscosity

References

Ahmed, R.M. and Takach, N.E. 2008. Fiber Sweeps for Hole Cleaning. Paper SPE 113746 presented at the SPE/ICoTA Coiled Tubing and Well Intervention Conference and Exhibition, The Woodlands, Texas, 1-2 April. DOI: 10.2118/113746-MS.

Alderman, N.J., Gavignet, A., Guillot, D. and Maitland, G.C. 1998. High-Temperature, High-Pressure Rheology of Water-Based Muds. Paper SPE 18035 presented at the SPE Annual Technical Conference and Exhibition, Houston, Texas, October 2-5. DOI: 10.2118/18035-MS.

Bivins, C.H., Boney, C., Fredd, C., Lassek, J. Sullivan, P., Engels, J., Fielder, E.O. et al. 2005. New Fibers for Hydraulic Fracturing. Schlumberger Oilfield Review 17 (2): 34-43.

Bulgachev, R.V. and Pouget, P. 2006. New Experience in Monofilament Fiber Tandem Sweeps Hole Cleaning Performance on Kharyaga Oilfield, Timan-Pechora Region of Russia. Paper SPE 101961 presented at the SPE Russian Oil and Gas Technical Conference and Exhibition, Moscow, Russia, 3-6 October. DOI: 10.2118/101961-MS.

Cameron C. 2001. Drilling Fluids Design and Management for Extended Reach Drilling. Paper SPE 72290 presented at the IADC/SPE Middle East Drilling Technology conference, Bahrain, 22-24 October. DOI: 10.2118/72290-MS.

Cameron, C., Helmy, H., and Haikal, M. 2003. Fibrous LCM Sweeps Enhance Hole Cleaning and ROP on Extended Reach Well in Abu Dhabi. Paper SPE 81419 presented at the SPE 13th Middle East Oil Show and Conference, Bahrain, 5-8 April. DOI: 10.2118/81419-MS.

Demirdal, B., Miska, S., Takach, N.E. and Cunha, J.C. 2007. Drilling Fluids Rheological and Volumetric Characterization Under Downhole Conditions. Paper SPE 108111 presented at the SPE Latin American and Caribbean Petroleum Engineering Conference, Buenos Aires, Argentina, 15-18 April. DOI: 10.2118/108111-MS.

Drilling Fluid Rheology. 2001. Kelco Oil Field Group, Houston, Texas (Rev. Sep 2005).

Gupta, V.K., Sureshkumar, R., Khomami, B. and Azaiez, J. 2002. Centrifugal Instability of Semidilute non-Brownian Fiber Suspensions. Physics of Fluids 14 (6): 1958-1971

Hemphill, T. and Rojas, J.C. 2002. Drilling Fluid Sweeps: Their Evaluation, Timing, and Applications. Paper SPE 77448 presented at the SPE Annual Technical Conference and Exhibition, San Antonio, Texas, 29 September-2 October. DOI: 10.2118/77448-MS.

Maehs, J., Renne, S., Logan, B. and Diaz, N. 2010. Proven Methods and Techniques to Reduce Torque and Drag in the Pre-Planning and Drilling Execution of Oil and Gas Wells. Paper SPE 128329

presented at the IADC/SPE Drilling Conference and Exhibition, New Orleans, Louisiana, 2-4 February. DOI: 10.2118/128329-MS.

Power, D.J., Hight, C., Weisinger, D. and Rimer, C. 2000. Drilling Practices and Sweep Selection for Efficient Hole Cleaning in Deviated Wellbores. Paper SPE 62794 presented at the IADC/SPE Asia Pacific Drilling Technology conference, Kuala Lumpur, Malaysia, 11-13 September. DOI: 10.2118/62794-MS.

Ravi, K.M. and Sutton, D.L. 1990. New Rheological Correlation for Cement Slurries as a Function of Temperature. Paper SPE 20449 presented at the SPE Annual Technical Conference and Exhibition, New Orleans, Louisiana, 23-26 September. DOI: 10.2118/20449-MS.

Robertson, N., Hancock, S., and Mota, L. 2005. Effective Torque Management of Wytch Farm Extended-Reach Sidetrack Wells. Paper SPE 95430 presented at the SPE Annual Technical Conference and Exhibition, Dallas, Texas, 9-12 October. DOI: 10.2118/95430-MS.

Swerin, A. 1997. Rheological properties of cellulosic fibre suspensions flocculated by cationic polyacrylamides. Colloids and Surfaces A: Physiochemical and Engineering Aspects 133 (3): 279-294

Valluri, S.G., Miska, S.Z., Ahmed, R.M. and Takach, N.E. 2006. Experimental Study of Effective Hole Cleaning Using "Sweeps" in Horizontal Wellbores. Paper SPE 101220 presented at the SPE Annual Technical Conference and Exhibition, San Antonio, Texas, 24-27 September. DOI: 10.2118/101220-MS.

Xu, A.H. and Aidun, C. K. "Characteristics of fiber suspension flow in a rectangular channel," International Journal of Multiphase Flow 31 (2005) 318–336.

Yu, M., Takach, N.E., Nakamura, D.R. and Shariff, M.M. 2007. An Experimental Study of Hole Cleaning Under Simulated Downhole Conditions. Paper SPE 109840 presented at the SPE Annual Technical Conference and Exhibition, Anaheim, California, 11-14ovember. DOI: 10.2118/109840-MS.

Zhou, L., Ahmed, R.M., Miska, S.Z., Takach, N.E., Yu, M., and Pickell, M.B. 2004. Experimental Study & Modeling of Cuttings Transport with Aerated Mud in Horizontal Wellbore at Simulated Downhole Conditions. Paper SPE 90038 presented at the SPE Annual Technical Conference and Exhibition, Dallas, Texas, 26-29 September. DOI: 10.2118/90038-MS.

Zhu, C. 2005. Cuttings Transport with Foam in Horizontal Concentric Annulus Under Elevated Pressure and Temperature Conditions. Ph.D. Dissertation, University of Tulsa, Tulsa, Oklahoma.

5. Settling Behavior of Particles in Fiber-containing Drilling Fluids

Fiber-containing fluids are utilized in many industrial applications. In the upstream petroleum industry, fiber suspensions are used to transport rock cuttings from the bottom of the hole to the surface. Moreover, fibrous fluids are applied in fracturing operations to transport proppant particle to the fractured space. Solids transport performances of these fluids largely depends on the settling behavior of suspended particles.

This section of the report presents results of experimental and theoretical investigations conducted on the settling behavior of spherical particles in fiber-containing fluid. Settling experiments were carried out in a 4-inch fully transparent cylinder that is sufficiently long (6.5 feet) to establish terminal settling conditions. Both Newtonian and non-Newtonian fluids were considered in the investigation. A moving digital camera system was used to track and locate a particle while it was settling in fully transparent test fluid. The camera records were used to determine the settling velocity of each particle as a function of time. Tests were performed with particles that have different sizes (2 mm to 8 mm). Fiber concentration was varied from 0.00 to 0.08 percent by weight.

When a particle settles in the fibrous fluid, it experiences fiber drag in addition to the conventional hydrodynamic resistance (i.e., viscous drag). Measured terminal velocity was used to compute the viscous component of the total drag. Subsequently, applying the momentum balance, the fiber drag component acting on the particle was determined from the total drag. Results showed that the fiber drag was a function of the projection area of the particle, settling velocity, fiber drag coefficient, and density difference between the fluid and particle. The fiber drag coefficient varied with Reynolds Number, fiber concentration, and fluid behavior index. Using the experimental data, a semi-empirical model was developed to predict terminal settling velocity of a particle in fiber-containing fluids. The correlation was validated for both Newtonian and non-Newtonian base fluids that have low concentrations of hole-cleaning fibers. The correlation is applicable to suspensions containing fully dispersed fibers with length of approximately 10 mm and diameter of 100 μm.

5.1 Introduction

Settling and sedimentation occur in many areas of the petroleum industry and process engineering operations. Typical applications of settling velocity include drill cuttings and proppants, transport prediction, design of separators and settling tanks, and hydraulic and pneumatic transportation of solids particle in mining, coal, and other industrial applications.

Studies on settling velocity of solids particles in Newtonian and non-Newtonian fluids have been well-documented (Shah 1982; Klessidis 2004; Chhabbra & Peri 1991; Dallon 1967; Prakash 1983; Lali et al. 1989; and Chhabra 1980). Shah (1982) developed a new approach to analyze proppant settling in non-Newtonian fluid. The study showed that the drag coefficient correlation is a function of Reynolds Number and fluid behavior index "n". Especially at low Reynolds numbers, the fluid behavior index "n" has a significant effect on the proppant settling velocity and this effect diminishes at high Reynolds Numbers. It also shows that the correlation developed for static settling velocity can predict the dynamic settling data. It was recommended to plot C_D^{2-n} versus Reynolds Number to get a better curve fit with a single straight line on a log-log plot. The method had been tested (Shah et al. 2007) with data from the previous studies (Dallon 1967; Prakash 1983; Lali et al. 1989; and Chhabra 1980) and satisfactory agreements had been obtained. An experimental study (Fang 1992) conducted on free settling of spherical particles in Newtonian and non-Newtonian fluids showed both stable and swinging settling patterns.

Particles in fluids with yield stress show different settling behavior. Fine and/or light particles can fully suspend in the fluid due the yield stress. Dedegil (1987) developed a method to predict settling velocity of particles in Herschel-Bulkley (Yield Power Law) fluid. The method relates the drag coefficient to the generalized Reynolds Number based on apparent viscosity calculated from the representative shear rate (V/d). The method accounts for the effect of yield stress on the settling velocity. It condensed most of the published data (Valentik and Whitmore 1965) into a single curve when the drag coefficient was plotted against the generalized Reynolds Number.

Many of the fluids used in the industry exhibit viscoelastic behavior. A study (Acharga 1986) conducted on particle settling in viscoelastic fluid indicated that the fluid elasticity does not affect the settling rate in the creeping flow region (low Reynolds Number). However, it enhances the sedimentation rate in the transition zone. Predictions from a theoretical model were compared with measurements and showed good agreement. Drag coefficient is strongly influenced by viscoelastic properties of the fluid. Experiments (Jin and Penny 1995) revealed the variation of drag coefficient with the Reynolds Number (N_{Rep}) and dimensionless viscoelastic parameter of the test fluid. In addition to fluid properties, the shape of a particle has substantial effect on its settling behavior. Empirical models (Peden and Luo 1987; Chien 1994) developed to predict settling velocities of non-spherical particles showed the relationship between the drag coefficient and shape factor.

Furthermore, the presence of a wall can create hydrodynamic interference with the settling particles. As particles settle in fluids, their motion is affected by the presence of other particles and/or container walls. The wall effect tends to reduce the settling velocity. The hydrodynamic effects of container walls have

been investigated (Brown et al. 1950; Lali et al. 1988; Di Felice et al. 1995) extensively. Experiments (Lali et al. 1988 and Brown et al. 1950) showed that the diameter ratio (i.e., the ratio of the diameter of the container to the diameter of the particle) and Reynolds Number determines the wall effect. Empirical correlations are available to determine correction factors that account for the presence of a wall. These factors relate the wall-free settling velocity to the actual velocity under both laminar and turbulent conditions.

The presence of neighboring particles creates hydrodynamic interference that hinders particle sedimentation. A number of experimental and theoretical studies (Richardson and Zaki 1954; Govier and Aziz 1972; Smith 1997; Daneshy 1978) were conducted to investigate sedimentation in concentrated suspensions, which demonstrated the reduction of settling velocity at high solids concentrations. Increasing the particle concentration tends to increase the hydrodynamic interference and particle collision, which are highly dependent on the flow regime (Govier and Aziz 1972). Uniformly-sized particles in laminar motion have identical velocities, and collision is not expected even as concentration increases. However, in turbulent flow collisions can occur due to settling speed differences that arise from random fluctuations of fluid velocity. Moreover, in actual situations the solids particles do not have uniform size distribution. As a result, even under laminar conditions, particle collision can exist. The collisions intensify with the increase in particle concentration and differences in particle settling speeds. Smith (1998) developed a theoretical model to predict the sedimentation velocity of uniformly-sized particles in Newtonian fluid under laminar conditions. The model was compared with the correlation of Richardson and Zaki (1954). Even though general agreement was obtained at high concentrations, discrepancies were observed at low concentrations.

Rheological behavior of fiber suspensions is very complex. The introduction of fiber can significantly alter the fluid rheology. Rajabian et al. (2008) developed a rheological model for fiber-containing polymer suspensions. The model includes the fiber-fiber and fiber-polymer interaction. The experimental measurements obtained from simple shear flows agreed with the model predictions. Another study of fiber suspensions (Marti et al. 2005) showed minor gains in viscosity as the fiber concentration was incrementally increased from an initial dilute suspension. However, at higher fiber concentrations, the viscosity showed greater sensitivity to fiber concentration.

In the drilling industry, sweep fluid is used to improve wellbore cleaning in inclined and horizontal wells when the regular drilling fluid fails to clean the wellbore sufficiently. Conventional sweeps are commonly categorized as i.) high-viscosity; ii.) high-density; iii.) low-viscosity; iv.) combination; and v.) tandem sweeps (Hemphill 2002). Sweeps provide a number of benefits, such as reducing cuttings beds and

subsequent decrease in annular pressure loss, as well as a reduction in torque and drag at the surface. As a result, it is often applied to reduce excessive annular pressure losses and clean the wellbore prior to tripping operation. Hole cleaning fiber is added to the sweep fluid to improve its performance with a negligible increase in viscosity and pressure loss. Previous studies (Ahmed and Takach 2008; Cameron et al. 2003; Bulgachev & Pouget 2006) reported that adding a small amount of hole cleaning fiber (less than 0.1 percent by weight) improves solid transport performance of the sweep with no noticeable change in fluid rheology.

Fiber has also shown considerable promise in well stimulation operations. Hydraulic fracturing requires extremely high downhole fluid pressure to induce cracks into the reservoir rock, fracturing the formation. A material that can withstand highly compressive forces, proppant, is necessary to prevent the fractures from closing after the fluid pressure subsides and hydrocarbon production begins. As the fracturing fluid is pumped downhole, the proppant travels with and behind it, and remains in the fracture after the fluid is imbibed into the formation and/or flows back. With insufficient particle suspension properties, the fracturing fluid will allow the proppant to settle before the fracture face closes and reduce the uniformity and effectiveness of the proppant within the fracture. Conventional fracturing fluids rely on viscosity for particle suspension, which precipitate excessive pressure losses and consequently require high pump pressures. Fiber has been added to stimulation fluids to achieve the suspension properties necessary to transport and deposit the proppant as designed, ensuring desired fracture conductivity and overall productivity of the well. The fiber fluid can achieve equivalent suspension characteristics with less viscosity, therefore requiring less pressure during stimulation operations. An experimental investigation was conducted to evaluate the benefits of using fiber to prevent proppant settling in hydraulic fractures (Bivins et al. 2005). Results showed a substantial reduction in the proppant settling velocity, which was attributed to fiber concentration.

The settling behavior of particles in fiber suspensions is more complex than in the base fluid (i.e., fluid without suspension). The interactions among the fiber particles, suspended solids and base fluid are difficult, if not impossible, to express mathematically. When the fiber is fully dispersed in fluid, it can form a stable network structure. The strength of the network depends on the fiber concentration and length. Suspensions with low fiber concentrations and/or short fiber length form a very weak network. The network structure created by the fiber particles tends to reduce the settling velocity of dense particles due to fiber-fiber and fiber-particle interactions. The origins of these interactions can be mechanical contact and/or hydrodynamic interference between fiber particles. Mechanical contact between fiber particles generate a strong friction force that hinders the settling of suspended particles or drill cuttings. A numerical investigation was conducted to study the settling of a small sphere through a suspension of

neutrally buoyant fibers (Harlen et al. 1999). The model considered fiber-fiber contact forces and long-range hydrodynamic interactions. An asymptotic solution was presented for the limit when the sphere diameter is much smaller than the fiber length and inter-fiber spacing. A greater understanding of particle settling behavior in fiber suspension is essential to develop effective fiber-containing sweep and fracturing fluid formulations.

5.2 Settling in Fiber Suspensions

Studies on the settling behavior of particles in both Newtonian and non-Newtonian fluid have been well documented. Theoretical models have been established to predict terminal velocity of a particle. When a particle settles in a homogeneous fluid, it experiences several forces. The major forces acting on the particle when it attains its maximum speed (terminal velocity) are gravity, buoyancy, and hydrodynamic drag. Considering these forces, the momentum balance for a settling particle is:

$$m\frac{dV}{dt} = F_g - F_b - F_{Dv} \quad \text{.....} \quad (5.1)$$

where F_g and F_b are the gravity and buoyancy forces, respectively. The hydrodynamic drag (viscous drag) force is expressed as:

$$F_{Dv} = \frac{1}{2}C_{Dv}V^2\rho_f A_p \quad \text{.....} \quad (5.2)$$

The above equation does not include the effect of fiber particles. After inserting the expressions for gravity (F_g = mg), buoyancy (F_b = mgρ_f/ρ_p), and drag forces into Eqn. (5.1), we obtain the following expression for the particle acceleration:

$$\frac{dV}{dt} = g\frac{\rho_p - \rho_f}{\rho_p} - \frac{C_{Dv}V^2A_p\rho_f}{2m} \quad \text{.....} \quad (5.3)$$

where m is mass of the particle; C_{Dv} is the viscous drag coefficient; and A_p is the projected area of the particle in the plane perpendicular to the direction of flow. Under steady state (i.e., terminal settling) condition, $\frac{dV}{dt} = 0$. Thus, the above equation reduces to:

$$g\frac{\rho_p - \rho_f}{\rho_p} - \frac{C_{Dv}V_s^2A_p\rho_f}{2m} = 0 \quad \text{.....} \quad (5.4)$$

When fiber is added to the fluid, an additional drag force (i.e., fiber drag) that opposes the particle motion will be created because of mechanical and hydrodynamic interactions between the fiber and the settling

particle. In this case, the total drag force (F_{DT}) acting on the particle is the sum of the viscous and fiber drags. Applying momentum balance for steady state condition (dv/dt = 0), the total drag is:

$$F_{DT} = F_B - F_g \quad \text{……………………………………………………………………} \quad (5.5)$$

Subsequently, the fiber drag can be determined from the total drag and viscous drag as:

$$F_{Df} = F_{DT} - F_{Dv} \quad \text{……………………………………………………………………..} \quad (5.6)$$

It is important to note that both total drag and viscous drag must be determined at identical settling conditions (i.e., at the same settling speed).

Despite the difference in origins between the fiber and viscous drags, similarities do exist. In less concentrated fiber suspensions with short fiber particles, the major components of the two forces originate from hydrodynamic effects. Considering this commonality, the fiber drag is modeled in a similar manner as the viscous drag, resulting in:

$$F_{Df} = \frac{1}{2} C_{Df} V_s^2 \left(\rho_p - \rho_f\right) A_p \quad \text{……………………………………………………………} \quad (5.7)$$

where C_{Df} is fiber drag coefficient. The major dissimilarity between the fiber drag and viscous drag equations is the use of density difference present in Eqn. (5.7), as compared to the singular fluid density term in Eqn. (5.2). This formulation is based on experimental observations and provides the best correlation with respect to the experimental measurements. Combining Eqns. (5.5), (5.6), and (5.7), particle-settling velocity in fiber-containing fluid is:

$$V_s^2 = \frac{\frac{4}{3} dg}{\left[C_{Df} + C_{Dv}\left(\frac{\rho_f}{\rho_p - \rho_f}\right)\right]} \quad \text{……………………………………………………………………} \quad (5.8)$$

In the case of fluid without fiber, the fiber drag coefficient in Eqn (5.8) becomes zero ($C_{Df} = 0$), and the equation reduces to the Stokes' law:

$$V_s^{\,2} = \frac{4}{3} \frac{dg}{C_{Dv}} \left(\frac{\rho_p - \rho_f}{\rho_f}\right) \quad \text{……………………………………………………………………} \quad (5.9)$$

5.3 Experimental Study

This investigation aimed at studying the settling behavior of solids particles in fiber suspensions and determining the contribution of fiber drag to the total drag force. To achieve these objectives, a baseline was first created to compare subsequent results. Settling velocity tests were conducted using base-fluids

(i.e., fluids without fiber), and correlations were developed to determine the viscous drag coefficients. Then, settling velocity experiments were repeated using the base fluids with differing fiber concentrations. The recorded terminal settling velocities of the particles in fiber suspensions, in conjunction with the base fluid correlations, were used to determine the Reynolds Number and corresponding viscous drag coefficient. Subsequently, the fiber drag coefficient was determined applying Eqn. (5.8).

5.3.1 Experimental Setup

Settling velocity experiments were conducted using a vertical cylinder with spherical particles, using both Newtonian and non-Newtonian base fluids. The settling velocity of each particle was measured by tracking the position of the particle as function of time. The experimental setup (**Fig. 5.1**) used in this study consisted of a 10-cm diameter and 2-m long fully transparent cylinder (i.e., polycarbonate tube). The ratio of the particle diameter to the cylinder diameter was maintained very low to reduce the wall effect. The test section was sufficiently long to ensure the establishment of steady state (terminal velocity) condition. A fully transparent ruler was attached to the cylinder to monitor the position of the particle while settling. A moving digital video camera tracked the settling particle. The camera captured videos that showed the exact position of the particles as a function of time. Back lighting was used to enhance the clarity of the videos. At the bottom the settling cylinder, a manual valve was installed to discharge test fluid when the experiment was completed. Experiments with non-Newtonian fluids were performed at ambient temperature conditions. Tests with mineral oil were carried out at different temperatures to increase the number of data points. Cooling water was circulated through a copper coil immersed in the cylinder to maintain a constant fluid temperature condition during the experiment.

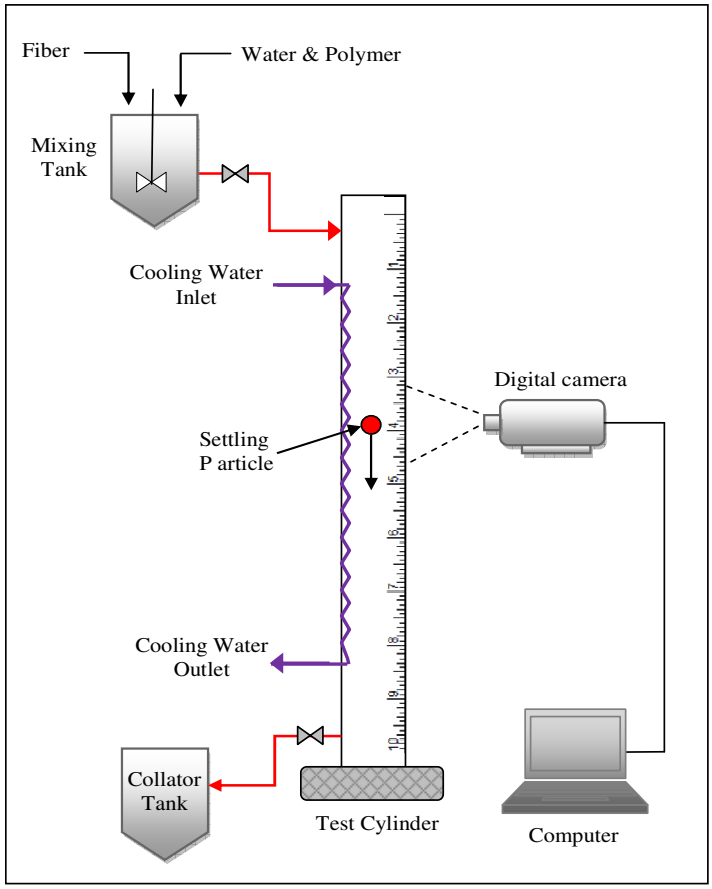

Fig. 5.1 Schematic of the experimental setup

5.3.2 Test Materials

Experiments were performed using three different base fluids: i) Mineral oil (Newtonian fluid); ii) 0.5 percent polyanionic cellulose (Polypac R) solution; and 0.25 percent xanthan gum (Xanvis) solution. Monofilament synthetic fiber particles (i.e., specific gravity of 0.9) were added to the base fluids to create suspensions of differing fiber concentrations (0.00, 0.02, 0.04, and 0.08 percent by weight). The fiber particles were flexible and easy to disperse in the fluid and had a relatively large aspect ratio (length = 10 mm and diameter = 100 μm). Spherical glass beads (2 mm to 8 mm) were used to carry out the experiments. To increase their visibility, all beads were painted red. In confirmation of the rheological study conducted in Section 4, the addition of fiber resulted in a negligible increase in shear stress **(Fig. 5.2**).

5.3.3 Test Procedure

A reliable test procedure was developed to measure settling velocity of solids particles in fiber suspensions. All the experiments were carried out using the same test procedure that consisted of the following:

Step 1. **Fluid Preparation:** Each experiment began by preparing the test fluid with desirable fiber and polymer concentrations. First powder polymer and water were mixed in a 5-gallon container. The polymeric fluid was left overnight to hydrate. The required amount of fiber was then added to the fluid and agitated using a stand mixer to achieve uniform dispersion. The rheology of the fiber suspension was measured using a rotational viscometer (Fann 35).

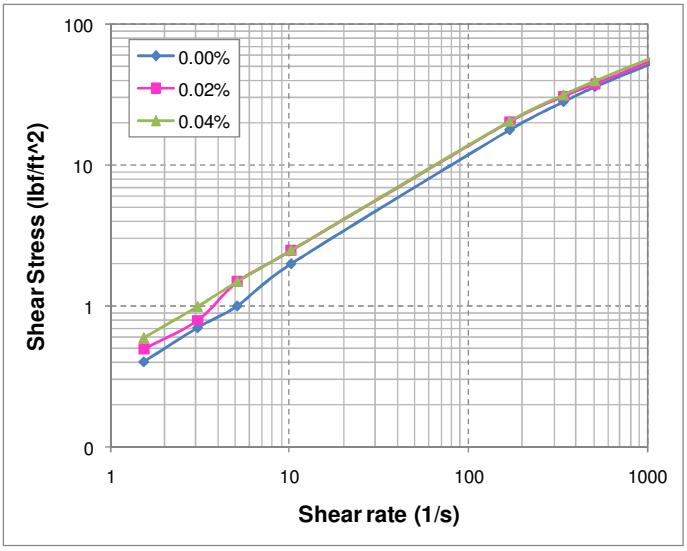

Fig. 5.2 Rheologies of 0.5% PAC based fluids with different fiber concentrations

Step 2. **Cylinder Filling:** The test fluid (base fluid or fiber suspension) was then transferred to the settling cylinder. The back-light bulb was turned on before dropping the particle into the settling container.

Step 3. **Particle Settling:** The glass particles were soaked in a separate container of test fluid. Then, each particle was brought to the center of the cylinder and released to settle in the fluid.

Step 4. **Particle Tracking:** As the particle settled through the fluid, it was tracked with the digital camera

to record its position as a function of time.

5.3.4 Test Results

Using recorded video clips, the position of the particle and corresponding time were determined over the length of the settling cylinder. The instantaneous settling velocity was determined from the position of the particle and settling duration (i.e., $V(t) = \Delta s/\Delta t$). **Fig. 5.3** presents the instantaneous settling velocity verses settling time. The figure shows both the transition and steady state settling regimes. At the experiment's initiation, the particle accelerated variably for a short time until a steady-state settling condition was established.

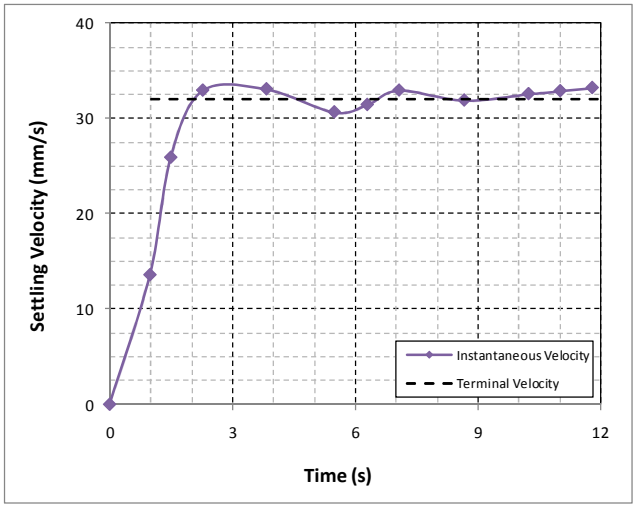

Fig. 5.3 Settling velocity of 6-mm spherical glass bead As a function of time in 0.7% PAC

The experimental measurements obtained from the base fluids (mineral oil and polymeric fluids) were analyzed and plotted on **Fig. 5.4** as the drag coefficient versus particle Reynolds Number (Re_p). Experiments with mineral oil were performed at different temperatures to cover a wide range of Reynolds Numbers (Re_p). For Re_p less than 0.8, the data points from the mineral oil experiments were highly correlated with the theoretical line ($C_{Dv} = 24/Re_p$), as was the Xanthan gum (XG)-based fluid. The viscoelastic properties of the polymer solutions tended to stabilize the flow and maintain the laminar flow conditions at higher particle Reynolds Numbers ($Re_p > 1.0$). XG- based fluids have been known to delay the onset of turbulence in pipes and annular flows (Escudier et al. 2009). Other high Re_p data points also match published measurements (Dedegil 1987) obtained from non-Newtonian fluids. The strong correlation between the theoretical line and the experimental data points indicated the accuracy of the measurements and minimal wall effect.

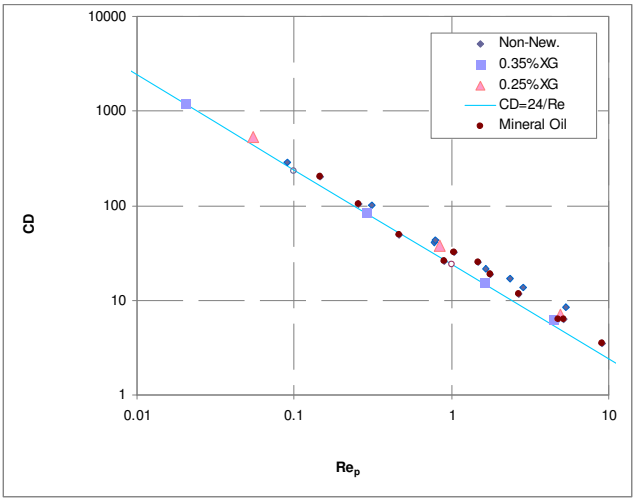

Fig. 5.4 Drag coefficient vs. particle Reynolds Number for base fluids

After establishing confidence in the measurements, settling tests were carried out using six different polymer base fluids (0.50 percent polyanionic cellulose (PAC), 0.70 percent PAC, 1.00 percent PAC, 0.15 percent XG, 0.25 percent XG, and 0.35 percent XG). **Fig. 5.5** shows the terminal settling velocity of particles versus particle size for different fiber concentrations in 0.50 percent PAC base fluid. The increase in fiber concentration consistently reduced the settling velocity. The smallest particle (2 mm) was fully suspended when the fiber concentration increased to 0.04 percent. At high fiber concentrations (greater than 0.04 percent), large particles were able to settle; however, at significantly reduced velocity. The high fiber concentration (0.08 percent) fluid was able to completely suspended 2-mm and 3-mm particles. Experimental results obtained from 0.25 percent xanthan gum solution (**Fig. 5.6**) showed a similar trend in reduction of settling velocity. Particles less than 5 mm were fully suspended when the fiber concentration was increased to 0.08 percent. In the XG-based fluids, the level of settling velocity reduction is highly pronounced at low concentrations. As the concentration increased, the impact of fiber diminished.

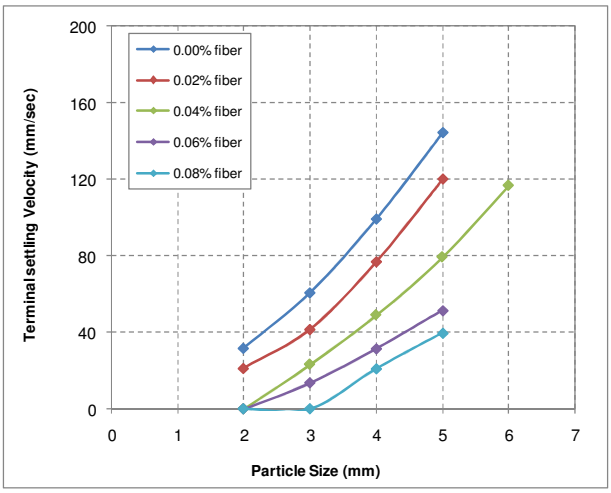

Fig. 5.5 Settling velocity particle in 0.5% PAC based fluid for different fiber concentrations

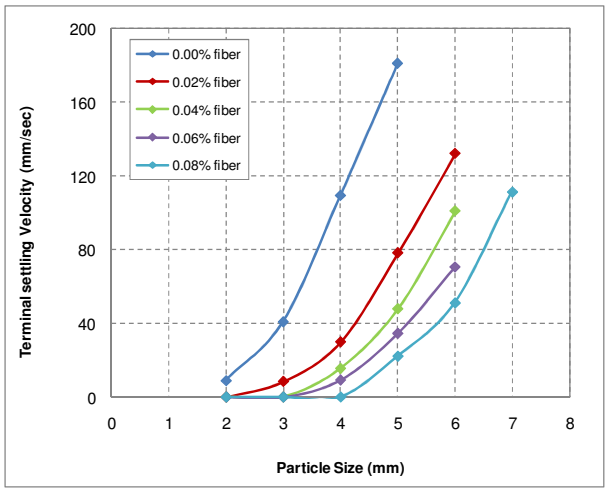

Fig. 5.6 Settling velocity particle in 0.25% XG based fluid for different fiber concentrations

No base fluids were able to suspend the particles fully. The base fluids tested did not exhibit high yield stress and therefore could not support the particles under static conditions. As shown previously, fiber has a minimal effect on fluid rheology. However, the fiber creates an additional drag mechanisms that can resist the motion of the particle. The additional drag due to the fiber can originate in different ways. Hydrodynamic effect of the fiber is critical at high settling velocities. As the settling velocity deceases, hydrodynamic resistance diminishes. The mechanical drag resulting from fiber network could be another mechanism that influences the behavior of particles. At low settling velocities, the mechanical drag becomes the dominant force. As a result, the fiber network provides the resistance required to suspend solids particles fully.

Figure 5.7 presents both the viscous and fiber drag forces as a function of fiber concentration. According to Eqn. (5.5), at steady state conditions the total drag force balances the difference between the weight and the buoyancy force. As a result, total drag remains constant as the fiber concentration increases. This is because the addition of fiber does not have significant effect on the density of the suspension, which affects the buoyancy force. In base fluid, the drag force develops only due to the viscous forces. However, as the fiber concentration increases, the fiber drag becomes substantial resulting in reduced settling velocity and viscous drag.

For a 5-mm particle (**Fig. 5.7a**), at approximately 0.04 percent the viscous and fiber drag forces became comparable and the force curves cross each other. Field experiences show that fiber sweeps containing nearly 0.04 percent provides optimum hole-cleaning with a limited quantity of fiber (Unnecessarily large quantity of fiber in the mud circulation system can cause operational problems such as plugging of downhole tools and surface separation equipment.). As the particle size decreased (**Fig. 5.7b**), the cross point shifted toward the left, indicating the reduction in the fiber requirement in the sweep fluids. As depicted from the figures, further increase in fiber concentration made the fiber drag asymptotically approach the value of the total drag force. Therefore, the effect of fiber diminished as the concentration increased.

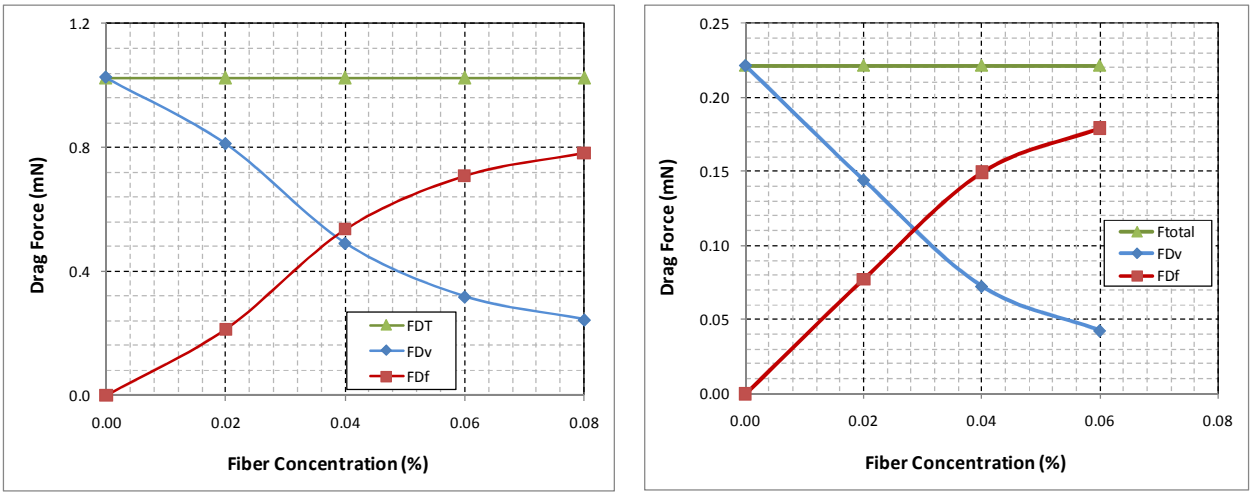

(a) **(b)**

Fig. 5.7 Comparison of fiber drag with viscous drag acting on a particle in 0.5% PAC based fluid as a function of fiber concentration: a) 5-mm diameter particle; and 3-mm diameter particle

5.4 Analysis of Results and Discussions

To develop generalized correlations for fiber drag coefficient, the experimental measurements (terminal velocities) were used to determine the viscous drag coefficient (C_{Dv}) and particle Reynolds Number (Re_p):

$$Re_p = \frac{\rho d V_s}{\mu_{app}} \quad \text{.....(5.10)}$$

where the apparent viscosity can be expressed as:

$$\mu_{app} = \tau_y + k(\dot{\gamma})^{n-1} \quad \text{.....(5.11)}$$

The representative shear rate $\dot{\gamma} = V_s/d$. The viscous drag coefficient is calculated from Eqn. (5.2) using the settling velocity data from the base fluid. Then, the fiber drag coefficient is determined from Eqn. (5.8).

Figure 5.8 shows the fiber drag coefficient as a function of particle Reynolds Number for different fiber concentrations. The data points formed a straight line on logarithmic plot with only minor deviations. In order to get a single curve, the fiber drag coefficient was normalized by the fiber concentration as C_{Df}/C^{α}. After normalization, the data points from different fluids (both Newtonian and non-Newtonian fluids) laid approximately on a single straight line on log-log plot (**Fig. 5.9**).

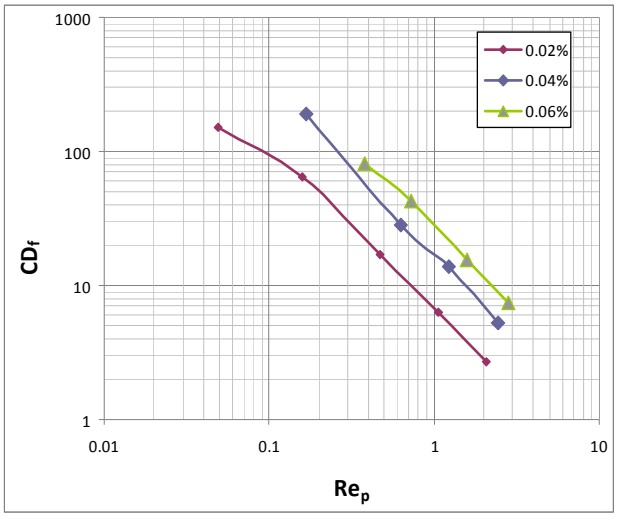

Fig. 5.8 Fiber drag coefficient vs. Reynolds Number for 0.7% PAC based fluid

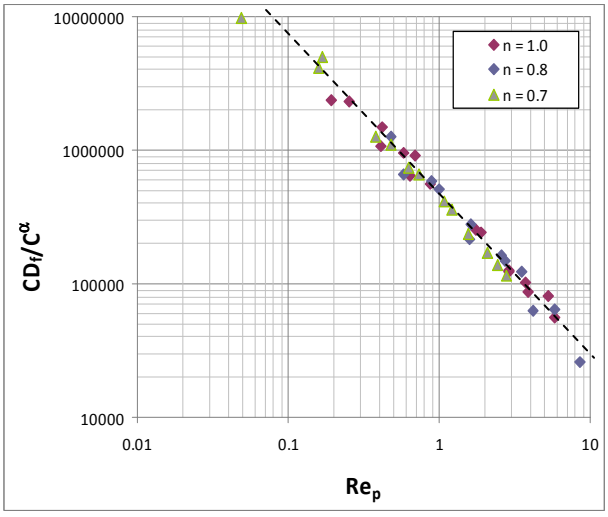

Fig. 5.9 Normalized fiber drag coefficient vs. Reynolds Number for different fluids

By applying regression analysis, the following correlation was developed to estimate the fiber drag coefficient in Newtonian and Power Law fluids:

$$\frac{C_{Df}}{C^{\alpha}} = 4.47 \times 10^{5} Re_{p}^{-1.176} \quad \text{..... (5.12)}$$

where the concentration exponent is:

$$\alpha = 1.4187 - 0.2397 \exp\left(-0.5\left(\ln\left(\frac{n}{0.8627}\right)/0.1763\right)^{2}\right) \quad \text{..... (5.13)}$$

5.5 Model Predictions

In order to assess the accuracy of Eqn. (5.12), model predictions were compared to experimental measurements (**Figs. 5.10** and **5.11**). The comparison of results showed a good agreement between measurements and predictions. This correlation demonstrated that fiber drag coefficient was a function of particle Reynolds Number, fiber concentration, and fluid behavior index. A similar correlation was developed to predict fiber drag coefficient in XG-based fluids, which exhibit yield stress. Results showed a satisfactory agreement between measurement and predictions.

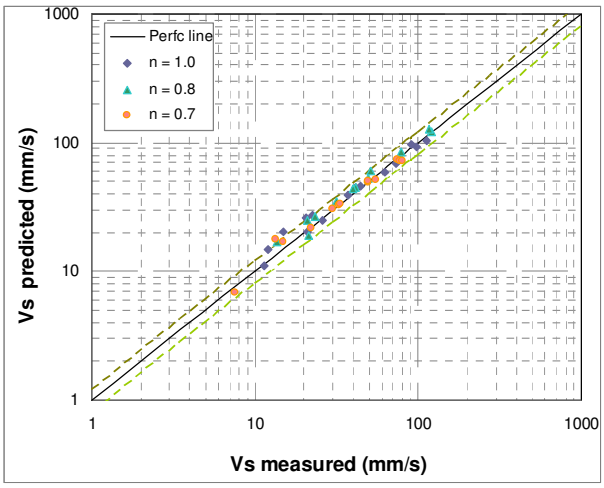

Fig. 5.10 Predicted vs. measured settling velocity for different PAC based fluids

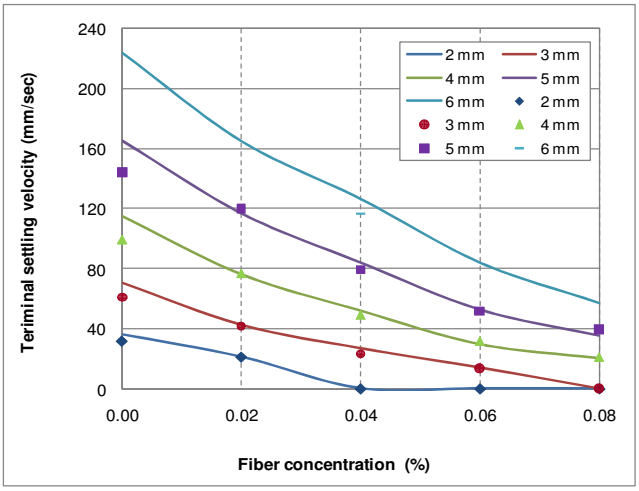

Fig. 5.11 Predicted and measured settling velocity vs. fiber concentration for 0.5% PAC

Figs. 5.10 and **5.11** provide better understanding of the level of settling velocity reduction due to the presence of fiber particles in the fluid system. Addition of fiber had a more pronounced effect on XG-based fluids than PAC-based fluids. When 0.02 percent of fiber was added into the XG-based fluid, a 50 percent or greater reduction in the settling velocity was observed. However, PAC-based fluids did not exhibit such a sharp reduction. This could be attributed to the difference in molecular structure. XG polymer has a branched structure that tends to entangle with fiber particles to create strong polymer-fiber network, which provides greater support to the particles.

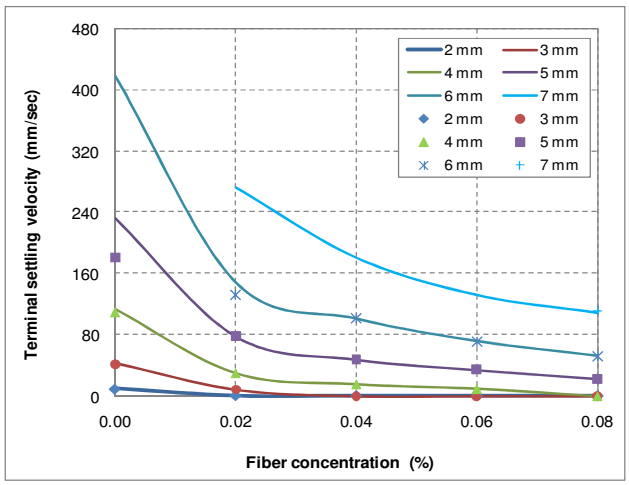

Fig. 5.12 Predicted and measured settling velocity vs. fiber concentration for 0.25% XG

5.6 Conclusions

Settling behavior of spherical particles in fiber-containing fluids was investigated. Fiber concentration was varied 0.00 to 0.08 percent. Measurements showed significant reduction in settling velocity in fiber-containing fluids. Based on the experimental results and theoretical analysis, the following conclusions were made:

- Fiber particles that were uniformly dispersed in fluids hinder the motion and reduce the settling velocity of suspended particles.
- Fiber concentration (up to 0.08 percent w/w) had a negligible effect on the rheological properties of the fluid.
- The fiber drag or the hinder effect of the fiber was related to the fiber concentration, properties of the fluid, and size, density, and settling velocity of the particle.
- Particles suspended in fiber sweep exhibited an additional drag force under both static and dynamic conditions. The correlations developed in this investigation provided reasonable settling velocity prediction in fiber suspensions.

Nomenclature

A_P = projection area of a particle

C_{Dv} = Viscous drag coefficient

C_{Df} = Fiber drag coefficient

d = diameter of a particle

F_B = Buoyancy force

F_D = Drag force

F_{Df} = Fiber drag force

F_{DT} = Total drag force

F_{Dv} = Viscous drag force

F_g = Gravitational force

g = gravitational acceleration

K = consistency index

m = Mass of a solids particle

N_{Rep} = Reynolds Number

n = fluid behavior index

Re = Reynolds Number

Re_P = Particle Reynolds Number

t = Time

V = Instantaneous settling velocity of a particle

V_s = Terminal settling velocity of a particle

Greek Letters

$\dot{\gamma}$ = Shear rate

μ = fluid viscosity

μ_{app} = Apparent fluid viscosity

ρ_f = Fluid density

ρ_p = Density of a particle

τ_y = yield stress

References

Ahmed, R.M. and Takach, N.E., 2008. Fiber Sweeps for Hole Cleaning. Paper SPE 113746 presented at the SPE/ICoTA Coiled Tubing and Well Intervention Conference and Exhibition, The Woodlands, Texas, 1-2 April.

Bivins. C.H., Bomey, CV., Fredd, C., Lassek, J., Sullivan, P., Engels, J., Fielder, E. O., Gorham, T., Judd, T., Mogollon, A E.S., Tabor, L., Munoz, A., and Willberg, D., 2005. New fibers for hydraulic fracturing. Oilfield Review, Vol. 17, Issue 2, Schlumberger.

Baldock, T.E., Tomkins, M.R., Nielsen, P., Hughes, M.G., 2004. Settling velocity of sediments at high concentrations. Coastal Eng. 51, 91-100.

Bulgachev, R.V. and Pouget, P., 2006., New Experience in Monofilament Fiber Tandem Sweeps Hole Cleaning Performance on Kharyaga Oilfield, Timan-Pechora Region of Russia. Paper SPE 101961, presented at the SPE Russian Oil and Gas Technical Conference and Exhibition, Moscow, 3–6 October. doi: 10.2118/101961-MS.

Cameron, C., Helmy, H., and Haikal, M. 2003., Fibrous LCM Sweeps Enhance Hole Cleaning and ROP on Extended Reach Well in Abu Dhabi. Paper SPE 81419 presented at the Middle East Oil Show, Bahrain, 9–12 June. doi: 10.2118/81419-MS.

Chhabra, R.P. and Peri, S.S. 1991., A simple method for the estimation of free fall velocity of spherical particles in Power Law liquids. Powder Technology 67 (1991), pp. 287–290.

Chhabra, R. P. 2007., Bubbles, drops, and particles in non-Newtonian fluids, Second Edition, Taylor and Francis Group, CRC Press, Florida.

Chhabra, R.P., 1980. Ph.D. Thesis, Monash University, Melbourne, Australia.

Chhabra. R.P., Agarwal. S. and Chaudhary. K., 2003. A note on wall effect on the terminal falling velocity of a sphere in quiescent Newtonian media in cylindrical tube. Powder Technology, 129, 53-58.

Chien. S.F., 1994. Settling velocity of irregularly shaped particles, SPE Drilling & Completion, Vol. 9, Num. 4, 281-289.

Dallon, D.S., 1967. A drag coefficient correlation for spheres settling in Ellis fluids. PhD Thesis, University of Utah, Salt Lake City, UT.

Daneshy, A.A., 1978. Numerical Solution of Sand Transport in Hydraulic Fracturing. Journal of Petroleum Technology, Vol. 30, Number 1, 132-140.

Dedegil, M.Y., 1987. Drag coefficient and settling velocity of particles in non-Newtonian suspensions. Journal of fluids engineering, vol. 109/319.

De Felice, R., 1996. A relationship for the wall effect on the settling velocity of sphere at any flow regime. Int. J. Multiphase Flow, vol. 22, No.3, 527-533.

Govier, G.W. and Aziz. K., 1972. The flow of complex mixtures in pipes, Second Edition, Krieger Pub Co., Malabar, Florida.

George, M., Ahmed, R. and Growcock, F., 2011. Rheological Properties of Fiber-Containing Drilling Sweeps at Ambient and High Temperature Conditions. Paper AADE-11-NTCE-35, presented at the 2011 AADE National Technical Conference and Exhibition, Houston, April 12-14.

Harlen, O.G., Sundararajakumar, R.R., Koch. D.L., 1999. Numerical simulations of a sphere settling through a suspension of neutrally buoyant fibers. J. fluid mech., vol. 388, pp. 355-388.

Hemphill, T. and Rojas, J.C., 2002. Exploration Drilling Fluid Sweeps: Their Evaluation, Timing, and Applications. Paper SPE 77448 presented at the SPE Annual Technical Conference and Exhibition, San Antonio, Texas, USA, 29 September–2 October. doi: 10.2118/77448-MS.

Highgate, D.J. and Whorlow, R.W., 1967. The viscous resistance to motion of a sphere falling through a sheared non-Newtonian liquid. J. Appl. Phys. 18 1019.

Holzer, A. and Sommerfeld, M., 2008. New simple correlation formula for the drag coefficient of non-spherical particle, Powder Technology, Vol. 184, Issue 3, 361-365.

Jin, L. and Penny, G.S., 1995. Dimensionless methods for study of particle settling in Non-Newtonian fluids. Journal of Petroleum Technology, Vol. 47, Num. 3, 223-228.

Kelessidis. V.C., 2004. An explicit equation for the terminal velocity of solid spheres falling in pesudoplastic liquid, Chem. Eng. 59, 4435-4445.

Lali, A.M., Khare, A.S. and Joshi, J.B., 1988. Behavior of solid particles in viscous Non-Newtonian solutions: settling velocity, wall effect and bed expansion in solid-liquid fluidized beds. Powder Technology, 57, 39-50.

Marti, I., Höfler,O., Fischer P. and Windhab, E.J., 2005 Rheology of concentrated suspensions containing mixtures of spheres and fibres, Rheol Acta, 44: 502–512

Prakash, S., 1983. Experimental evaluation of terminal velocity in non-Newtonian fluids in the turbulent region, Ind. Chem. Eng. 25 (1983), pp. 1–4.

Phani, B.G., Yajun, L., Jay, N., Roger, B. and Mukul, M.S., 2004. Modeling proppant settling in water-Fracs, paper SPE 89875, presented at the SPE Annual Technical Conference and Exhibition, 26-29 September, Houston, Texas.

Rajabian, M., Dubois, C., Grmela, M. and Carreau, P.J., 2008. Effects of polymer–fiber interactions on rheology and flow behavior of suspensions of semi-flexible fibers in polymeric liquids. Rheol Acta 47:701–717.

Sadowski.Z., Mager. J. and Laskowski. J. 1978., Hindered settling of coagulating suspensions. Powder Technology, Vol. 21, Issue 1, 73-79.

Shah, S.N., El Fadili. Y. and Chhabra. R.P., 2007. New model for single spherical particle settling velocity in power law (visco-inelastic) fluids. Int. J. multiphase flow. 33, 51-66.

Shah, S.N., 1982. Proppant settling correlations for Non-Newtonian fluids under static and dynamic conditions. SPE Journal, Vol. 22, Num. 2, 164-170.

Smith, T.N., 1998. A model of settling velocity. Chemical Eng. Science, Vol. 53, Issue 2, 315-323.

6. Hole-cleaning Performance of Fiber Sweeps

An experimental study was performed to investigate the rheology, hydraulics, and wellbore cleaning (sweep tests) performance of aqueous and non-aqueous based fiber-containing fluids. The overall focus of this entire body of research was to determine wellbore cleaning effectiveness of fiber-containing fluid under actual field conditions. Despite the desire to simulate an operational scale environment, the atmospheric conditions and functional variables were limited by the test equipment. As such, the system was open to the atmosphere (standard atmospheric condition) and the operating fluid temperature could be slightly elevated above ambient, as the water-based and synthetic-based fluids flowed through the recirculation pump installed on the flow loop. In order to calibrate the equipment and perfect the experimental procedures, some initial rheology and hole-cleaning experiments were run with water-based xanthan gum fluid. The WBM sweep experiments were also used to correlate the critical cuttings velocity model with experimental predictions (Section 7).

6.1 Introduction

Multiple field-tested techniques have been introduced over the years to prevent and reduce the proclivity of drilled cuttings to settle within the wellbore, therefore improving hole-cleaning and cuttings transport. Previous studies indicated that cuttings transport in directional wells is dependent on fluid rheology, wellbore inclination angle, rotary speed of the drillpipe, flow rate, wellbore geometry, and other drilling parameters (Valluri et al. 2006). Considering these factors, the easiest and most economical procedures involve adding weighting agents and viscosifiers to the drilling fluid to increase the fluid's cutting transport capability. As such, sweeps conventionally utilized in the industry are commonly categorized as i) high-viscosity; ii) high-density; iii) low-viscosity; iv) combination; and v) tandem sweeps (Hemphill 2002). Sweeps provide a number of benefits, such as reducing cuttings beds and subsequent decrease in annular pressure loss, as well as a reduction in torque and drag at the surface. Increasing the flow rate also provides extra lifting potential of the sweeps but must be closely monitored depending on the characteristics of the well. Pressure losses along the wellbore, as well as the equivalent circulating density (ECD), must be considered when designing and applying sweep fluids. As a result, hole-cleaning fiber is added to the sweep fluid to improve its performance with a negligible increase in viscosity and pressure loss (George et al. 2011). Previous studies (Marti et al. 2005; Rajabian et al. 2005; Guo et al. 2005) also showed similar trends, as the apparent viscosity of fiber-polymer suspensions slightly increased linearly with increasing fiber concentration up to an approximate critical fiber concentration. At this critical concentration, the apparent viscosity increased exponentially with a small increase in fiber concentration. For field applications and for this study, fiber concentrations are relatively insignificant and well below the critical threshold.

Previous experimental studies (Ahmed and Takach 2008) and field applications (Cameron et al. 2003; Bulgachev & Pouget 2006) reported that adding a small amount of synthetic monofilament fiber (less than 0.1 percent by weight) improves solid transport and hole-cleaning efficiency of the sweep over comparable non-fiber sweeps, and with no noticeable change in fluid rheology. This favorable performance may be attributed to the dynamic influence between the adjacent fibers. When fully dispersed in the sweep fluid, fiber can form a stable network structure that tends to support cuttings due to fiber-fiber and fiber-fluid interactions. The fiber-fiber interactions can be by direct mechanical contact and/or hydrodynamic interference among fiber particles. Mechanical contact among fibers improves the solids-carrying capacity of the fluid (Ahmed and Takach 2008). The mechanical contact between the fibers and the cuttings beds aids in resuspending cuttings deposited on the low-side of the wellbore. As the fibers flow through the annulus, mechanical stresses develop between the settled cuttings and the fibers. These mechanical stresses result in a frictional force, which helps to re-suspend the cuttings, while the fiber networks carry the solids to the surface. Also aiding in the solids transport is the fiber-fiber interaction that enables the fiber network to move as a plug. Hence, at the surface of the cuttings bed the fiber may have a higher velocity than the fluid phase, which is typically very low. These fast moving fibers can therefore transfer more momentum to the deposited solids, overcoming the static frictional forces and initiating particle movement.

6.2 Experimental Setup

Hole-cleaning abilities of fiber-containing fluids (fiber sweep), which are similar to those used for sweeps in real wells, were investigated. Fiber sweep performance tests were conducted using a flow loop apparatus (**Fig. 6.1**) available at the Well Construction Technology Center (WCTC). This device, as currently configured (**Fig. 6.2**), provides the capability to perform pipe viscometer and annular hydraulic measurements on any given fluid, as well as cuttings removal tests. The primary mechanical components of the flow loop system are:

a. 150 gal mixing tank
b. Centrifugal pump
c. 4” x 2” annulus
d. 1.75” pipe viscometer
e. Two (2) hydrocyclones
f. Cuttings collection tank
g. Cuttings injection tank
h. Data Acquisition System (DAS)

The test fluid was mixed in the 150 gallon tank using a shaft and propeller agitator. The fluid then flowed through the centrifugal pump, through 2-inch steel piping and the cuttings injection tank (when opened), and into the two (2) parallel polycarbonate test sections. The two (2) test sections, 1.75-inch pipe viscometer and 4 inch by 2 inch annulus, contained differential pressure (DP) meters which were connected to a central desktop computer that contained the data acquisitions and control system (DAS). All readings from the DP meters were recorded by the DAS. The DAS also controlled the flow rate and drillpipe rotation and recorded all the system information, such as fluid temperature, pressure, density, flow rate, and test time. Two coriolis flow meters (F1 and F2) were installed at the inlet and outlet of the test sections. The flow meters measured mass flow rate and density of the fluid. The entire test section was constructed as an independent unit that was connected to the pump and tanks by quick-connecting hoses. The simply supported, hinged test section truss could be elevated at the free end to allow for an inclined orientation.

The fluid from the test sections was then routed to a set of parallel hydrocyclones, which in turn routed the cuttings to a collection tank below and returned the fluid to the mixing tank. During cuttings collection, the valve between the collection and injection tanks was open. However, during cuttings injection the valve was closed to prevent fluid backflow up through the hydrocyclones.

Fig. 6.1 Flow loop in inclined position

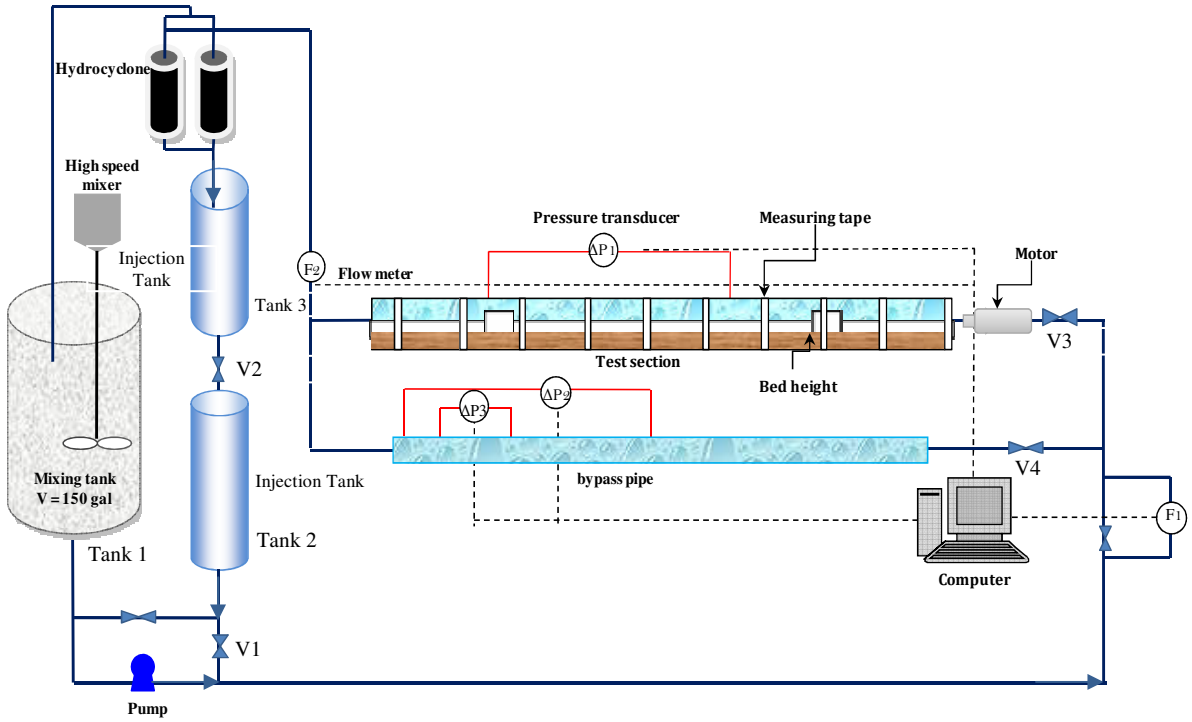

Fig. 6.2 Flow loop schematic

To simulate the cuttings that would be found in the wellbore during drilling, 8/16-mesh silica sand was used. The sand particles were circulated through the system and used to create a bed in the annulus for wellbore cleaning experiments. During the removal process, the sand was diverted back to the collection tank through the hydrocyclones. According to the sieve analysis (**Fig. 6.3**), 91 percent of the sand was 1.20 mm in diameter or greater

SIEVE SIZE	% PASSING
3/8 inch	100
No. 4	100
No. 8	96
No. 16	9
No. 30	1
No. 50	0
No. 100	0
No. 200	0.0
Fineness Modulus	3.93

Fig. 6.3 Sieve analysis of silica sand, 8/16 mesh (Test Methods: AASHTO T27, T11, T255, T248)

6.3 Experimental Procedure

Before wellbore cleaning experiments were run, the pipe viscometer and annulus hydraulic measurements were taken for the xanthan gum drilling fluid, unweighted SBM, and the weighted SBM plus the incremental fiber concentrations. The process required from fluid formulation to hole-cleaning efficiency results was as follows:

Step 1. Preparation of Base Fluid: The fluids used for the wellbore cleaning experiments were unweighted xanthan gum drilling fluid (WBM) and a weighted synthetic-based drilling fluid system (SBM). This synthetic-based, invert emulsion fluid system consisted of multiple components (**Fig. 6.4**):

a) Synthetic-base (Internal Olefin, IO 16-18, 6.45 ppg)
b) Viscosifier
c) Lime
d) Primary and secondary emulsifiers
e) Brine

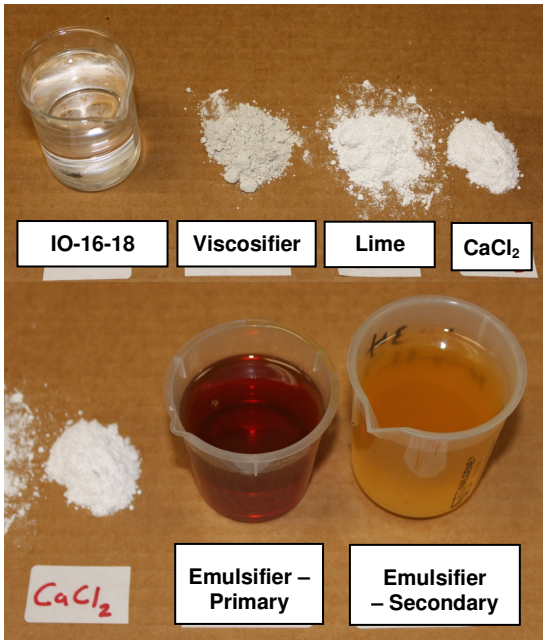

Fig. 6.4 Synthetic-based fluid constituents

This fluid system shipped piecewise (**Fig. 6.5**), i.e., we were responsible for mixing the components at the specified concentrations in order to achieve the proper invert emulsion properties. Based on the required proportions in **Fig. 6.6**, the fluid was mixed using a high-speed mixer (**Fig. 6.7**) and the following procedure:

a. Add base oil
b. Mix in lime and clay for 10 minutes
c. Add emulsifier(s) and mix for 10 minutes
d. Add brine and mix for 20 minutes

In order to utilize the available mixer, the fluid had to be mixed five (5) gallons at a time. Had a larger mixer or dispersator been available, the mixing time would have been reduced considerably. Each mixed five-gallon batch of synthetic-based fluid was then transferred to the flow loop mixing tank (Tank 1).

Fig. 6.5 Packaged components of synthetic-based fluid

Fluid Formulation	*SBM*
IO 16-18, bbl	0.66
LVT-200, bbl	-
VG-PLUS, ppb	6.0
LIME, ppb	3.0
SUREMUL, ppb	7.0
SUREWET, ppb	2.0
MEGAMUL, ppb	-
*$CaCl_2$, ppb	29.43
*Water, bbl	97.64

Fig. 6.6 SBM component concentrations

Fig. 6.7 High-speed mixer

Step 2. Weighting up (SBM): The WBM hydraulics and sweep experiments were conducted with unweighted fluids (i.e., specific gravity of 1). By not introducing barite into the WBM, the experimental error was reduced, and the cuttings behavior was easily observed in the annulus. Adding barite would have resulted in a dark brown, murky colored fluid that would have prohibited visual observation of cuttings beds removal.

Approximately 35 batches of unweighted SBM were mixed and transferred to the flow loop mixing tank (Tank 1), with an estimated total weight of 955 lb. The unweighted SBM was agitated in the mixing tank (Tank 1) to ensure homogeneity, and multiple samples were taken to measure density, which equaled 7.43 lb/gal. For the wellbore cleaning experiments, the desired fluid weight was 10.5 ppg. In order to achieve this fluid density, 675 lb. of barite were slowly added to the mixing tank while the fluid was being agitated. In order to achieve maximum barite dispersion and homogeneity, the fluid and barite were circulated through the flow loop, while also being agitated in the mixing tank. After a sufficient length of time, multiple samples were again taken from the mixing tank (Tank 1) and the density was checked. Taking the average of the measurements, the density of the weighted fluid was calculated to be 10.6 lb/gal.

Step 3. Addition of Fiber: In a similar manner to the rheology and stability experiments, incremental amounts of the synthetic monofilament fiber were added to the base fluid. A test matrix shows the different variables and fiber concentrations used for the pipe viscometer and hole-cleaning experiments (**Tables 6.1 and 6.2**). Based on the desired weight percentage, the quantity of fiber needed for the experiment was determined and prepared.

The manufacturing and packaging process used for the fibers resulted in a compact mixture of isotropic fiber clumps. When adding fiber to the sweep fluid on a rig, the fiber goes through the hopper and exits the drillstring through the drill bit nozzle. The restriction at the bit results in exponentially increased velocity, which immediately disperses the fiber. However, in the flow loop, no such restriction existed, and the system pressure and maximum flow rate were incapable of dispersion on their own. In order to promote a homogeneous fiber dispersion, the fiber clumps were meticulously pulled apart before they were added to the system. The pulled fiber was added to the mixing tank while the fluid was being circulated through the system. This was done to enhance dispersion of the fiber and prevent the formation of clumps in the fluid.

Step 4. Pipe Viscometer Measurements: The test fluid (base fluid and fiber) was first thoroughly homogenized by circulating through the flow loop at a high flow rate until the fluid temperature reached approximately 40°C due to viscous heating. Once the fluid increased to proper temperature, the flow was diverted through the 1.75-inch pipe viscometer. Starting with a flow rate of 10 gpm, the fluid was allowed to flow until the data acquisition system stabilized the flow rate and a sufficient number of data points were recorded. The flow rate was then adjusted accordingly.

Step 5. Cuttings Bed/Accumulation in Annulus: Once all pipe viscometer measurements were taken, the flow was diverted back to the annulus. The valve (V1) below the cuttings injection tank (Tank 2) was then opened, while the valve (V2) between the collection tank (Tank 3) and injection tank (Tank 2) was closed. The flow was again initiated at a medium rate (~ 40 gpm) until cuttings begin to appear in the annulus. The flow rate was then decreased (~ 10 gpm) to allow the cuttings to settle out of the fluid and form a bed on the low side of the annulus. This process was continued until the cuttings bed was sufficiently deep and is no longer increasing in depth. For the high-inertia, SBM this process took up to 30 - 45 minutes, since the cuttings did not easily settle out of the high yield stress, plug flow zone.

Step 6. Flush Cuttings from System: Once the cuttings bed was established, the injection tank (Tank 2) outlet valve (V1) was closed, and the middle valve (V2) was opened. Then the valve to the annulus (V3) was closed while the pipe viscometer valve (V4) was opened. Once the valve configurations were complete, the fluid was pumped through the system at a high flow rate to clear the piping of any remaining cuttings. This process was continued until no cuttings were observed in the transparent pipe viscometer, and until the density readings of the inlet and outlet coriolis flow meters (F1 and F2) were approximately equivalent.

Step 7. Sweep Fluid Circulation/Cuttings Removal: Once the latent cuttings were flushed from the system, the flow was stopped and the annulus and pipe viscometer valves were opened and closed, respectively. Flow again was initiated at a low flow rate (10 gpm), with or without pipe rotation, depending on the test matrix. The fluid was circulated through the annulus until the density readings the coriolis meters at the entrance and exit of the annulus converged to within 0.015 g/cc.

Step 8. Change in Inclination: The initial experiments were conducted with the annulus in the horizontal position ($\theta = 90°$). For each SBM and fiber formulation, the test matrix was followed varying flow rate and pipe rotation in the horizontal orientation. Then, one end of the annulus test section was elevated ($\theta = 72°$) to simulate an inclined wellbore, as shown in **Fig. 6.1**. At this annulus orientation, the test matrix experiments were ran again.

Modified Procedure in Step 6 for SBM Tests

Theoretically, after a certain amount of time at a steady flow rate, the fluid will have removed all the cuttings possible at that given flow rate. That is, all possible cuttings from the top of the cuttings bed will be swept away for a given fluid velocity and inertia. An increase in the flow rate would result in an increase in velocity and accompanying inertia, which would remove another layer of cuttings from the bed. However, with the weighted SBM, the density difference between the annulus entrance and exit would never converge to 0.015 g/cc. This is attributed to the barite in the fluid, which may result in some inconsistencies in density. One of the advantages of using the non-aqueous fluid systems is their ability to suspend cuttings, and this may have attributed to the non-converging densities. In other words, the fluid may have still been holding very fine sand particles in suspension in the mixing tank and throughout the system.

Due to the difficulty in attaining a satisfactory density difference, the test procedure had to be modified. In order to minimize error between the experiments, the sweep experiment time was held constant at 30 minutes. The 30-minute duration was sufficient to establish equilibrium conditions in the test section. The cuttings removal/sweep experiments were timed, the flow was stopped after 30 minutes, and the data was recorded. This process was repeated for each flow rate interval.

6.4 Experimental Test Matrix

Two hole-cleaning experiments (WBM and SBM) were conducted. The research was compartmentalized to accommodate two diverging deliverables. The culmination of the first set of experiments allowed for the subsequent modeling work and the initiation of the second set of experiments.

6.4.1 WBM Test Matrix

The first group of experiments focused on unweighted xanthan gum (FLO-VIS L) drilling fluid (WBM). A test matrix of critical cuttings transport velocity experiments was developed to achieve the study objectives presented in Section 7. The final matrix is shown in **Table 6.1**.

Sand particles with an average diameter of 2 mm were used in the experiment. The tests were performed at different flow rates (20, 30 ... 100 gpm) to provide a wide range of bed height measurements. The rheological properties of the test fluids were measured using rotational viscometers and presented in Table 6.1. Two test fluids with similar flow curves were used in the sweep experiments.

Table 6.1 WBM flow loop test matrix and rheological properties

Fluid	Fiber concentration % by w/w	Drill pipe rotation (rpm)	Hole angle Degree	Fluid properties		
				K ($Pa.S^n$)	n	T_y (Pa)
0.70%	0.00	0,25,50,75	90º, 70º	0.9	0.32	1.58
	0.02	0,25,50,75	90º, 70º	0.9	0.32	1.58
	0.04	0,25,50,75	90º, 70º	0.9	0.32	1.58
	0.06	0,25,50,75	90º, 70º	0.9	0.32	1.58

6.4.2 SBM Test Matrix

The second set of hole-cleaning experiments was conducted using weighted synthetic-based mud (SBM). With respect to the original objectives of this project, these experiments were in accordance with the project deliverables and provided insight into the performance of fiber-containing synthetic-based drilling fluids. The test matrix for the SBM tests, shown in **Table 6.2**, contains the same variables.

Table 6.2 SBM flow loop test matrix

Sweep Fluid	Weighting Agent	Fiber Concentration (%)	Inclination Angle	Flow Rate Q (gpm)	Pipe Viscometer	Sweep Experiment
XG-based Fluid	None 8.33 ppg	0.00	72°	10 □80	Y	Y
(15.7 lb Flovis ® / 175 gal Water)	None 8.33 ppg	0.02	72°	10 □80	Y	Y
Synthetic-based Fluid	None 7.50 ppg	0.00	90°, 72°	10 □80	Y	N
Synthetic-based Mud (SBM)	Barite 10.6 ppg	0.00	90°, 72°	10 □80	Y	Y
	Barite 10.6 ppg	0.02	90°, 72°	10 □80	Y	Y
	Barite 10.6 ppg	0.04	90°, 72°	10 □80	Y	Y
	Barite 10.6 ppg	0.06	90°, 72°	10 □80	Y	Y

6.5 Experimental Results

Using the previously described experimental setup and procedure, multiple tests were conducted and data recorded. After Step 5 of the experimental procedure, the height of the cuttings bed was recorded at all 15 locations along the annulus. The measurement locations were demarcated by measuring tapes that have been attached to the outside circumference of the annulus (**Fig. 6.8**). The average of these measurements was calculated and recorded as the initial bed height. From the circumferential bed height measurements, the fluid flow area could be calculated, as well as the cuttings bed wetted perimeter, hydraulic radius and depth (Appendix D). **Fig. 6.9** shows the average dimensionless bed height versus varying flow rates.

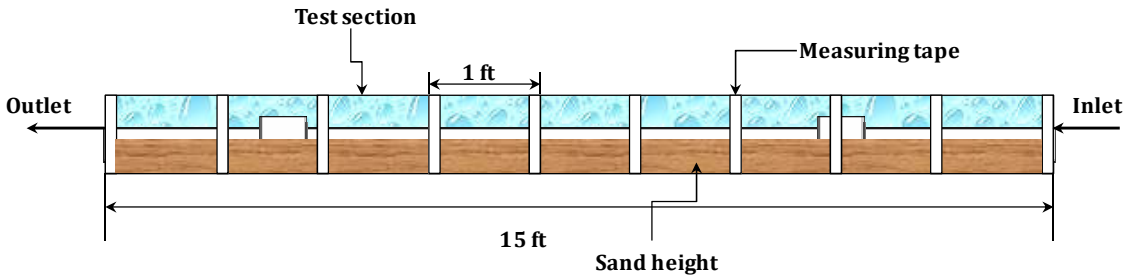

Fig. 6.8 Annulus test section bed height measuring tapes

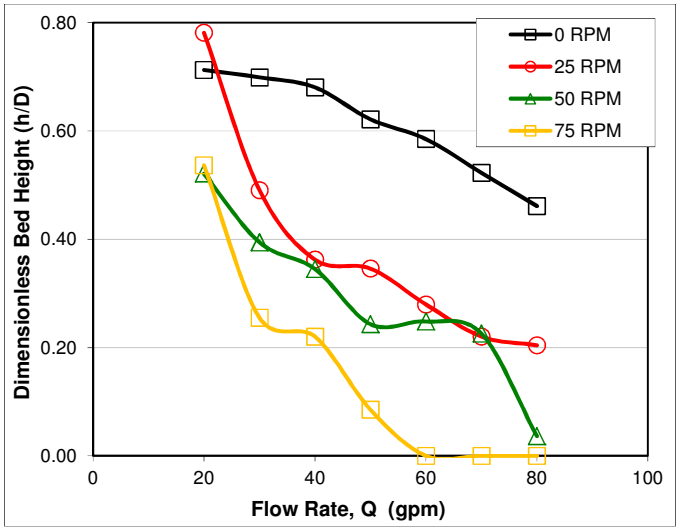

Fig. 6.9 Bed height vs. flow rate for XG based fluid sweep (no fiber), inclined annulus (8.33 ppg)

6.5.1 Dynamic Variation of Cuttings Bed Height

The purpose of the annular test section in the flow loop was to provide a visual basis for measurements and an understanding of flow behavior. In order to achieve the required visibility, the outer pipe must be transparent, which requires relatively low strength pipe compared to the traditional casing or drillpipe.

Polycarbonate was used for this outer pipe, and due to its susceptibility to cracking, a hollow, thin-walled pipe was used to simulate the drillstring. As such, the drillpipe was not overly heavily, and did not rest in a completely centered eccentric position within the annulus. This became particularly apparent during pipe rotation because the pipe wobbled in a random, unpredictable fashion down the entire length of the annulus, hitting the sides of the outer polycarbonate tube.

After the cuttings bed built in the annulus, the drillpipe was completely covered by the sand particles, therefore eliminating the possibility of visually confirming its eccentric location. In order to eliminate error and provide repeatable results, the drillpipe was manually rotated to the same position every time measurements are taken. During the prosecution of the sweep experiments when utilizing pipe rotation, the cuttings bed height was observed to vary in rhythm with the drillpipe rotation. As the pipe rotated, one side of the cuttings bed rose while the other side dipped (**Fig. 6.10**). As the pipe continued to rotate, this phenomenon was reversed.

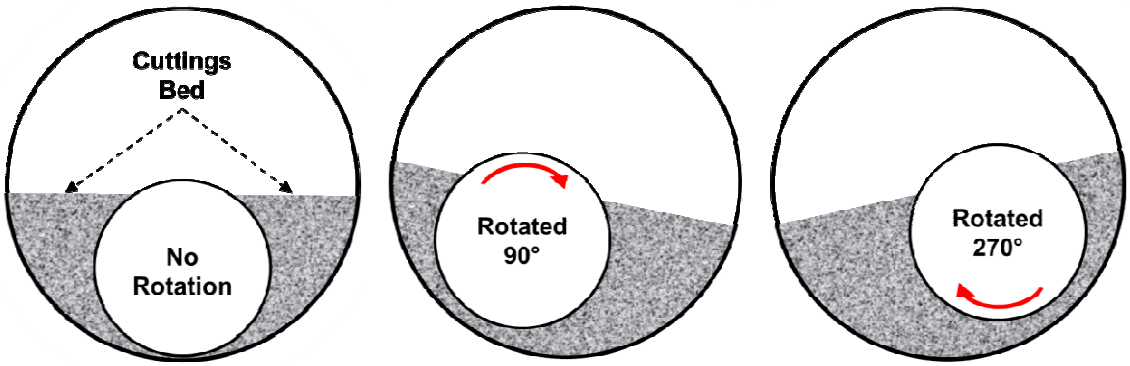

Fig. 6.10 Fluctuation of cuttings bed height due to drillpipe rotation

After the sweep experiment concluded, the drillpipe was manually rotated to the previously determine set position. Once the drillpipe was static and in the correct position, the bed height measurements were recorded. By repeating the same process for subsequent data collection, the possible error associated with the varying bed height was eliminated.

6.5.2 Effect of Fluid Types

The emphasis of this study was on synthetic-base mud (SBM) and the effect of introducing synthetic fiber on its ability to clean the wellbore. Due to the high cost of the SBM, only one test batch was created and used for the sweep experiments. In order to perfect the experimental procedure, and for use as a comparison to previous studies, a XG-based, unweighted, polymeric fluid was mixed in the flow loop. The XG fluid was used to run the sweep experiments following the same experimental procedure and data

gathering processes. For the sake of time, the entire text matrix was not completed, stopping after the addition of 0.02 percent w/w of fiber.

The WBM and SBM sweep experiments initiated with the base fluid (no fiber). The cuttings removal efficiency was plotted as a function of flow rate (**Figs. 6.11** and **6.12**). Despite the limited amount of data gathered for the polymeric fluid sweep experiments, a trend emerged that could be extrapolated to compare to other fluid sweep tests.

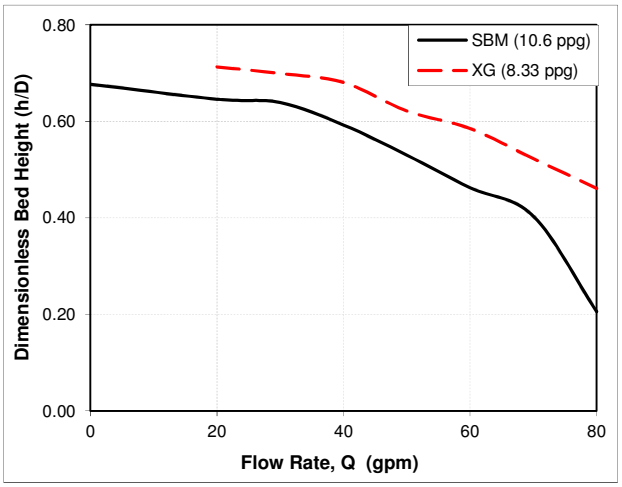

Fig. 6.11 Bed height vs. flow rate for WBM and SBM, no rotation, inclined annulus

When comparing the WBM and the SBM fluids, the density and rheology of the two fluids must be taken into consideration. Weighted fluid provides a significantly increased inertial force over unweighted fluids. This alone can provide an increased cuttings carrying capacity and improved hole-cleaning. To make a fair comparison, the SBM sweep data should be handicapped to eliminate the density benefit. Even so, prediction will still favor the SBM, since the fluid system shows an unequivocal advantage in cuttings suspension and flow. It should also be noted in **Fig. 6.11** that the lines diverge at high flow rates. In essence, the SBM provides an overall cleaner wellbore at the experiment culmination, despite similar trends between the two fluids at lower flow rates.

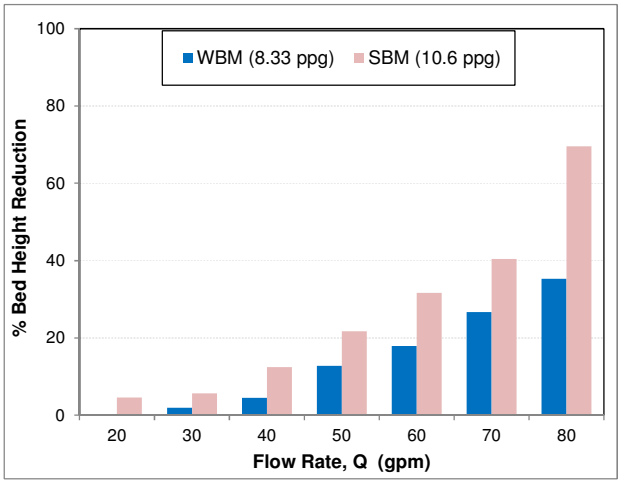

Fig. 6.12 Percent reduction of bed height of WBM and SBM, no rotation, inclined annulus

Another visible difference between the two fluids was physical and macroscopic appearances. The XG-based fluid was lightly colored, and the cuttings particles were easily identified within the fluid. This enabled very accurate bed height measurements. This contrasts with the experiences from the SBM sweep experiments. The base, unweighted synthetic-base drilling fluid (7.6 ppg) was slightly off-white in color

and clean. Once barite was added to the system, the color changed to dark brown, and small barite clumps could be seen floating in the fluid. This provided difficulty in precisely measuring the bed height because the dark color of the fluid closely matched that of the cuttings particles. Therefore, bed height measurements were taken based on the shaded areas of the annulus, present from the cuttings beds inside. Individual cuttings particles could no longer be identified. Due to the density of the fluid and the particles suspended within, the coriolis flow meters were constantly measuring relatively large differences in density. The difference was apparent during rheology and hydraulics measurements, but it was exacerbated during sweep experiments. The ability of the fluid to suspend the cuttings and the presence of the barite clumps, provided for a constantly changing fluid density.

The greatest advantage evident from the experimental results was the greater ability of the SBM over the XG-based fluid to reduce the cuttings beds with a reduced pressure loss. Using strictly water-based muds, an increase in viscosity or density would be required to increase cuttings removal, but it would detrimentally result in increased pressure loss in the annulus and pipe. However, the weighted SBM is able to eliminate cuttings beds and the accompanying measured apparent viscosity is less than that measured for the unweighted WBM (**Fig. 6.13**).

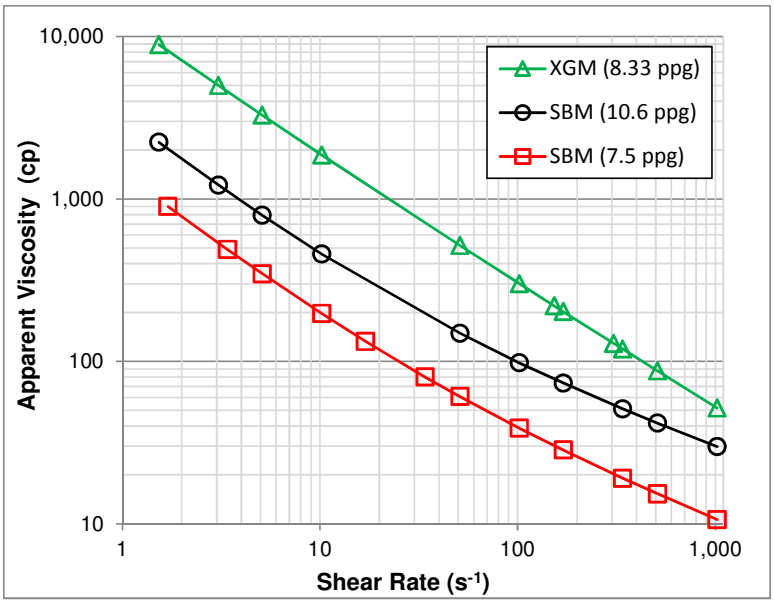

Fig. 6.13 Apparent viscosity vs. shear rate for sweep base fluids, 95°F

6.5.3 Effect of Fiber Concentration

In accordance with the test matrix, four (4) fluid formulations were tested; base fluid, 0.02, 0.04, and 0.06 percent by volume. In theory, with each incremental increase in fiber concentration, the wellbore cleaning effect should improve. In essence, more fiber equates to less cuttings beds. This hypothesis is based partly on conventional wisdom and partly on previous experimental studies. Previous works have shown that adding small amounts of fiber to the sweep fluid can improve cuttings removal (Ahmed and Takach 2008). This phenomenon may hold true unless the fiber concentration is great enough to influence the rheology of the suspending fluid drastically, at which point the advantages of fiber are no longer relevant. The test matrix for this experimental phase of the work only includes fiber concentrations proven to provide little to no rheological influence.

The fiber was added to the system after each successive round of experiments, and in accordance with the experimental setup and procedure. As stated previously, two (2) test batches of XG-based fluid (WBM) were mixed to test the experimental procedure and provide a comparison to the ensuing SBM tests. As shown in **Fig. 6.14**, adding a small amount of fiber (0.07 lb/bbl) to the fluid resulted in an overall increase in cuttings bed removal. This advantage is particularly noticeable at high flow rate. At the maximum flow rate of 80 gpm, the bed height after the fiber sweep was almost 50 percent of the bed height after the base fluid sweep.

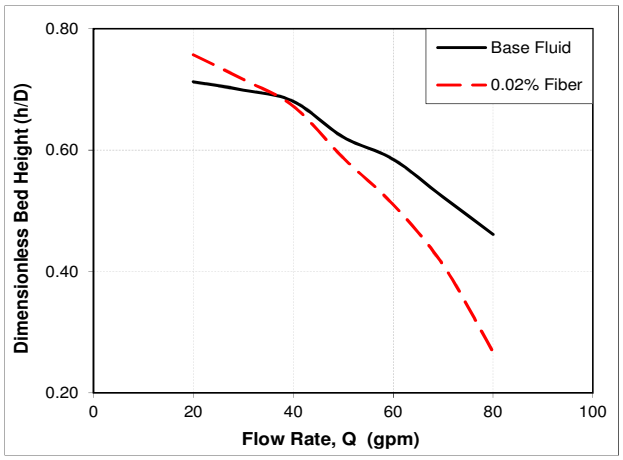

Fig. 6.14 Bed height vs. flow rate for WBM, no rotation, inclined annulus

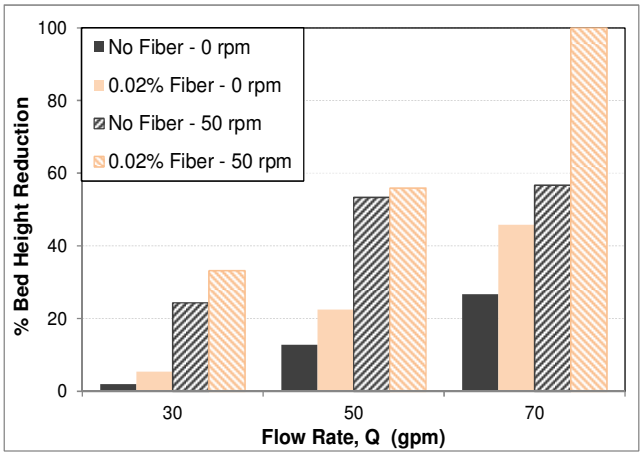

Fig. 6.15 Comparison of fiber effectiveness for hole-cleaning with WBM (8.33 ppg), inclined annulus

It should also be noted that only the fiber fluid could completely clean the wellbore during the sweep experiment (**Fig. 6.15**). While this required some pipe rotation, the fiber provided obvious benefits, since the base fluid alone could not completely clean the wellbore unless high pipe rotation speeds (75 rpm and 60 gpm)

were applied.

Introducing fiber into the weighted synthetic-based fluid (SBM) provided slightly different results. Due to the weight of the fluid, the inertial force of the moving fluid in the annulus was greater than that of the unweighted XG-based fluid. This factor alone could have provided enhanced hole-cleaning performance over the WBM. The inertia of the SBM could have limited the significance of the addition of the fiber. As shown in **Figs. 6.16** to **6.18**, the addition of fiber in the horizontal and inclined annulus, without pipe rotation, provided no real predictable or reliable benefit to cuttings bed eradication. This was in contrast with the results from the WBM sweep experiments, in which the addition of a small amount of fiber resulted in a decrease in bed height over the base fluid (**Fig. 6.14**).

When the annulus was in the horizontal position, the inertial force pushing the cuttings through the annulus was at the maximum. This left little room for improvement with the addition of fiber. However, in the inclined position, the cuttings wanted to slide down the annulus, creating more work for the sweep fluid. Critical evaluation of **Fig. 6.18** showed that in the inclined position, the high concentration fiber sweep provided visual and measurable improved wellbore cleaning over the base fluid. This trend was slightly apparent at low flow rates, but it became unequivocally obvious at high flow rates. The addition of fiber may have increased the lifting capacity of the sweep fluid, which enabled the fluid to carry the cuttings through the annulus and return them to the collection/accumulation tank.

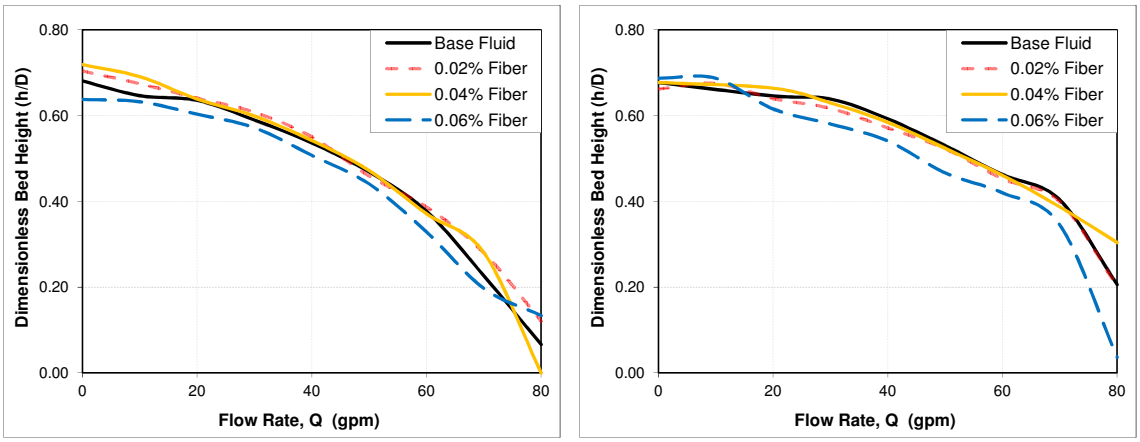

Fig. 6.16 Dimensionless bed height vs. flow rate for SBM, no pipe rotation
a) Horizontal annulus, and b) Inclined annulus

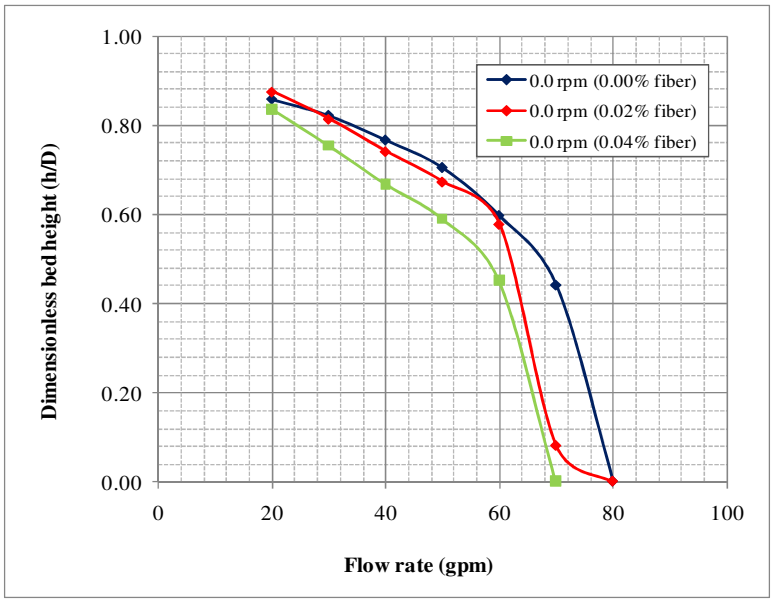

Fig. 6.17 Dimensionless bed height vs. flow rate for WBM, no pipe rotation, horizontal annulus

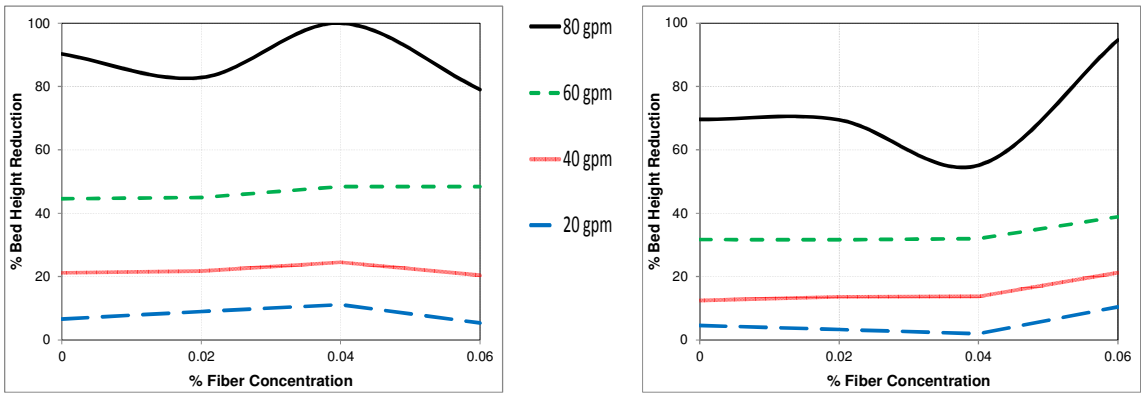

Fig. 6.18 Percent bed height reduction vs. fiber concentration for SBM, no pipe rotation
a) Horizontal annulus, and b) Inclined annulus

With pipe rotation, the benefits of fiber became more apparent. Sweep experiments conducted without pipe rotation left residual cuttings in the annulus after 80 gpm (**Fig. 6.19**). Compare this with tests conducted at 25 rpm pipe rotation, as the wellbore is completely cleaned with a flow rate of 40 gpm (**Fig. 6.20**). As stated previously, the benefits were negligible in the horizontal position. However, adding fiber to sweep fluids in the inclined annular position provided marked improvement in wellbore cleaning.

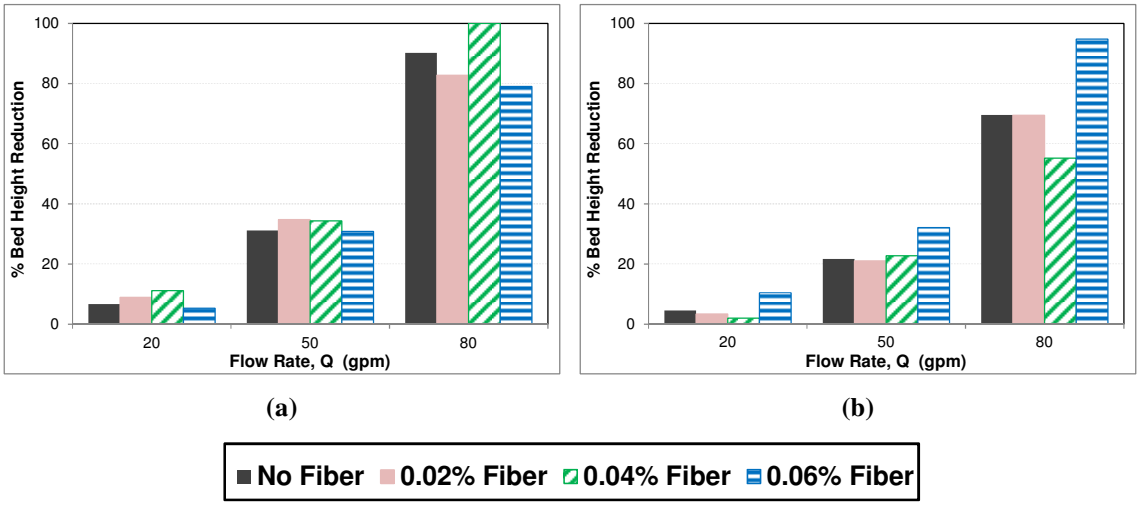

Fig. 6.19 Percent bed height reduction vs. flow rate for SBM, no pipe rotation
a) Horizontal annulus, and b) Inclined annulus

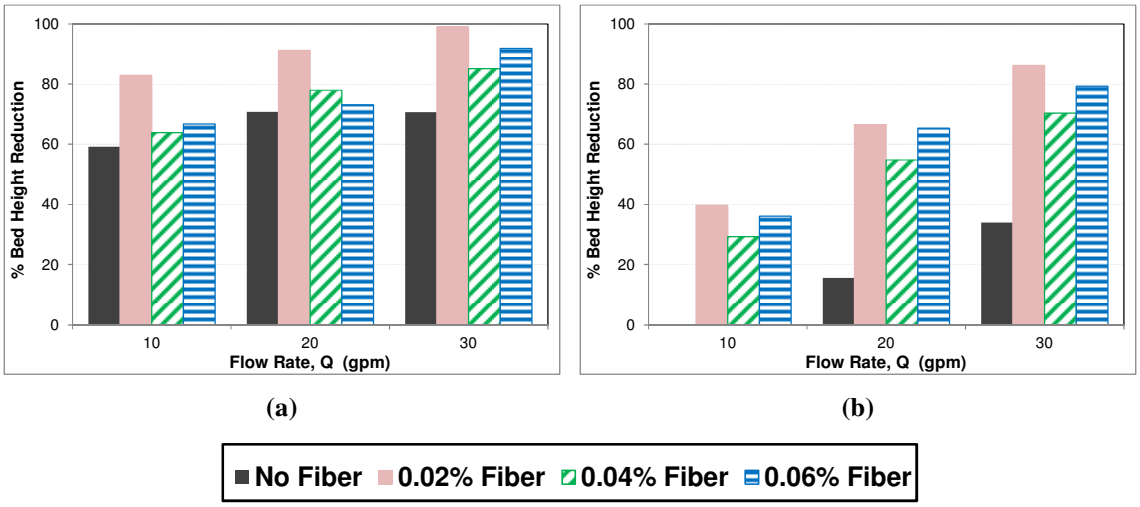

Fig. 6.20 Percent bed height reduction vs. flow rate for SBM, 25 rpm pipe rotation
a) Horizontal annulus, and b) Inclined annulus

6.5.4 Effect of Inclination Angle

In accordance with the test matrix, the sweep experiments were conducted in horizontal (90°) and inclined (72°) annular orientations. The 72° inclination angle represents the approximate maximum safe height the end of the annulus test section could be raised. This required reconfiguring of the support braces and the rerouting and stabilization of the fluid return lines.

Inclination angle played an important role in visualizing the effectiveness of the fiber sweeps. As stated previously, the fiber sweeps provided no real significant improvement over the base sweeps in the horizontal annular position. The wellbore cleaning effectiveness of the base weighted synthetic-based fluid was so great that the addition of any hole-cleaning aid would be inconsequential. However, in the

inclined annular position, the addition of fiber provided observable decreases in bed height (**Fig. 6.21**). At most flow rates, adding fiber to the sweep fluid provided an approximate two-fold decrease in bed height over the base sweep fluid.

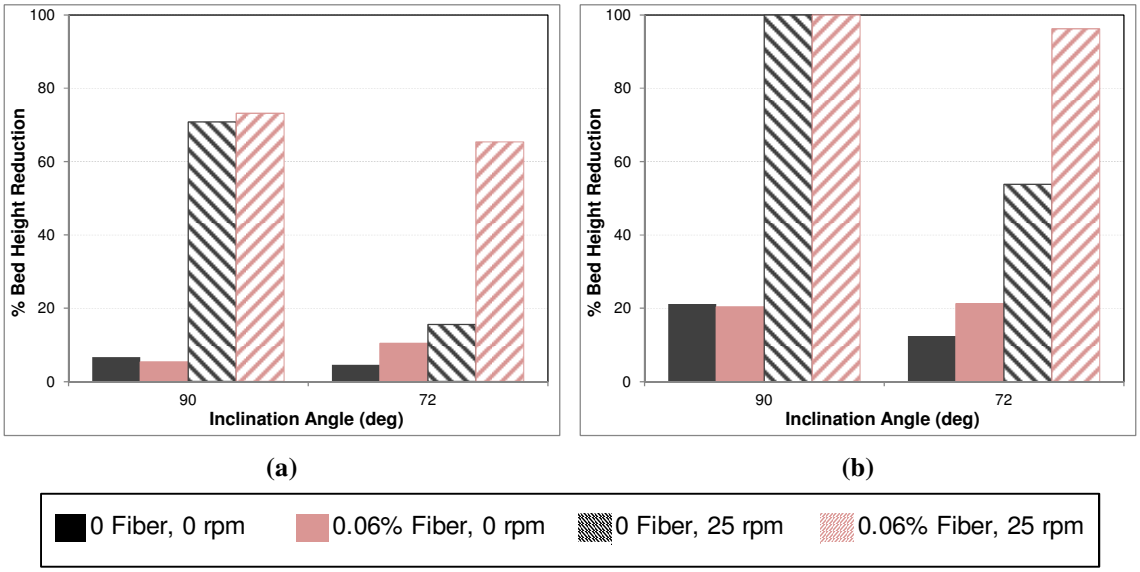

Fig. 6.21 Percent bed height reduction vs. inclination angle for SBM a) 20 gpm, and b) 40 gpm

Fig. 6.22 presents equilibrium bed high measurements obtained under horizontal and inclined configurations with WBM. In general, the inclination effect on the bed height was moderate. Without pipe rotation, an inclined wellbore was slightly easier to clean than horizontal. However at high flow rates (above 80 gpm), this trend changed. The horizontal test section was completely cleaned while some cuttings were still in the inclined annulus at the same flow rate.

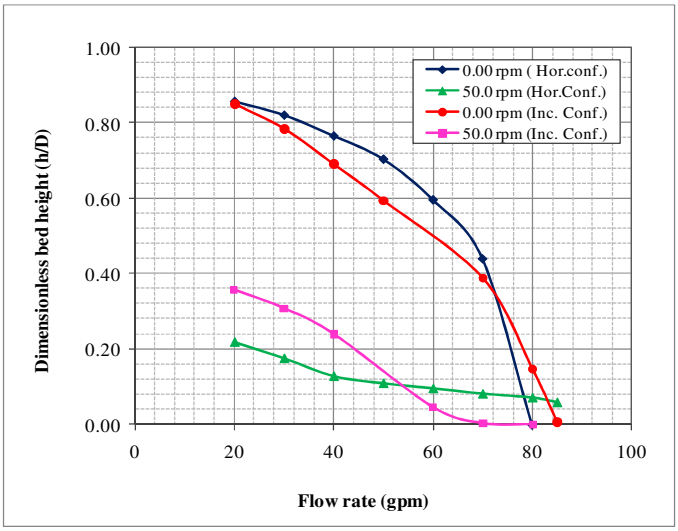

Fig. 6.22 Dimensionless bed height vs. flow rate for WBM base fluid, horizontal and inclined annulus

6.5.5 Effect of Flow Rate

As mentioned previously, the maximum allowable flow rate is a critical component in designing sweeps used in the field. The best cleaning results are typically obtained at maximum pump rate. However, the maximum rate may cause an undesirable increase in the equivalent circulating density, which is limited by the pore and fracture pressures.

Aside from fiber concentration, flow rate was the most critical variable in determining the effectiveness of fiber sweeps on cuttings removal. Per the experimental procedure, the flow rate was varied from 10 gpm to approximately 80 gpm, the system's maximum attainable flow rate. Cuttings bed measurements were taken after each 30-minute, static flow rate sweep experiment. As predicted, cuttings removal increased as flow rate increased (**Fig. 6.23**). This trend persisted regardless of the inclination angle, pipe rotation, or fiber concentration. However, a phenomena developed during some of the sweep experiments. As shown in **Figs. 6.9** and **6.23**, a flat spot appeared in the cuttings removal/flow rate graphs. This plateau was immediately followed by another positive-slope bed height reduction trend. This was thought to be attributed to some critical cuttings transport velocity. Essentially, a small range of flow rates existed that could no longer remove cuttings from the cuttings bed. Once the flow rate threshold was exceeded, the sweep was able to remove cuttings again, reducing the bed height.

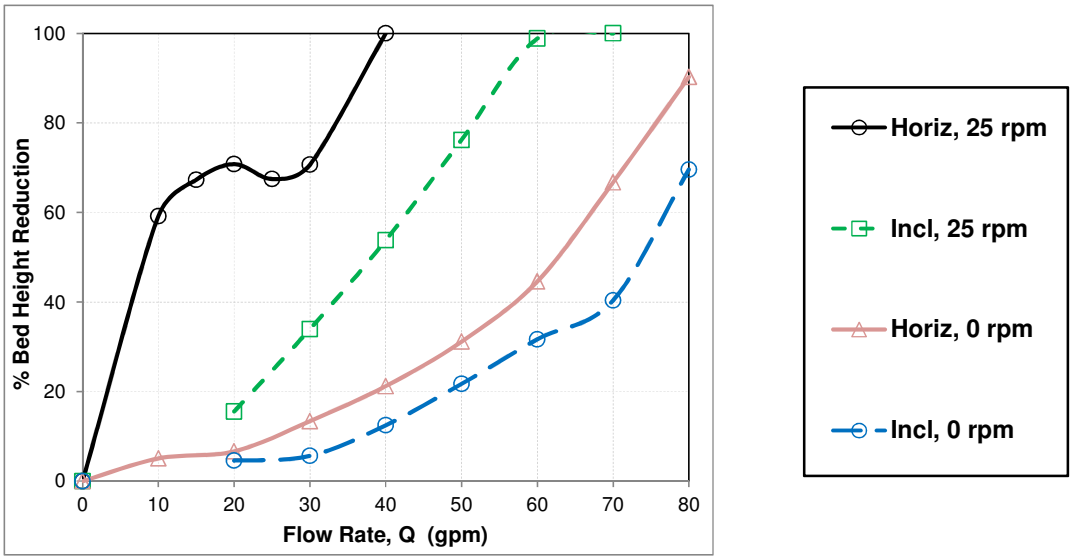

Fig. 6.23 Percent bed height reduction vs. flow rate for SBM base sweep (no fiber)

6.5.6 Effect of Pipe Rotation

In accordance with the test matrix, two rotational speeds were chosen to provide similarity with actual field practices. The maximum revolutions per minute for the sweep experiments was held at 50. At 50 rpm, the cuttings removal efficiency was comparatively high. Increasing the rotational speed above 50 rpm provided no real significant increase in cuttings removal. In addition, the eccentricity of the drillpipe resulted in rhythmic contact and vibration between the 2-inch drillpipe and the 4-inch polycarbonate tube (casing). At 50 rpm, the vibrations caused by the wobbling drillpipe were severe, and increasing the rotational speed would have increased the vibrations and possibly reduced the life expectancy or damaged the flow loop apparatus.

For a given flow rate and fluid formulation, the cuttings removal was significantly improved when the drillpipe was rotated (**Figs. 6.24** and **6.25**). The benefit of pipe rotation was more noticeable in the inclined annulus (**Fig. 6.24b**). Increasing the pipe rotation speed from 25 to 50 rpm resulted in a larger measured increase in cuttings removal for a given fiber concentration over that measured at similar test conditions in the horizontal position. The rotation of the pipe agitated the bed, lifted bed particles, and facilitated the removal process of cuttings. Regardless of the inclination, it provided substantial improvement in the hole-cleaning performance of the fluid at low and intermediate flow rates.

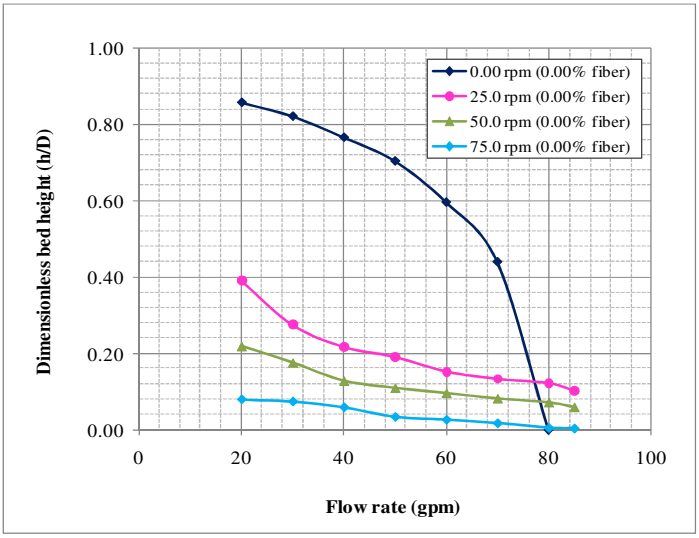

Fig. 6.24 Effect of different pipe rotation speeds on the hole-cleaning for WBM

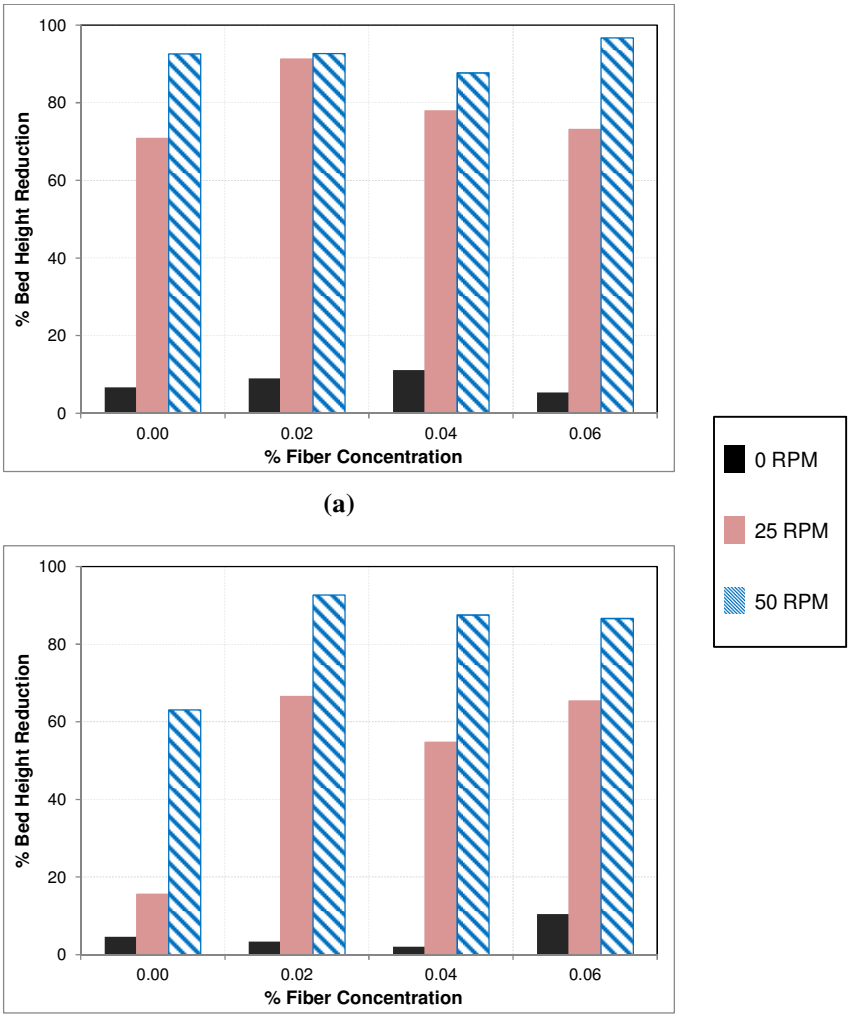

Fig. 6.25 Percent bed height reduction vs. fiber concentration for SBM, Q = 20 gpm
a) Horizontal annulus, and b) Inclined annulus

6.6 Pipe Viscometer Measurements

Measuring fluid rheology in a pipe viscometer provides a relatively greater knowledge of fluid behavior under actual flow conditions. It also provides another metric of quantitatively identifying the influence of different additives on the flow behavior of the base fluid. A number of pipe viscometer tests were performed to: i) study the effect of fiber concentration on a critical Reynolds number for the transitional from laminar to turbulent condition; ii) compare flow curves of base fluid and fiber sweeps; iii) evaluate theoretical model prediction using experimental results; and iv) investigate drag reduction behavior of fiber suspension. Base fluid and fiber sweep exhibit similar pressure loss behavior. However, fiber tends to reduce the pressure loss slightly. The results are consistent with previously reported studies (Ahmed

and Takach 2008; Xu and Aidum 2005), which showed that small amounts of fiber have a negligible effect on the pressure loss.

The pipe viscometer is one of the two parallel test sections (**Fig. 6.2**) and contains two differential pressure (DP) meters (**Fig. 6.26**). The spacing between the two capillary lines for each DP meter is different to serve as a redundant check for evaluating the flow data.

Pipe viscometer experiments were conducted to determine the flow behavior effect of introducing fiber into the sweep fluid. Pipe viscometer rheology was recorded for every fluid+fiber formulation listed in the test matrix (**Tables 6.1** and **6.2**).

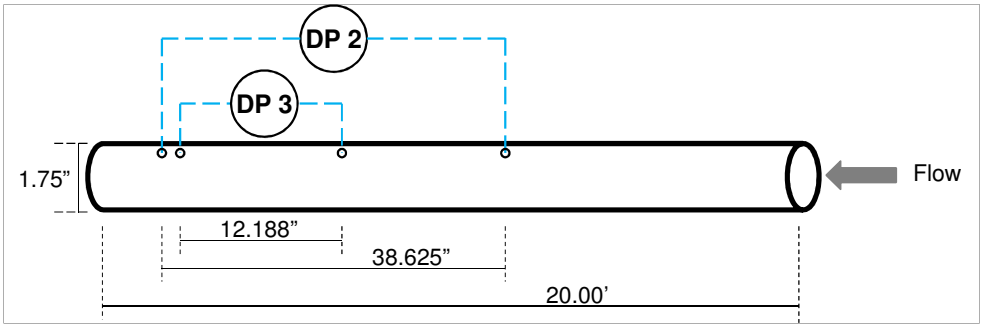

Fig. 6.26 Pipe viscometer schematic

The DP meters functioned as transducers, converting the hydraulic differential pressure energy into an electrical current, which was then sent to the Data Acquisition System (DAS). The DAS controlled the flow rate of the centrifugal pump, and recorded flow rate, pressure drop, temperature, pressure, and density. Therefore, the pipe viscometer experiments measured pressure loss as a function of flow rate (**Fig. 6.27**). For the WBM, the base fluid and fiber sweeps showed similar pressure loss (**Fig. 6.27a**). The addition of fiber even slightly reduced pressure loss at higher flow rate. This trend conflicted with that observed with the SBM. The measured pressure loss as a function of flow rate showed that under low flow rates (laminar conditions) the addition of fiber resulted in an increase in pressure loss (**Fig. 6.27b**).

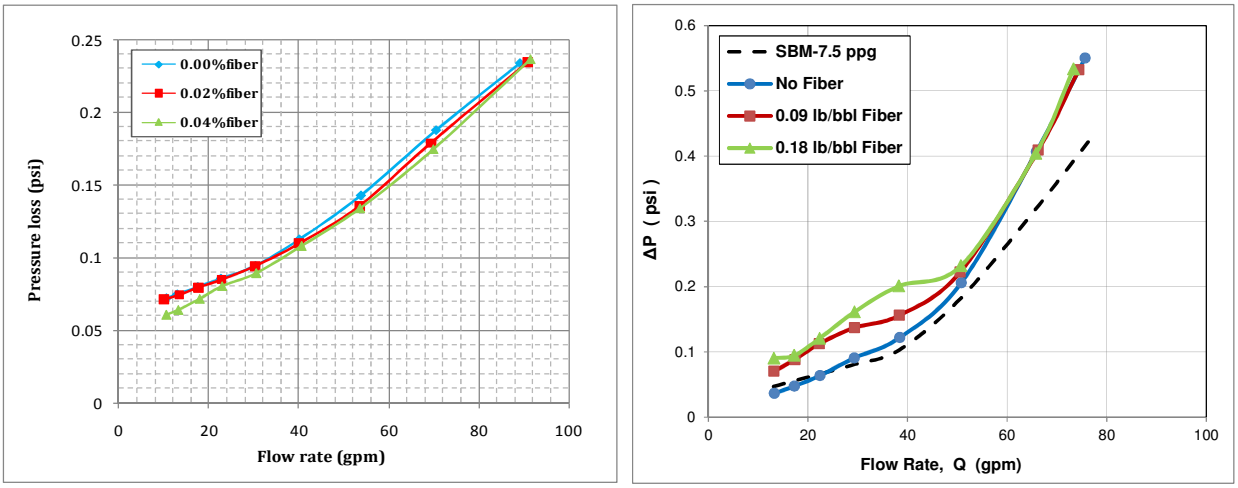

(a) **(b)**

Fig. 6.27 Measured pressure loss as a function of flow rate in pipe viscometer, 90° orientation: a) WBM; and b) SBM

The measured pressure losses were converted to the Reynolds numbers and associated friction factors for the varying flow rates (**Fig. 6.28**). For the WBM, the critical Reynolds number (Re) was approximately 2700. The fiber concentration had a minor effect on the critical Reynolds number. Under laminar conditions, slight reduction in pressure loss or friction factor was observed. After evaluating the dimensionless groups for the SBM, the flow was laminar at all flow rates, which was attributed to the weight of the fluid because the density prevented the onset of turbulence given the flow rate and pipe diameter.

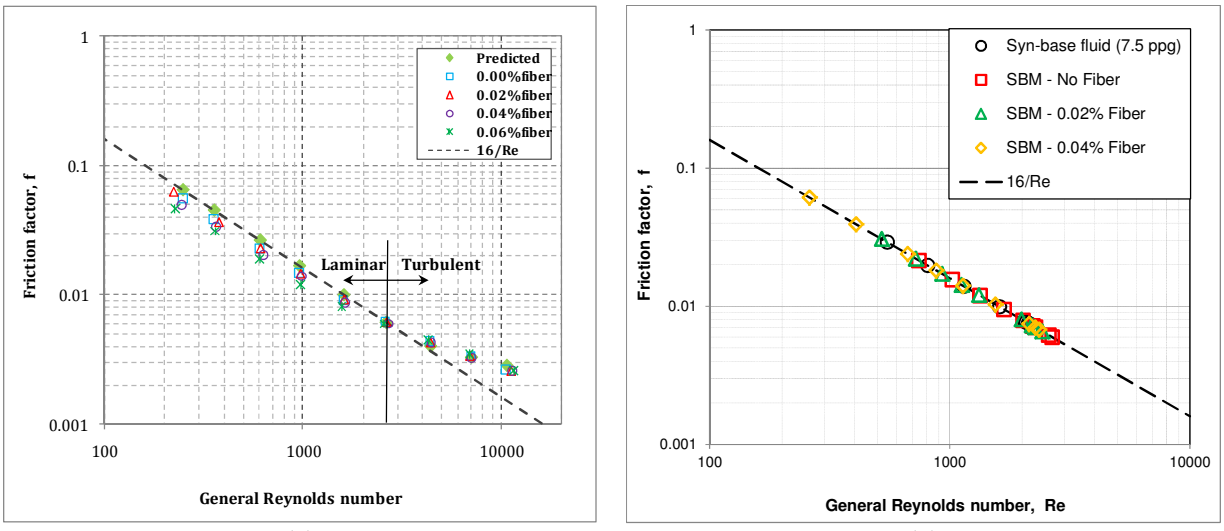

(a) **(b)**

Fig. 6.28 Fanning friction factor vs. generalized Reynolds number in pipe viscometer: a) WBM; and b) SBM

6.7 Wellbore Hydraulics

In a similar manner to the pipe viscometer experiments, hydraulics studies were conducted with fluid flowing through the annulus test section. The annulus test section sat parallel to the pipe viscometer, and a differential pressure meter that was attached to the annulus with capillary lines approximately four feet apart measured pressure drop as a function of flow rate (**Fig. 6.29**). Hydraulic measurements were taken of every fluid+fiber formulation listed in the test matrix (Tables 6.1 and 6.2). The differential pressure measurements were recorded and graphed (**Fig. 6.30**). However, the pressure measurements for the fiber sweep fluids were in error, as the recorded data provided illogical results. It was speculated that this was the result of fiber plugging of the capillary lines. Therefore, the SBM fiber sweep pressure data was left off of Fig. 6.30.

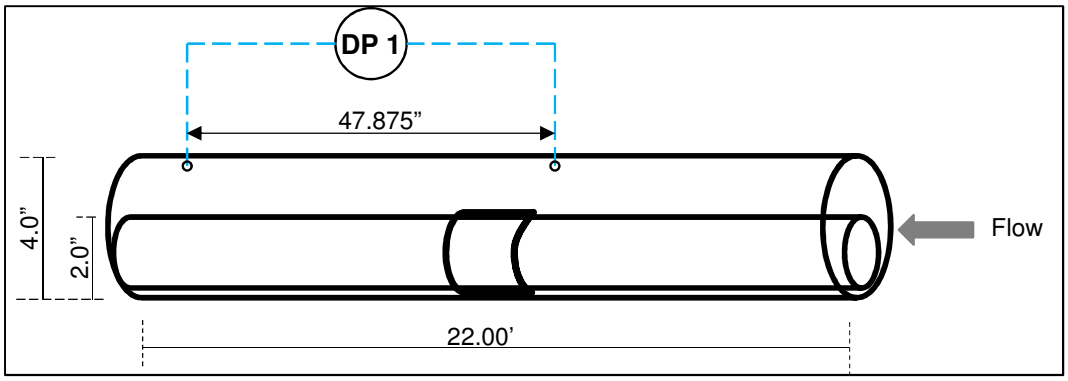

Fig. 6.29 Annulus test section schematic

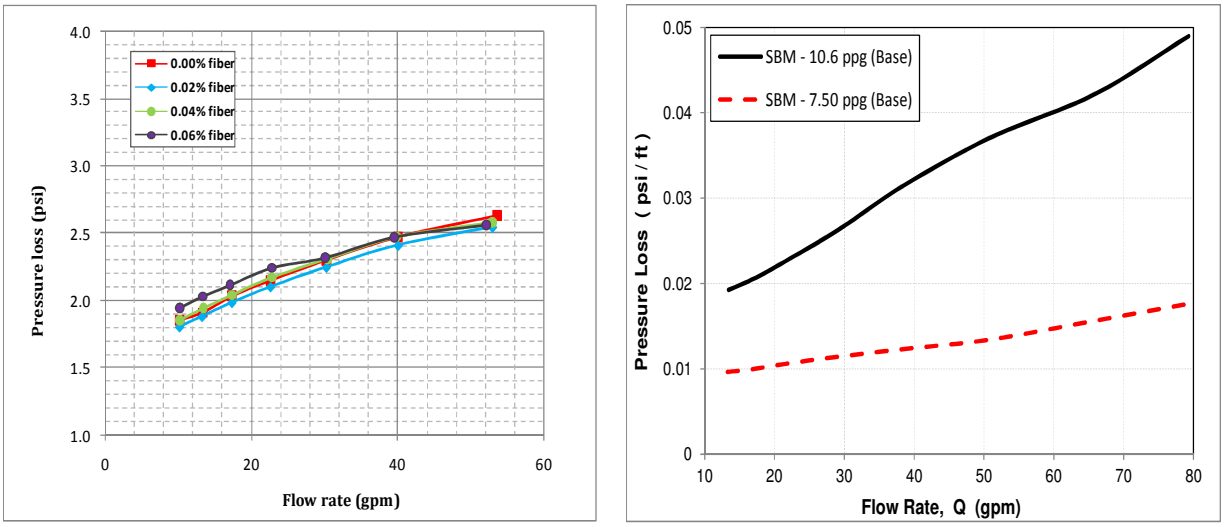

(a) **(b)**

Fig. 6.30 Measured pressure loss as a function of flow rate in annulus, 90° orientation: a) WBM; and b) SBM

In **Fig. 6.31**, measurements are presented as Fanning friction factor versus Reynolds number for the WBM. Per the figure, every test was carried out under laminar flow conditions. The pump rate and annular dimensions did not promote turbulent flow.

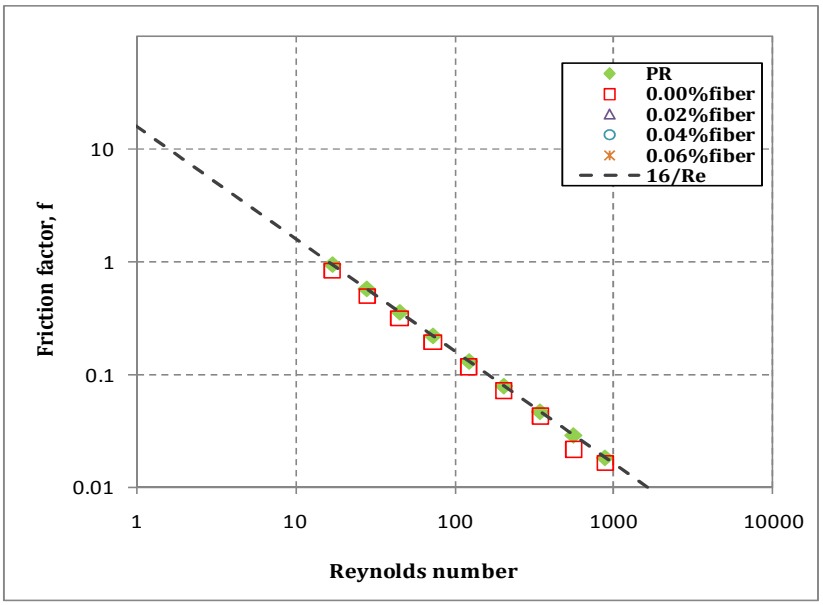

Fig. 6.31 Fanning friction factor vs. generalized Reynolds number in annulus

6.8 Conclusions

An experimental study was conducted on the wellbore cleaning efficiency of fiber-containing water-based and synthetic-based fluids. These fluids represent commonly used drilling fluids in the industry, and satisfy the requirement of using fluids relevant to offshore, deepwater operations. The two fluids, unweighted xanthan gum-based fluid and weighted synthetic-based mud, were each mixed with varying fiber concentrations. A flow loop test apparatus was utilized to conduct the cleaning experiments, as well as measure pressure drop in a pipe viscometer. By varying flow rate, inclination angle, fiber concentration, and pipe rotation, a great amount of data were gathered that was used to evaluate the optimum conditions to use these fiber sweeps. The following were concluded from the experiments:

- Very dilute concentrations of fiber in the XG based fluid had no significant influence in measureable pressure loss compared to the fiber-free base fluid.
- Introducing fiber into synthetic-based fluid resulted in an increase in pressure loss at low flow rates. However, this disparity disappeared as the flow rate increased, and the pressure loss versus flow rate curves converged at high flow rates.

- For a non-rotating pipe case, noticeable increase in cuttings removal was not observed with increasing fiber concentration. The inertia of the weighted fluid is great enough to mask any slight improvement that might be gained by adding fiber to the system.
- With pipe rotation, cuttings removal increased with the introduction of fiber to the system. Only a slight amount of fiber was necessary to observe the improved wellbore cleaning performance of the fiber sweep over the base fluid sweep.
- Maximum wellbore cleaning performance with a very dilute concentration of fiber was achieved at maximum flow rate and pipe rotation.

6.9 Guidelines

The applicability of this study to the industry is apparent in the experimental results. As this study was oriented towards offshore, deepwater drilling operations, the results regarding oil-based muds and synthetic-based muds are of the utmost importance. The rheological studies implicate that the addition of fiber up to 0.08 percent will have no significant impact of rheology, and subsequently the hydraulics and ECD will remain unaffected. The sweep experiments and pipe viscometer rheology also reinforce the usefulness of fiber in sweep fluids. Under similar conditions, fiber sweeps improved wellbore cleaning over base fluid sweeps. Taking this into consideration, the recommendations here-to-fore in the use of fiber-containing sweeps are as follows:

- Utilize base sweep fluids that have gelling property (i.e., measurable yield stress). The presence of yield stress is necessary to achieve stable and homogeneous suspension of fiber particles within the sweep fluid.
- Use fiber concentration of approximately 0.04 percent. As shown in Section 5.3.4, the best hole-cleaning performance is generally achieved with an optimum fiber concentration that makes the fiber drag comparable with the viscous drag force. Increasing fiber concentration beyond this optimum value results in minimal cleaning improvement. In addition, using optimum fiber concentration will ensure a minimal ECD influence.
- Rotate the drillstring while applying fiber sweep material to optimize wellbore cleaning. Without drillstring rotation, the performance improvement obtained from the application of fiber sweep is minimal.

Nomenclature

bbl = Barrel

cp = Centipoise

DAS = Data acquisition system

DP = Differential pressure

ECD = Equivalent circulating density

gpm = Gallons per minute

K = consistency index

n = fluid behavior index

ppg = Pounds per gallon

Q = Flow rate

Re = Reynolds number

rpm = Rotations per minute

SBM = Synthetic-based mud

T_y = yield stress

WBM = Water-based mud

XG = Xanthan Gum

Greek Letters

θ = Inclination angle

$\dot{\gamma}$ = Shear rate

μ = fluid viscosity

References

Ahmed, R.M. & Takach, N.E. 2008. Fiber Sweeps for Hole Cleaning. Paper SPE 113746 presented at the SPE/ICoTA Coiled Tubing and Well Intervention Conference and Exhibition, The Woodlands, Texas, 1-2 April.

Bulgachev, R.V. & Pouget, P. 2006. New Experience in Monofilament Fiber Tandem Sweeps Hole Cleaning Performance on Kharyaga Oilfield, Timan-Pechora Region of Russia. Paper SPE 101961 presented at the SPE Russian Oil and Gas Technical Conference and Exhibition, Moscow, Russia, 3-6 October.

Cameron, C., Helmy, H., & Haikal, M. 2003. Fibrous LCM Sweeps Enhance Hole Cleaning and ROP on Extended Reach Well in Abu Dhabi. Paper SPE 81419 presented at the SPE 13th Middle East Oil Show and Conference, Bahrain, 5-8 April.

George, M.L., Ahmed, R.M. **&** Growcock, F.B. 2011. Rheological Properties of Fiber-Containing Drilling Sweeps at Ambient and High Temperature Conditions. Paper AADE-11-NTCE-35 presented at the AADE National Technical Conference & Exhibition, Houston, Texas, USA, 12-14 April.

Guo, R., Azaiez, J., & Bellehumeur, C. 2005. Rheology of Fiber Filled Polymer Melts: Role of Fiber-Fiber Interactions and Polymer-Fiber Coupling. *Polymer Eng. and Sci.* **45** (3): 385-399.

Hemphill, T. **&** Rojas, J.C. 2002. Drilling Fluid Sweeps: Their Evaluation, Timing, and Applications. Paper SPE 77448 presented at the SPE Annual Technical Conference and Exhibition, San Antonio, Texas, 29 September-2 October.

Marti, I., Hofler, O., Fischer, P. & Windhab, E.J. 2005. Rheology of Concentrated Suspensions Containing Mixtures of Spheres and Fibres. *Rheologica Acta* **44** (5): 502–512

Rajabian, M., Dubois, C., & Grmela, M. 2005. Suspensions of Semiflexible Fibers in Polymeric Fluids: Rheology and Thermodynamics. *Rheologica Acta* **44** (5): 521–535.

Valluri, S.G., Miska, S.Z., Ahmed, R.M. & Takach, N.E. 2006. Experimental Study of Effective Hole Cleaning Using "Sweeps" in Horizontal Wellbores. Paper SPE 101220 presented at the SPE Annual Technical Conference and Exhibition, San Antonio, Texas, 24-27 September.

7. Mechanistic Modeling of Hole Cleaning with Fiber Sweeps

The mechanistic model presented in this study is an extension of existing cuttings transport models (Ahmed et al. 2002; Duan 2005; Larsen et al. 1997; Clark et al. 1994). It was developed to predict critical transport velocity (CTV) in fiber-containing fluid. The CTV for fiber-containing fluid is different from that of the fluid without fiber (base fluid). Adding fiber to the base fluid creates additional force, fiber drag force, acting on bed particles in the same direction as the viscous drag force. The fiber drag can initiate particle movement even at low fluid velocities in which the viscous drag is minimal. As shown in Eqn. (5.7), the fiber drag is a function of the fiber drag coefficient, and a reliable correlation is needed to estimate the coefficient. A mathematical model for the CTV has been developed considering linear and angular momentum balances of a bed particle.

7.1 Introduction

Mathematical hole-cleaning models are often preferred because of their wide range of applicability. Clark and Bickham (1994) presented a mechanistic model for predicting the minimum fluid velocity for transporting cuttings without formation of a cuttings bed. This model considers major forces acting on a single stationary cuttings particle deposited on the surface of the bed. To verify the model, they performed flow loop tests using different test fluids (water, solution of HEC, and xanthan gum). The tests were run at angles ranging from near vertical (20° minimum) to horizontal (90°). The model prediction showed a good agreement with the experimental results. Recently, an improved mechanistic model (Ahmed et al. 2002) was developed to predict the critical transport velocity (CTV). The model was verified using experimental data obtained using water and polypnoinic cellulose suspension as test fluids. The average cuttings size was varied from 0.125 mm to 3.5 mm. The model predictions showed satisfactory agreement with experimental measurements.

Although mechanistic models provide general CTV predictions for different drilling applications, their accuracy is lower than that of the empirical models. To improve the accuracy of the mechanistic models, studies were conducted to develop models that combine both mechanistic models and empirical correlations. Rasi (1994) presented a semi-empirical model that combines fluid mechanics-based analytical model with correlations developed using experimental and field data. Later, an improved semi-empirical model (Larson et al. 1997) was developed to predict the required critical transport velocity in high angle wells. The model was developed after performing an extensive experimental study using a medium-scale flow loop. The model predicted critical transport velocity and annular cuttings concentration under different drilling conditions for highly deviated and horizontal wells. The study concluded that cuttings start to accumulate in the wellbore if the annular velocity becomes insufficient,

below the critical transport velocity. More recently, Ozbayoglu et al. (2007) developed a three-layer cuttings transport model applying the principles of mass and momentum balance for steady, isothermal flow condition. The model is valid for both compressible and incompressible drilling fluids.

Basic Assumptions

The following basic assumptions are made to develop the present model:

1. A flat and uniform layer of cuttings bed forms in the wellbore.
2. The variation in bed thickness along the length of the wellbore is negligible.
3. Cuttings particles are assumed spherical with uniform size and density.
4. Flow is steady and isothermal.
5. Solid concentration in the fluid layer above the bed is negligible.
6. Particle collision has a minor effect on the critical transport velocity.

Assuming uniform bed thickness greatly simplified the modeling, even though in some cases ripples and dunes form in the wellbore. The formation of ripples and dunes complicate the flow geometry and make the modeling extremely difficult. Ripples and dunes usually form when the flow velocity is close to the critical transport velocity and bed particle size is comparable with the thickness of viscous sub-layer. By using the average bed thickness, it was more convenient to define the critical transport velocity.

Another important simplifying assumption was that there were no suspended solids in the fluid. The presence of suspended particles tends to create collision phenomena. In addition to hydrodynamic forces, the collision helps to initiate the movement of bed particles. This phenomena is largely dependent on the size of both suspended and bed particles. The effect of the collision is negligible when the suspended particles are very small compared to bed particles.

7.2 Forces Involved in Particle Transport

Analyzing solids bed removal process and resuspension phenomena requires a good understanding of the forces acting on a single bed particle. The momentum exchange between the bed particle, and the fluid represents the external force that is imposed on the particle. As depicted on **Fig. 7.1**, a single particle located on the cuttings bed surface is subjected to the three major forces: weight of the particle (gravity), buoyancy force hydrodynamic drag and lift forces, and plastic force due to the gelling characteristics of the fluid. The hydrodynamic drag and lift forces are created due to the fluid flow over bed particles. When they become strong enough, these forces can initiate particle movement either in the form of rolling or

lifting of the particles. Net non-hydrodynamic torque is the sum of torque generated by gravity, buoyancy, and plasticity at point P. The net torque is independent of fluid velocity. Particle rolling is initiated when the moment generated by the hydrodynamic forces at point P overcome the net torque. Similarly, the lifting occurs when the y-component of the resultant force developed by gravity, buoyancy, plasticity and hydrodynamic forces becomes positive (upward).

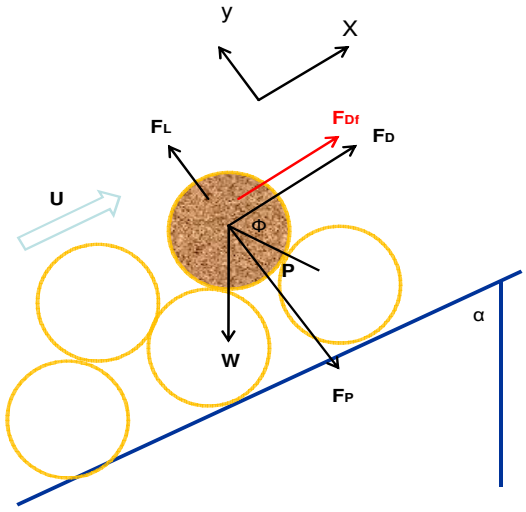

Fig. 7.1 Forces acting on single bed particle

7.2.1 Gravity and Buoyancy Forces

Gravity and buoyancy forces are major forces that act on the bed particle under dynamic and static conditions. These forces act in opposite directions and have contradictory effects on hole cleaning. Cuttings particles deposit on the borehole wall and form beds because gravity dominates the buoyancy force. Buoyancy force is a function of density of the fluid and hence weighted muds have the potential to provide effective hole cleaning. Nevertheless, due to ECD limitation mud weight cannot be increased substantially for improving hole-cleaning. The buoyancy force acting on a bed particle is expressed as:

$$F_b = \frac{\pi}{6} d_p^3 \rho_f g \quad \text{.....(7.1)}$$

And the weight of the particle is calculated as:

$$F_g = \frac{\pi}{6} d_p^3 \rho_p g \quad \text{.....(7.2)}$$

where ρ_p and ρ_f are particle and fluid density, respectively.

7.2.2 Hydrodynamic Forces

The hydrodynamic drag (F_D) and lift force (F_L) develop under dynamic conditions. These forces generate when a body moves relative to its surrounding fluid. The hydrodynamic drag (viscous drag) acts in the direction of the fluid upstream velocity. The lift force acts perpendicular to upstream velocity. These forces develop as a result of pressure and stress variations on the surface of the particle due to the action of the surrounding fluid. They can be determined by integrating the wall shear stress and pressure distributions on the surface of the particle (**Fig. 7.2**):

$$F_D = \oint P \cos\theta dA + \oint \tau_{dis} \sin\theta dA \quad \text{.....(7.3)}$$

$$F_L = -\oint P \sin\theta dA + \oint \tau_{dis} \cos\theta dA \quad \text{..... (7.4)}$$

where P is pressure normal to the small surface area, dA, τ_{dis} is the wall shear stress tangent to the surface area, and θ_w (or θ) is the angle between upstream velocity and pressure direction.

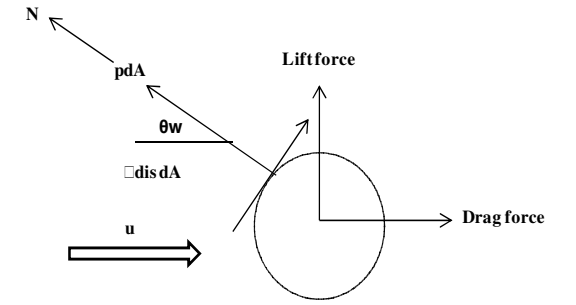

Fig. 7.2 Drag and lift force acting on the surface of a bed particle

The wall shear stress and pressure distributions are required to determine the lift and drag forces using Eqns. (7.3) and (7.4). However, it is difficult to obtain these distributions experimentally or mathematically. Therefore, experimentally obtained drag and lift coefficients are commonly utilized to determine these forces. The viscose drag force acting on the flow protruding bed particle is:

$$F_D = \frac{1}{2} C_{Dv} \rho_f u^2 A \quad \text{..... (7.5)}$$

Similarly, the lift force is expressed as:

$$F_L = \frac{1}{2} C_L \rho_f u^2 A \quad \text{..... (7.6)}$$

where u is the local velocity and A is the projected area of the particle above the mean bed surface where the hydrodynamic forces are acting perpendicular to this area.

Drag Coefficient

Various analytical, numerical, and experimental investigations (Guogui 1992; Dedegil 1987) have been conducted to estimate drag coefficient for both Newtonian and non-Newtonian fluids. A commonly used correlation (White 1991) for a wide range of particle Reynolds number can be used to determine the drag coefficient. The correlation is valid for both creeping and turbulent flow regimes.

$$C_{Dv} = \frac{24}{R_{ep}} + \frac{6}{1+R_{ep}^{0.5}} + 0.4 \quad \text{..... (7.7)}$$

The drag coefficient is a function of the bed particle properties such as shape, size, orientation, and surface roughness, as well as fluid properties and flow parameters. This equation can be applied for Newtonian and non-Newtonian fluids if the particle Reynolds number is defined in generalized form (Dedegil 1987).

$$R_{ep} = \frac{u^2 \rho_f}{\tau} \quad (7.8)$$

The shear stress, τ, is evaluated at the representative shear rate of (u/d_p). Eqn. (7.7) was developed and used to predict drag coefficient of a single particle without considering the effect of neighboring particles. In order to predict reasonable values of drag force, the equation should be modified to account for the variation of drag coefficient due to the presence of other particles on the surface of the solids bed (Ahmed et al. 2002). An extensive experimental study (Liang et al. 1995) performed to determine the effect surrounding particles on drag coefficient presented a correction factor, D_r, which varies from 1.05 to 0.35. The correction factor is 1.05 without the presence of particles and 0.35 with the presence of several neighboring particles. Due to the presence of many particles on the surface of the bed, more realistic value for the correction is 0.35. However, during model testing and calibration, the best drag correction factor was found to be 0.4.

Lift Coefficient

Lift force exists due to the asymmetry in the flow field around the particle. The asymmetry flow condition is established because of the no-slip boundary condition at the cuttings bed surface. This phenomenon is responsible for the lift mechanism. A small spherical particle moving through very viscous liquid in slow shear flow experiences a lift force resulting from the velocity gradient (Saffman 1964). Two assumptions are made in the development of Saffman's lift force equation: i) the particle is not influenced by solid boundaries, and ii) constant fluid velocity gradient. The equation is expressed as:

$$F_L = 1.615 \frac{4 d_p^2 \mu}{\nu^2} \left(\frac{du}{dy}\right)^{0.5} \quad (7.9)$$

where ν is the kinematic viscosity and y is the vertical distance from the mean bed level. The validation of his formula is limited to instances in which certain values of gradient Reynolds number, $R_{eG} = d_p(du/dy)\,\nu$, R_{ep} and R_{eG} is less than unity. By combining Eqns. (7.6) and (7.9), lift coefficient can be expressed as:

$$C_L = 4.11 \left[\frac{d_p}{u\, R_{ep}} \frac{du}{dy}\right]^{0.5} \quad (7.10)$$

7.2.3 Fiber Drag Force

When fiber is introduced to pure liquid, an additional drag force will develop if the particle slips in the fluid or the fluid flows past the particle. Fiber drag force, F_{Df}, acts in the same direction as the viscous drag force (**Fig. 7.1**). In order to estimate this force, a model has been developed. Even though limited

studies (Bivins et al. 2005; Harlen et al. 1999) have been conducted on the settling behavior of particle in liquid, the settling mechanisms present in fiber-containing fluid have not been fully understood.

In this study, the contribution of fiber drag to the total drag force was experimentally investigated. Empirical correlations that relate the fiber drag coefficient to the fiber concentration were developed. The definition for the fiber drag force is presented in Section 5.2. The fiber drag coefficient for fluid without yield stress is expressed as:

$$\frac{C_{Df}}{C^{\alpha}} = 4.47 \times 10^{5} Re_{ep}^{-1.176} \quad (7.11)$$

where the concentration exponent is:

$$\alpha = 1.4187 - 0.2397 \exp\left(-0.5\left(\ln\left(\frac{n}{0.8627}\right)/0.1763\right)^{2}\right) \quad (7.12)$$

The concentration is a function of the fluid behavior index for Power Law fluids. Xanthan gum-based fluids exhibit yield stress under ambient temperature. The drag coefficient for these fluids does not follow the same trend. It is also affected by the yield stress in addition to the fluid behavior index. Hence, the following drag coefficient correlation has been developed for these types of fluids.

$$\frac{C_{Df}}{C^{\alpha}} = 1335\ Re_{ep}^{-0.962} \quad (7.13)$$

The concentration exponent is calculated as:

$$\alpha = 3.2271 n'^{2} - 3.3965 n' + 1.441 \quad (4.14)$$

where $k' = \tau_y + k$, and

$$n' = \frac{1}{2}\log\left(\frac{\tau_y + k\,(100)^{n}}{\tau_y + k}\right) \quad (7.15)$$

7.2.4 Plastic Force

Pore spaces are occupied by drilling fluid. The upper portion of the cuttings bed is exposed to the dynamic of the liquid phase while the fluid in the interstitial can be stagnant (**Fig. 7.3**). The stagnant fluid can form gel that tends to hold bed particles and prevent them from moving. The plastic force acting on a single particle that is fully surrounded by stagnant fluid is estimated as $F_p = 0.5\pi d_p^2 \tau_y$, where τ_y is the yield stress. Clark and Bickham (1984) introduced a method to estimate plastic force for bed particles that are partially surrounded by stagnant fluid. The plastic force that holds a spherical bed particle is expressed as:

$$F_p = 0.5\pi d_p^2 \tau_y \left[\emptyset + \left(\frac{\pi}{2} - \emptyset\right)\sin^2\emptyset - \cos\emptyset\sin\emptyset\right] \quad (7.16)$$

where $\emptyset$ is the angle of repose.

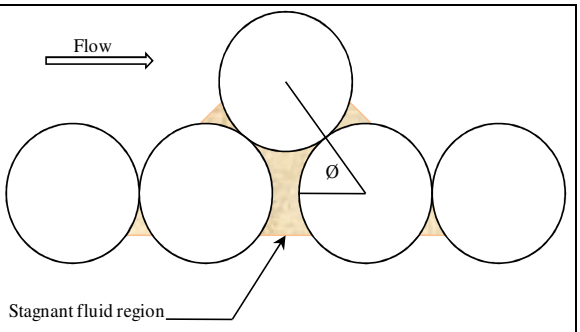

Fig. 7.3 Stagnant fluid surrounding a bed particle (Ahmed et al. 2002)

7.3 Near-Bed Velocity Profile

Forces that are developed under dynamic condition such as hydrodynamic force and fiber drag are affected by the local velocity close to the center of the particle. Therefore, in order to predict these forces, a model that describes the local velocity at the bed particles is necessary.

7.3.1 Newtonian Fluid

The law of the wall is often used to describe the near-bed velocity profile under turbulent flow condition. Person (1972) developed a general formula of the law of the wall for Newtonian fluid. This correlation is valid for both the viscous sub-layer as well as the turbulent boundary layer.

$$y^+ = \frac{w}{k} + A(e^w - 1 - w - 0.5w^2 - 0.33w^3 - 0.0417w^4) \quad (7.17)$$

where $w = u^+k$, A=0.1108, the Von karman constant, ko = 0.4, and dimensionless velocity $u^+ = \frac{u}{U_\tau}$. When the dimensionless bed particle size, $d_p^+ = \frac{d_p U_\tau}{v}$, is greater than 70, the roughness of the bed largely affects the velocity profile. As a result, the above formulation of the law of the wall will not be applicable (Gerhart et al. 1992; White 1991).

7.3.2 Non-Newtonian Fluid

In order to apply the law of the wall for non-Newtonian fluids, the apparent viscosity can be used instead of Newtonian viscosity. However, using the apparent viscosity concept to calculate velocity profile for fluid with yield stress does not provide reliable velocity predictions. Desouky and Al-Saddique (1999) developed a formula to predict local velocity profile of Yield Power Law fluid.

Velocity Profile in the Viscous Sub-layer

Most modern drilling fluids are expected to have a thick laminar sub-layer due to their high yield stress. The velocity profile in the viscous sub-layer ($y^+ < \delta^+$) defined as:

$$u^+ = y^+ \quad (7.18)$$

where y^+ is the dimensionless distance from the mean bed surface and is expressed as $y^+ = y^n U_\tau^{2-n}\left(\frac{\rho_f}{K}\right)$, y is the distance from the mean bed surface, $U_\tau = \left(\frac{\tau_{bed}}{\rho_f}\right)^{0.5}$, and τ_{bed} is average of bed shear stress, $\tau_{bed} = f_{bed}\frac{\rho_f U^2}{2}$. Dimensionless thickness of the laminar sub-layer, δ^+ is calculated as:

$$\delta^+ = \delta^n U_\tau^{2-n}\left(\frac{\rho_f}{K}\right) \quad (7.19)$$

where

$$\delta = \frac{5D_{hyd}}{R_{eg}}\left(\frac{2}{f_{bed}}\right)^{0.5} \quad (7.20)$$

Substituting u^+ and y^+ into Eqn. (7.18) and rearranging it:

$$u = y\left(\frac{\tau_{bed}}{K}(1-x)\right)^{1/n} \quad (7.21)$$

Hence, the local velocity gradient can be determined from the above equation.

$$\frac{du}{dy} = \left(\frac{\tau_{bed}}{K}(1-x)\right)^{1/n} \quad (7.22)$$

$$X = \frac{\tau_y}{\tau_{bed}} \quad (7.23)$$

where n is the fluid behavior index, and K is the consistency index.

Velocity Profile outside the Viscous Sub-layer

Outside the viscous sub-layer, the velocity profile for Yield Power Law fluid is determined using the following formula.

$$u = \frac{U_\tau}{K}\left[\sqrt{1-\frac{2y}{Dh}} + \ln\left(1-\sqrt{1-\frac{2y}{Dh}}\right)\right] + U_{max} \quad (7.24)$$

where U_{max} is the maximum fluid velocity that can be expressed as:

$$U_{max} = \left[\left(\frac{\tau_{bed}}{K}(1-x)\right)\right]^{1/n}\delta - \frac{U_\tau}{k_0}\left[1+\ln\left(\frac{\delta}{Dh}\right)\right] \quad (7.25)$$

Similarly, the velocity gradient can be obtained from the above equation.

$$\frac{du}{dy} = \frac{U_\tau}{k_0}\left[\frac{-1}{Dh\sqrt{\frac{2y}{Dh}}} + \frac{1}{Dh\left(\sqrt{1-\frac{2y}{Dh}}-\left(1-\frac{2y}{Dh}\right)\right)}\right] \quad (7.26)$$

The annular flow Reynolds number can be expressed in a generalized form.

$$R_{egn} = \frac{8U^2\rho_f}{\tau_w} \quad (7.27)$$

where τ_w is the wall shear stress. According to Ahmed and Miska (2009), the average wall shear stress in a concentric annulus can be calculated using the narrow slot approximation technique.

$$\frac{12U}{D_o - D_i} = \frac{\left(\tau_w - \tau_y\right)^{\left(\frac{1+n}{n}\right)}}{K^{\frac{1}{n}}\tau_w^2}\left(\frac{3n}{1+2n}\right)\left(\tau_w + \left(\frac{n}{1+2n}\right)\tau_y\right) \quad (7.28)$$

In order to calculate average bed shear stress, τ_{bed}, the bed friction factor, f_{bed}, must first be obtained. Many correlations (Dodge and Metzner 1959; Colebrook 1939) have been developed to estimate friction factor for Newtonian and non-Newtonian fluids under turbulent flow conditions for both smooth and rough pipes and annuli. Reed and Pilehvari (1993) proposed the following correlation for non-Newtonian turbulent flow in rough pipe.

$$\frac{1}{\sqrt{f}} = -4\log\left(\frac{0.27\varepsilon}{D_{eff}} + \frac{1.26^{n-1.2}}{\left(R_{egn} f^{(1-n/2)}\right)^{n-0.75}}\right) \quad (7.29)$$

where ε is absolute pipe roughness, which is a function of the angle of repose, ∅; effective diameter, D_{eff}; and general Reynolds number, R_{egn}, that can be obtained from Eqn. (7.27). According to Duan (2005), pipe roughness, $\varepsilon = \frac{d_p}{2}(1 + \sin\emptyset)$. The hydraulic diameter, D_{hyd} is used to approximate the effective diameter.

$$D_{hyd} = \frac{A_f}{S_o + S_i + S_b} \quad (7.30)$$

where A_f is the flow area above the cuttings bed, S_o is the wetted perimeter of the wellbore, S_i is the wetted perimeter of the drill pipe wall, and S_b is the wetted perimeter of the cuttings bed. Calculation procedure for the area and perimeter is shown in Appendix A. For the laminar regime, bed friction factor reads:

$$f_{bed} = \frac{16}{R_{egn}} \quad (7.31)$$

7.4 Mechanistic Model Formulation

In order to determine the mechanical equilibrium status of a single bed particle, the net torque at the contact point, P (**Fig. 7.1**), and the resultant left force in the lateral direction must be determined. Lifting of the particle occurs when the inclination angle is low (nearly vertical). However, in horizontal and highly deviated wells bed particles that are exposed to the fluid movement start rolling when the net rotating torque has a positive value. Forces acting on a single particle are shown on **Fig. 7.1**. The contact point P is considered as the axis of rotation during rolling. Particles rolling over the surface of the bed have been visually observed during laboratory experiments at high inclination angles. Applying the angular momentum balance at point P, the rotating torque, Γ_P, can be expressed as:

$$\Gamma_P = \frac{d_p}{2}\left[F_D \sin\phi + F_{Df}\sin\phi + F_L\cos\phi - F_p\cos\phi - \left(F_g - F_b\right)\sin(\alpha+\phi)\right] \quad \text{(7.32a)}$$

where α and ϕ are the inclination angle and angle of repose, respectively. By substituting the force expressions developed in the Section 7.2 into Eqn. (7.32a), the following simplified equation for torque can be obtained.

$$\Gamma_P = \frac{\pi d_p^3 \rho_f}{4}\left[\frac{C_{Df}\sin\emptyset + D_r C_{Dv}\sin\phi + C_L\cos\phi}{4}u^2 - \frac{\tau_y\cos\emptyset}{2\rho_f} - \frac{d_p g(s-1)\sin(\alpha+\emptyset)}{3}\right] \quad \text{(7.32b)}$$

where, s is the ratio of the density fluid to that of the solid and D_r is the drag correction factor. The following steps show the numerical procedure:

1. A constant flow rate is set at a certain value.
2. Maximum and minimum bed height values are selected to determine the average bed height.
3. Hydraulic diameter and generalized Reynolds number are calculated.
4. Bed friction factor is obtained from Eqn. (7.29) or (7.31).
5. The local velocity and velocity gradient should be determined from Eqns. (7.21 to 7.26).
6. Reynolds number is calculated particle using Eqn. (7.27).
7. Drag and lift coefficients are estimated using Eqns. (7.7 to 7.15).
   The forces acting on the particle are predicted using V_r. Eqn. (7.5) and (7.6) and substituted into Eqn. (7.32a).
8. If $\Gamma_P > 0.0$, then the maximum value of bed height is replaced by the average value. Otherwise, the minimum value of bed height is replaced by the average value and the procedure requires repeating Steps 2 to 8 until Γ_P converges to a certain value.

7.5 Experimental Results

Fiber sweeps of varying base fluid, density, and fiber concentrations were tested in the flow loop to evaluate their hole cleaning performance (Section 6). In addition, the data from the XG-based drilling fluid (WBM) was used to evaluate the mechanistic CTV model shown in Section 7.4. The wellbore cleaning characteristics observed with the WBM fiber sweeps was subsidiary to the evaluation of the model.

7.5.1 Comparison of Model Predictions with Test Measurements

The mechanistic model developed in Section 4 was formulated to predict the equilibrium bed height in the annulus for a given flow rate. The model is valid for annuli without inner pipe rotation. Therefore, to evaluate the performance of the model, predictions were compared with experimental measurements obtained without inner pipe rotation. **Fig. 7.4** presents dimensionless bed height (H/D) as a function of flow rate for base fluid and fiber-containing fluid (fiber sweep) in horizontal annulus orientation. For the base fluid (**Fig. 7.4a**), the model showed good prediction at low flow rate (up to 50 gpm); however, it over-predicted the bed height at higher flow rates. Careful examination of results from the model indicate that the discrepancies between the model predictions and experimental measurements at high flow rates (more than 50 gpm) could have been due to poor local velocity predictions when the flow protruding bed particle, which was considered in the mechanistic model analysis, was out of the viscous layer.

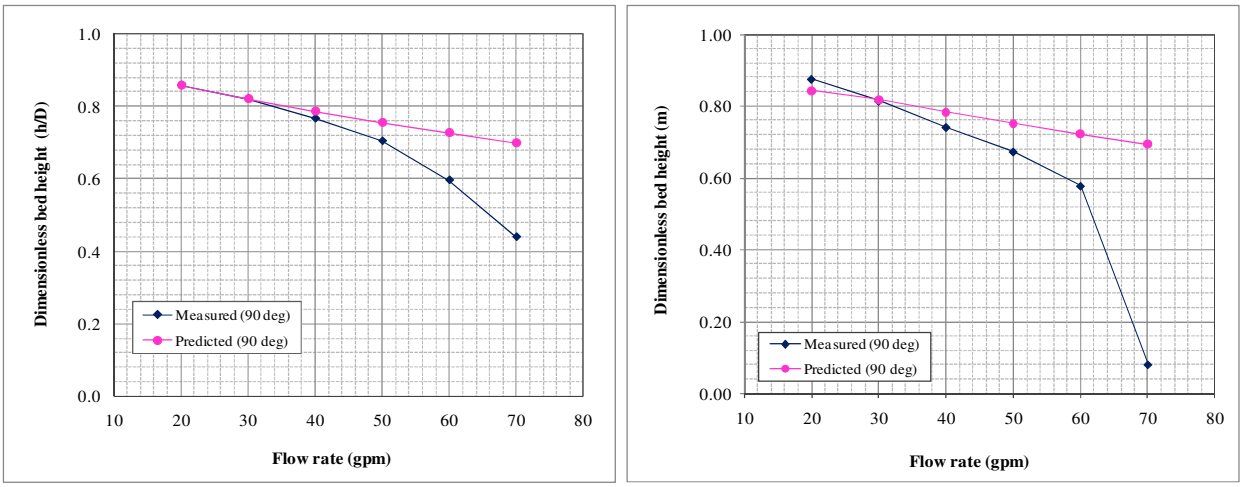

(a) **(b)**

Fig. 7.4 Bed height vs. flow rate for 2 mm cuttings in horizontal configuration
a) Base fluid, and b) Fiber sweep

The mechanistic model was formulated to account for the presence of fiber in the bed height prediction. The model predictions for the horizontal test section were compared (**Fig. 7.4b**) with measurements obtained from the fiber sweeps. At low flow rates (i.e., less than 60 gpm), predictions showed satisfactory

agreement with experimental measurements. Similar to the base fluid experiments, discrepancies between predictions and measurements were high at higher flow rates.

Flow loop experiments were also carried out in the inclined annular orientation (i.e., 70º from vertical). **Fig. 7.5** compares the model predictions with experimental measurements in terms of dimensionless bed height for the base fluid and fiber sweeps. As shown in the figures, the model predictions and measurements were in good agreement at low flow rate. As previously noted, as the flow rate increased, the discrepancies between the model predictions and experimental measurements also increased.

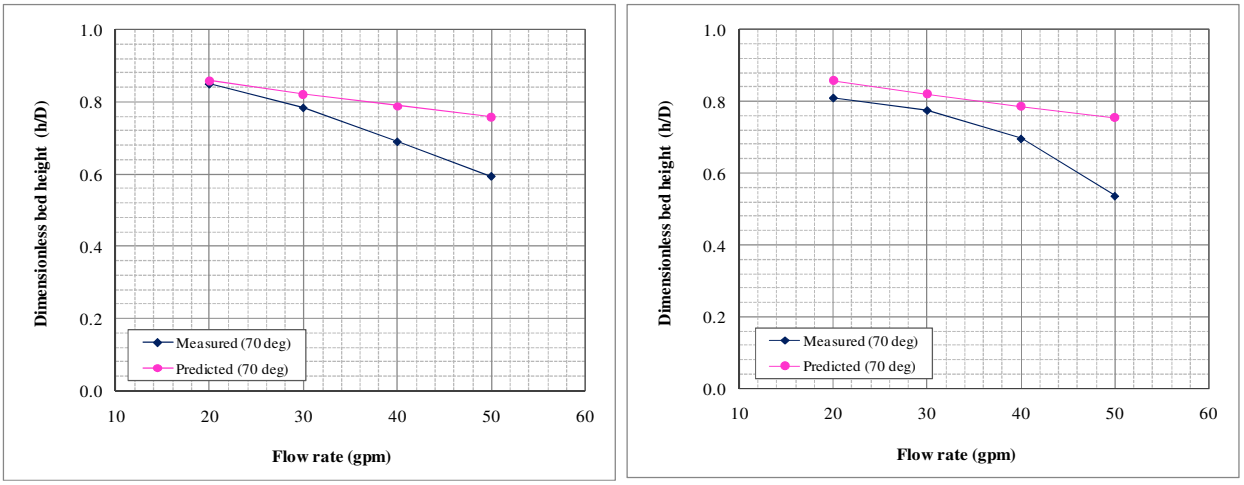

Fig. 7.5 Bed height vs. flow rate for 2 mm cuttings in inclined (70°) configuration a) Base fluid, and b) Fiber sweep

7.5.2 Comparison of Model Predictions with Published Data and Existing Model

In order to ensure the accuracy of the model, predictions were compared with published measurements (Duan, 2005) obtained from large-scale flow experiments conducted to study cuttings transport velocity in horizontal and highly deviated wells. Two different fluids (water and PAC) and solids particles with various sizes (0.45 mm; 1.4 mm) were used to perform the experiments. **Fig. 7.6** compares experimental measurements with model predictions for fine cuttings (0.45-mm average diameter) in horizontal and inclined annuli. A similar plot is presented in **Fig. 7.7** for coarse cuttings (1.4-mm average diameter) in horizontal and inclined annuli. As depicted in the plots, as flow rate increased, the bed cross-sectional area (bed area) decreased, resulting in an increase in flow area. For coarse cuttings (i.e., 1.4 mm particle), the new model predictions showed good agreement with the experimental measurements. Discrepancies increased slightly as the flow rate increased, reaching its maximum value (20 percent difference) at 400 gpm in an inclined annulus. For fine cuttings, the trend was similar and the maximum discrepancy (which

was roughly 20 percent) observed was at higher flow rates in inclined configuration. Despite some noticeable discrepancies at high flow rate, in general the performance of the new model was better than that of the existing model. The existing model showed discrepancy level of up to 90 percent.

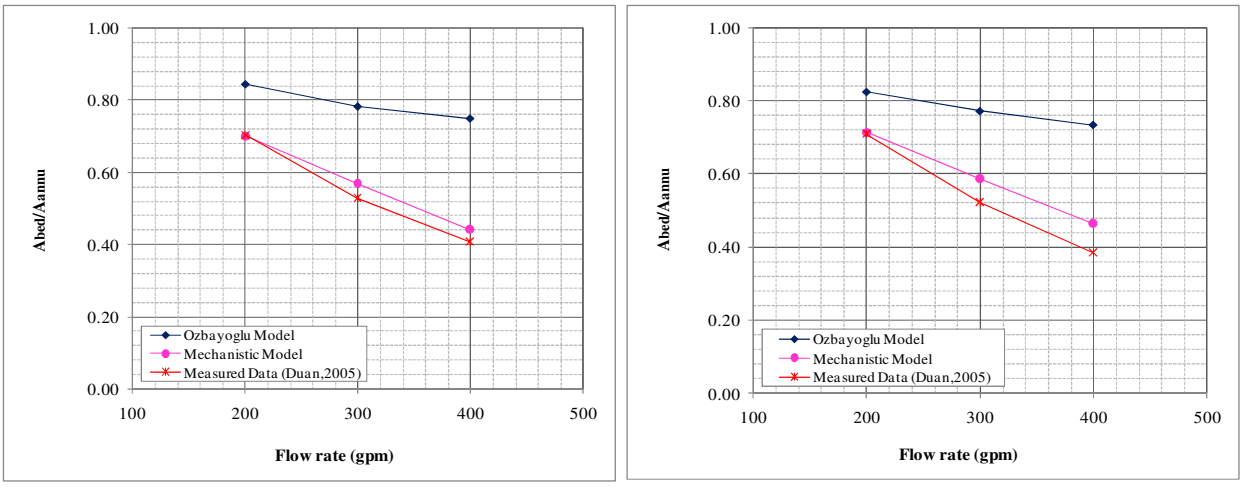

(a) **(b)**

Fig. 7.6 Bed area vs. flow rate for 0.45 mm cuttings with PAC based fluid a) Horizontal (90°), and b) Inclined (70°) orientation

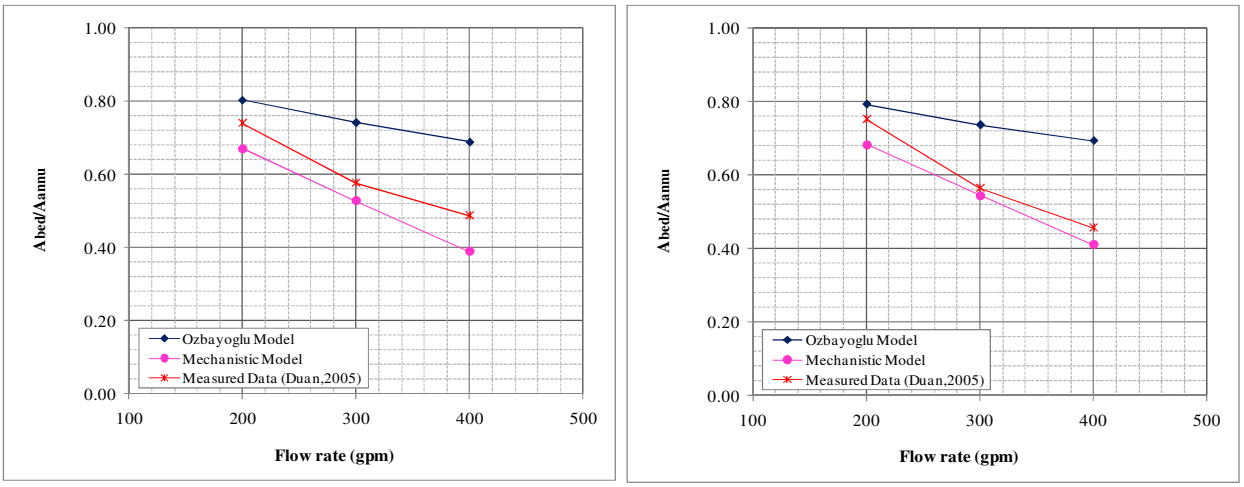

(a) **(b)**

Fig. 7.7 Bed area vs. flow rate for 1.40 mm cuttings with PAC based fluid a) Horizontal (90°), and b) Inclined (70°) orientation

7.6 Conclusions

Hole-cleaning performance of fiber-containing sweep fluid was investigated by varying inclination angle, fiber concentrations, pipe rotation, and flow rate. Experimental measurements showed that adding fiber to the fluid had a significant effect on the hole cleaning efficiency when applied in conjunction with inner pipe rotation. Based on the outcomes of this study, the following conclusions are drawn:

- Fiber sweep provides better hole cleaning than the base fluid in horizontal and highly inclined configurations.
- In the presence of the pipe rotation, adding fiber substantially improves sweep fluid efficiency. Increasing fiber concentration with pipe rotation tends to improve considerably the cuttings transport.
- Pipe rotation has a substantial effect on the bed erosion and fiber sweep applications.
- Based on pipe viscometer and rotational viscometer measurements, the quantity of fiber added to the sweep fluid has a minor effect on rheological and hydraulic characteristics of the fluid.
- Mechanistic modeling provides better prediction than the existing model.
- Cuttings transport model predictions agree with the experimental data at low flow for both base fluid and fiber-containing fluid.

Nomenclature

A_P = projection area of a particle

A_f = flow area above the cuttings

A = constant

B = constant

C_{Dv} = viscous drag coefficient

C_L = lift coefficient

C_{Df} = Fiber drag coefficient

$C_{\square}$ = correction of the angle of repose

C = fiber concentration

d_p = diameter of a particle

D_h = hydraulic diameter of a layer

D_{eff} = effective diameter

dV_r/dy = velocity gradient

Re_P = particle Reynolds number

Re = Reynolds number

R_{eG} = gradient Reynolds number

S_o = wetted perimeter of the outer wellbore

S_i = wetted perimeter of inner drill pipe wall

S_b = wetted perimeter of the cuttings bed

t = Time

U= mean flow velocity in the channel

U_{max} = maximum fluid velocity in the channel

U_τ = friction velocity

u^+ = dimensionless velocity

V_r = local velocity at the center of a bed particle

V = Instantaneous settling velocity of a particle

d_p^+ = particle diameter dimensionless

D_r = correction factor of the drag coefficient

F_b = buoyancy force

F_D = drag force

F_{Df} = fiber drag force

f_{bed} = friction factor of the bed

F_L = lift force

f = friction factor

F_{DT} = total drag force

F_{Dv} = viscous drag force

F_g = gravitational force

F_p = plastic force

g = gravitational acceleration

K = consistency index

k' = equivalent consistency index

m = mass of a solids particle

n' = equivalent fluid behavior index

n = fluid behavior index

p = pressure

V_s = Terminal settling velocity of a particle

y = vertical distance from the mean bed level

y^+ = dimensionless distance

Greek Letters

Γ_p = rotating torque at point p

ε = pipe roughness

$\prod$ = angle of repose

α = angle of inclination from vertical

α = exponent power of the fiber concentration

$\dot{\gamma}$ = Shear rate

δ^+ = dimensionless of thickness laminar sub-layer

μ = fluid viscosity

ρ_f = Fluid density

ρ_p = density of a particle

ϑ = kinematic viscosity

τ_y = yield stress

τ_{bed} = average bed shear stress

τ_w = wall shear stress

τ_{dis} = shear stress distribution around a bed particle

References

Ahmed, R.M., Skalle. P. and Johansen. S.T. 2002. A Mechanistic Model to Determine the Critical Flow Velocity Required to Initiate the Movement of Spherical Bed Particles in Inclined Channels. Chemical engineering science , 58 (2003) 2153-2163, 4 November.

Ahmed, R.M, Takach, N.E. and Savitri. 2009. Experimental Study on Fiber Sweeps in Horizontal and Highly Deviated Configurations. Paper SPE 120644 presented at the production operation Symposium held in Oklahoma city, USA, 4-8 April.

Ahmed, R.M. and Miska, S.Z. 2009. Drilling Hydraulics: Advanced Drilling and Well Technology, Edited by: Aadnoy, B.; Cooper, I.; Miska, S.; Mitchell, R.F.; Payne, M.L., Society of Petroleum Engineering, Chap 4.1, 191-220.

Bivins, C.H., Bomey, C.V., Fredd, C., Lassek, J., Sullivan, P., Engels, J., Fielder, E. O., Gorham, T., Judd, T., Mogollon, A E.S., Tabor, L., Munoz, A. and Willberg, D. 2005. New Fibers for Hydraulic Fracturing. Oilfield Review, Vol. 17, Issue 2, Schlumberger.

Clark, R.K. and Bickham, K.L. 1994. A Mechanistic Model for Cuttings Transport. Paper SPE presented at 69th annual technical conference and Exhibition held in New Orleans, La, USA, 25-28 September.

Colebrook, C.F. 1939. Friction Factors for Pipe Flow, *Inst. Civil Eng.*, **11**, 133

Dedegil, M.Y. 1987. Drag Coefficient and Settling Velocity of Particles in Non-Newtonian Suspensions. Journal of fluids engineering, vol. 109/319.

Dodge, D.W. and Metzner, A.B. 1959. Turbulent flow of non-newtonian systems. *AIChE Journal*, Vol. 5, No. 2, pp. 189-204.

Duan, M. 2005. An Experimental Study of Small Sand- Size Cuttings Transport in Horizontal and High Angle Wellbores. The University of Tulsa.

Desouky, S.E.D.M. and Al Saddique, M.A. 1999. Turbulent Pressure Loss of Yield Fluids in Pipes. Journal of Canadian petroleum technology, Vol. 38, No. 13.

Gerhart, P. M, Gross, R. J., & Hochstein, J. I. (1992). Fundamental of Fluid Mechanics (pp. 480–650). New York: Addison Wesley Publishing Company.

Guogui, F. 1992. An Experimental Study of Free Settling of cuttings in Newtonian and Non-Newtonian Drillings Fluids: Drag Coefficient and Settling Velocity. Technical University of Berlin.

Harlen, O.G., Sundararajakumar, R.R. and Koch. D.L. 1999. Numerical Simulations of a Sphere Settling through a Suspension of Neutrally Buoyant Fibers. J. fluid mech., Vol. 388, pp. 355-388.

Larsen, T.I., Pilehvari, A.A. and Azar. J.J. 1997. Development of a New Cuttings-Transport Model for High-Angle Wellbore Including Horizontal Wells. SPE drilling & completion, June.

Liang, S.C., Hong. T. and Fan. L.S. 1995. Effect of Particle Arrangements on the Drag Force of a Particle in the Intermediate Flow Regime. International journal multiphase flow, Vol. 22, No.2, pp.285-306.

Duan, M., Stefan. M., Mengjiao. Y., Nicholas. T. and Ahmed. R. 2006. Transport of Small Cuttings in Extended Reach Drilling. Paper SPE 104192 presented at international Oil and Gas conference , China , 5-7 December.

Ozbayoglu, M., Saasen, A., Sorgun, M. and Svanes, K. 2007. Estimating Critical Velocity to Prevent Bed Development for Horizontal-Inclined Wellbores. Paper SPE/IADC 108005 presented at middle east technology conference and exhibition held in Cairo, Egypt, 22-24 October.

Persen, L. N. (1972). Boundary Layer Theory (pp. 83–130). Trondhiem:Tapir.

Rasi, M. 1994. Hole Cleaning in Large, High Angle Wellbore. Paper IADC/SPE 27464 presented at the drilling conference held in Dallas, Texas, 15-16 February.

Reed. T.D. and Pilehavari. A.A. 1993. A New Model for Laminar, Transitional and Turbulent Flow of Drilling Muds. Paper SPE 25456 presented at the production operation Symposium held in Oklahoma city, USA, 21-23 March.

Saffman. P.G. 1964. The Lift on a Small Sphere in a Slow Shear Flow. Journal fluid mechanic, Vol.22, part 2, pp. 385-400.

White, F. M. (1991). Viscous Fluid Flow (2^{nd} ed .) (pp. 181–200). New York: McGraw-Hill.